EXPLORATIONS OF siRNA THERAPEUTICS USING MOLECULAR DYNAMICS SIMULATIONS: STRUCTURAL IMPACTS OF 2'-RIBOSE MODIFICATIONS ON RNA DUPLEX AND INTERACTIONS WITH HUMAN ARGONAUTE-2

RIDWAN OLAYIWOLA TAJUDEEN
Bachelor of Science, University of Ilorin, 2018

A thesis submitted
in partial fulfilment of the requirements for the degree of

MASTER OF SCIENCE

in

CHEMISTRY

Department of Chemistry and Biochemistry
University of Lethbridge
LETHBRIDGE, ALBERTA, CANADA

EXPLORATIONS OF siRNA THERAPEUTICS USING MOLECULAR DYNAMICS SIMULATIONS: STRUCTURAL IMPACTS OF 2'-RIBOSE MODIFICATIONS ON RNA DUPLEX AND INTERACTIONS WITH HUMAN ARGONAUTE-2

RIDWAN OLAYIWOLA TAJUDEEN

Date of Defense: July 25th, 2025

Dr. Stacey Wetmore Supervisor	Professor	PhD
Dr. Marc Roussel Thesis Examination Committee Member	Professor	PhD
Dr. Jean-Denys Hamel Thesis Examination Committee Member	Assistant Professor	PhD
Dr. Michael Gerken Chair, Thesis Examination Committee	Professor	PhD

DEDICATION

To my wife, for her unwavering love and support, and to my daughter whose arrival brought new light and purpose to my life. Your love, strength, and presence gave me purpose, and made every challenge worthwhile.

ABSTRACT

RNA interference (RNAi) is a natural mechanism by which short strands of RNA, such as small interfering RNA (siRNA), directly control the activities of genes through targeted gene suppression. RNAi can theoretically degrade any disease-related gene in a sequence-specific manner, thereby preventing disease. As a result, siRNA is a promising therapeutic. Indeed, drugs based on siRNA have emerged to treat various diseases, including cancer, viral infections, and genetic disorders. Despite their potential, siRNA-based therapeutics pose developmental challenges due to several inherent properties such as easy degradation *in vivo* and unwanted off-target effects, which reduce their potency. The introduction of chemical modifications into nucleotides has been employed to improve the drug-like properties of siRNA, with five such drugs having been approved by the United States Food and Drug Administration (FDA). These drugs are used to treat diseases such as hereditary transthyretin mediated amyloidosis, acute hepatic porphyria, and primary hyperoxaluria type 1, and hypercholestomia. However, to rationally design improved drugs, we must know how existing versions work. Although an important step in this process is understanding the chemical structure of the drugs and other chemically-modified siRNA duplexes, this information is currently limited, primarily due to the extensive time requirements associated with experimental procedures. To bridge the gap in our understanding of useful siRNA modifications and thereby accelerate the transition from discovery and development to clinical trials, this research uses long-timescale molecular dynamics (MD) simulations to analyze the structural preferences of the 5 siRNA drugs approved by the FDA, namely Patisiran, Givosiran, Lumasiran, Inclisiran, and Vutrisiran, and to examine how diverse chemical modification patterns influence the overall siRNA structure and interactions with human argonaute-2, the

protein that facilitates gene suppression. My findings provide valuable insight into the changes in the structural dynamics, and interactions induced by chemical modifications, offering valuable information to assist the development of new siRNA drug with enhanced therapeutic efficacies.

CONTRIBUTION OF AUTHORS

This thesis comprises two results chapters. The contributions of each contributor are detailed below in accordance with the CRediT (Contributor Roles Taxonomy) system.

The manuscript for Chapter 2 is currently being drafted. Contributors to this chapter include Stacey D. Wetmore, Tyler Quinn, Sara Kozub, and I. I contributed to the conceptualization of the project, carried out the model building of all duplexes, prepared the systems, and conducted the molecular dynamics simulations. Additionally, I performed all formal analysis, interpreted the findings, generated all figures, and wrote the initial draft of the manuscript. Tyler Quinn and Sara Kozub contributed by performing some molecular dynamics simulations on the different nucleobase sequences with drug modification patterns while under my mentorship. Stacey D. Wetmore was responsible for project conceptualization and administration, supervision, funding and resource acquisition, data visualization and interpretation, and contributed to writing and reviewing the manuscript and chapter drafts.

Chapter 3 has not yet been prepared for publication. For this chapter, I contributed to the project conceptualization, model building, system preparation, and molecular dynamics simulations. I also carried out all analysis and interpretation of the results. Stacey D. Wetmore contributed to project conceptualization and administration, supervision, funding and resource acquisition, data visualization and interpretation, and contributed to writing and reviewing the chapter draft.

ACKNOWLEDGEMENT

I would like to express my deepest appreciation to my supervisor, Dr. Stacey Wetmore, for her unwavering support, guidance, and encouragement throughout the years. Her mentorship has been instrumental in helping me navigate the challenges of graduate school, and I could not have asked for a more dedicated and invested supervisor. I am truly grateful for her commitment to my success. I would also like to thank my committee members, Dr. Marc Roussel and Dr. Jean-Denys Hamel, for their insightful feedback and constructive advice, which have significantly contributed to the quality and direction of my research. My sincere thanks to Dr. Michael Gerken for agreeing to serve as the chair of my thesis defense. Finally, I am grateful for the financial support I received during my graduate studies. I would like to acknowledge RNA Innovation, Alberta Innovates–Technology Futures, and the School of Graduate Studies for their generous funding throughout my studies.

To my fellow Wetmore lab members, thank you for creating such a supportive and enjoyable environment. Your camaraderie made the lab a place of both productivity and fun. Whether it was bouncing ideas off each other or sharing laughs during breaks, I truly appreciated every moment. From my fellow master's students, Mark Lea and Angela Frederickson to Rebecca Jeong, Dr. Briana Boychuk, Makay Murray, Dylan Nikkel, Umer Yaqoob, Dr. Indu Negi, Dr. Mansour Basel, and Dr. Austin Pounder—each of you has played a meaningful role in my journey, and your presence has been deeply valued. I would also like to thank the undergraduate student Tyler Quinn and HYRS student Sara Kozub, with whom I had the pleasure of working, your contributions and enthusiasm did not go unnoticed.

Finally, to my family and friends, your love, encouragement, and prayers have been my anchor throughout this journey. I couldn't have done this without you.

TABLE OF CONTENTS

LIST OF TABLES

LIST OF FIGURES

LIST OF ABBREVIATION

2′-MOE	2′-Methoxyethyl
2'-F	2'-Fluoro
2'-*O*-Me	2'-*O*-Methyl
AHP	Acute Hepatic Porphyria
AML	Acute Myeloid Leukemia
CD	Circular Dichroism
cryo-EM	Cryo-electron Microscopy
DFT	Density Functional Theory
DNA	Deoxyribonucleic Acid
dsRNA	Double Stranded RNA
ENA	Ethyl-bridged Nucleic Acid
FDA	Food and Drug Administration
FNA	Fully 2'-F substituted Nucleic Acid
FTD	Trifluorothymidine
FTO	Fat mass and Obesity Associated Protein
GAFF2	Generalized Amber Force Field
GalNac	*N*-acetylgalactosamine
GB	Generalized Born
GNA	Glycol Nucleic Acid
hAgo2	Human Argonaute-2
hATTR	Hereditary Transthyretin-Mediated Amyloidosis
LNA	Locked Nucleic Acid
lncRNA	Long Noncoding RNA
m^1A	N^1-methyladenosine
m^5C	5-methylcytosine
m^6A	N^6-methyladenosine
MD	Molecular Dynamics
miRNA	MicroRNA
MM	Molecular Mechanics
MM/PBSA	Molecular Mechanics/Poisson-Boltzmann Surface Area
MM-GBSA	Molecular Mechanics/Generalized Born Surface Area
mRNA	Messenger RNA
ncRNA	Noncoding RNA
NMR	Nuclear Magnetic Resonance
OMeNA	Fully 2'-*O*-Me substituted Nucleic Acid
PAZ	PIWI-Argonaute-Zwille
PDB	Protein Data Bank
PH1	Primary Hyperoxaluria Type 1
piRNA	PIWI-interacting RNA
poly A	Polyadenylic Acid
PS	Phosphorothioate
QM	Quantum Mechanical
RESP	Restrained Electrostatic Potential
RISC	RNA Inducing Silencing Complex

RMSD	Root-Mean-Square Deviation
RMSF	Root-Mean-Square Fluctuation
RNA	Ribonucleic Acid
RNAi	RNA Interference
RoG	Radius of Gyration
SAS	Small Angle Scattering
shRNA	Short Hairpin RNA
siRNA	Small Interfering RNA
snRNA	Small Nuclear RNA
tRNA	Transfer RNA
TtAgo	*Thermus thermophilus* Argonaute
Ψ	Pseudouridine

Single- and Triple-Letter Abbreviations for the Amino Acids

A	Ala	Alanine
C	Cys	Cysteine
D	Asp	Aspartate, aspartic acid
E	Glu	Glutamate, glutamic acid
F	Phe	Phenylalanine
G	Gly	Glycine
H	His	Histidine
I	Ile	Isoleucine
K	Lys	Lysine
L	Leu	Leucine
M	Met	Methionine
N	Asn	Asparagine
P	Pro	Proline
Q	Gln	Glutamine
R	Arg	Arginine
S	Ser	Serine
T	Thr	Threonine
V	Val	Valine
W	Trp	Tryptophan
Y	Tyr	Tyrosine

CHAPTER 1: INTRODUCTION

1.1 Thesis Overview

The importance of RNA-based medicines came into the global spotlight during the COVID-19 pandemic, when mRNA vaccines played a crucial role in controlling the spread of the virus. [1] These vaccines demonstrated how powerful RNA technologies can be in treating and preventing disease. A key reason mRNA vaccine worked so well during the pandemic was the use of chemical modifications,[1-5] which are small, chemical changes to the RNA building blocks that typically make the drugs more stable and less likely to trigger immune reactions.

The success of mRNA vaccinees has sparked growing interest in using similar approaches for other types of RNA treatments, including a promising class of drugs called small interfering RNAs (siRNAs). These molecules can block harmful genes associated with a particular disease and have already been approved for treating diseases like hereditary transthyretin mediated amyloidosis, acute hepatic porphyria, primary hyperoxaluria, and high cholesterol.[6-8] However, despite their proven potential, many challenges remain in the use of siRNA therapeutics. Indeed, siRNA molecules can break down quickly in the body, and sometimes cause side effects by interacting with the wrong targets. [9] To overcome these issues, scientists have turned to using chemical modifications to improve drug performance.[7,9] To design even better drugs to treat more diseases, information about the impact of the chemical modifications on the structure and function of the RNA-based drug is required. However, this information is currently lacking in the literature, at least in part because of difficulties gaining this information for a range of chemical modifications through traditional ‘wet’ lab experiments.

My research uses the tools of computational chemistry to explore how chemical modifications commonly used in existing siRNA drugs affect RNA structure and function. While some previous computational studies have looked at how small chemical changes impact siRNA behavior, most have focused on molecules with only one or two modifications.[10-12] In contrast, real-world siRNA drugs include many modifications across the entire drug and therefore my work will fill an important void in the literature. In addition to detailing the structure and dynamics of both unmodified and fully modified siRNA molecules, I will look at how modified siRNAs interact with a key protein in the body that helps them do their job (called human Argonaute-2). The overarching goal of my work is to better understand how different types and patterns of chemical modifications influence structure and functions of siRNA, which could guide the development of safer and more effective RNA treatments in the future. In the remainder of this chapter, I outline the basic structure of nucleic acids and RNA modifications in biology, introduce the therapeutic relevance of siRNA and its mechanism of action through RNA interference (RNAi), discuss the importance of chemical modifications in siRNA drug development, review key experimental and computational findings related to siRNA modifications, and summarize the main approach used in my work.

1.2 Nucleic Acid Structure

Nucleic acids are fundamental macromolecules that exist in two naturally occurring forms: deoxyribonucleic acid (DNA) and ribonucleic acid (RNA).[13,14] These biomolecules play essential roles in cellular processes, with DNA primarily serving as a stable, double-stranded repository of genetic information, while RNA participates in diverse functions, including gene expression, catalysis, and regulatory mechanisms.[13,15] In the central role of

RNA in the flow of genetic information, messenger RNA (mRNA) serves as an intermediary carrier of genetic instructions,[16] while transfer RNA (tRNA) acts as a molecular adaptor that facilitates the translation of this information into a functional protein.[17] This translation process is catalyzed by the ribosome, a large ribonucleoprotein complex that ensures the accurate pairing of mRNA codons with the corresponding aminoacylated tRNAs and catalyzes peptide bond formation.[18] Beyond its role in protein synthesis, RNA performs numerous gene regulatory and expression roles, particularly in eukaryotic and multicellular organisms. Small interfering RNA (siRNA), microRNA (miRNA), PIWI-interacting RNA (piRNA), and small nuclear RNA (snRNA) are critical for gene expression regulation, RNA silencing, and other cellular processes.[19-32] Consequently, RNA can be broadly categorized into protein-coding RNA and noncoding RNA (ncRNA), with the latter comprising the majority of RNA species and playing essential roles in gene expression, and cellular regulation.[32]

The basic structural unit of both DNA and RNA is the nucleotide (Figure 1.1).[14] A nucleotide consists of three components: a nitrogenous base, a pentose sugar, and a phosphate group. The combination of only the nitrogenous base and the sugar (without the phosphate group) is referred to as a nucleoside.[33] In nucleoside and nucleotides, the sugar component is either β-D-2'-ribose in RNA or β-D-2'-deoxyribose in DNA. A phosphate group is attached at the 5' position and a nitrogenous base covalently linked at the C1' position via a β-glycosidic bond in a nucleotide.[34] The nitrogenous bases fall into two categories: purines (adenine and guanine) and pyrimidines (cytosine, uracil, and thymine, Figure 1.2). While both DNA and RNA contain adenine (A), guanine (G), and cytosine (C), RNA uniquely incorporates uracil (U) instead of thymine (T), which features an additional methyl group at position 5 and is present in DNA.

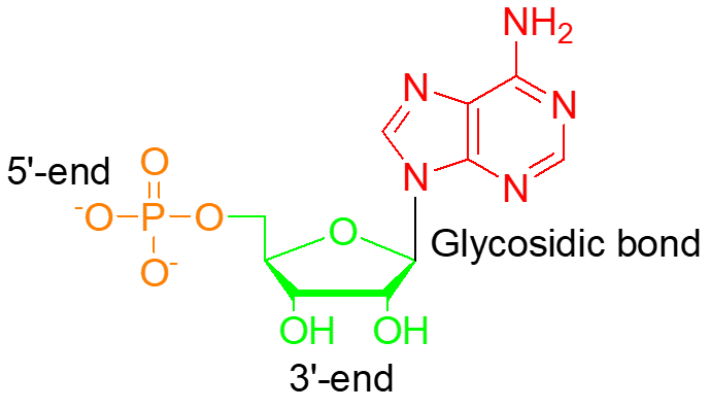

Figure 1.1: Structural representation of an RNA nucleotide, highlighting the three main components: the phosphate moiety (orange), ribose (green), and the nucleobase (red).

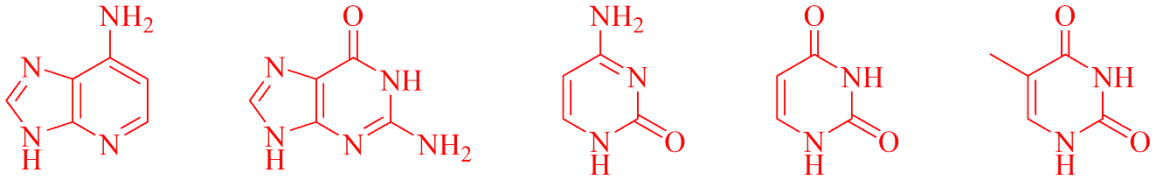

Figure 1.2: Chemical structures of the five standard nucleobases from left to right: adenine, guanine, cytosine, uracil, and thymine. Adenine and guanine are purines, while cytosine, uracil, and thymine are pyrimidines. Uracil is found in RNA, whereas thymine is its DNA counterpart.

Nucleotides polymerize to form polynucleotide chains with directionality, meaning they have chemically distinct 5′ and 3′ ends. The 5′ end of the chain has an exposed phosphate group from the first nucleotide, while the 3′ end has a free hydroxy group in the last nucleotide. During polymerization, new nucleotides are added exclusively to the 3′ end, with the 5′ phosphate of an incoming nucleotide forming a phosphodiester bond with the 3′ hydroxy of the growing strand. The so-called phosphodiester linkage establishes the sugar–phosphate backbone that is essential for nucleic acid stability and function.[33, 35-37]

Early X-ray diffraction studies identified two predominant duplex conformations of nucleic acids: the B-form and A-form (Figure 1.3).[15,36-38] The B-form is the most common conformation, particularly in DNA, and is characterized by a thin, elongated helical

structure, with approximately 10 base pairs per turn and a helical rise of >3.0 Å per base pair.[39,40] In contrast, RNA predominantly adopts the A-form, which is shorter and wider, featuring an average of 11 base pairs per turn and a helical rise of ~2.6 Å per base pair.[41] Within the double strand of DNA, each nucleobase is engaged in Watson-Crick hydrogen bonds with the complementary base in the opposing strand to form G:C and A:T base pairs (Figure 1.4).[42] The genetic code is stored in the specific sequence of nucleotides, with accurate hydrogen bonding between complementary bases preserving the integrity.[32]

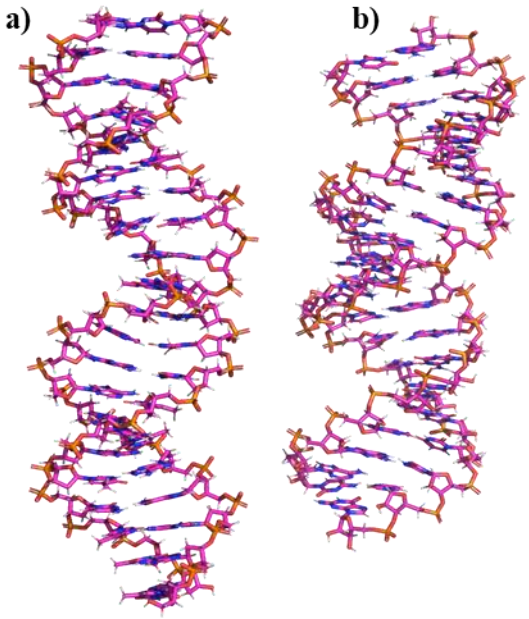

Figure 1.3: Structural representations of (a) B-form and (b) A-form nucleic acid duplexes.

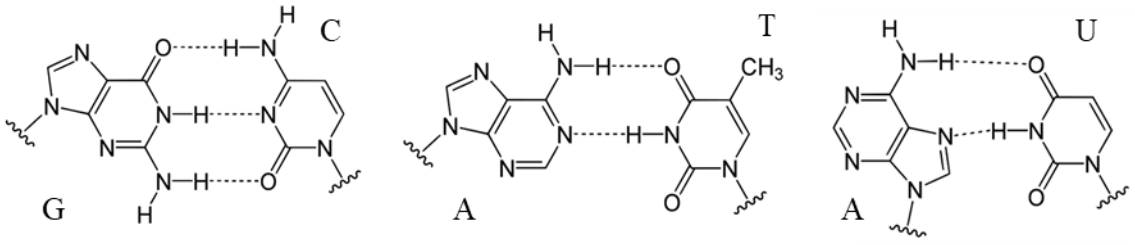

Figure 1.4: Structures of the adenine–thymine (A:T), adenine–uracil (A:U), and guanine–cytosine (G:C) canonical Watson-Crick base pairs, illustrating specific hydrogen-bonding patterns and base complementarity.

RNA mostly exists in the single-stranded form, but there are several RNA that are

double-stranded like viral RNA and siRNA.[32] Like DNA, RNA duplexes are composed of four nucleotide monomers (A, C, G, and U) engaged in Watson-Crick hydrogen bonds to form G:C and A:U base pairs (Figure 1.4). The presence of the 2′-hydroxy (2′-OH) group in ribose introduces structural and chemical differences between RNA and DNA. This functional group reduces the chemical stability of RNA by promoting intramolecular cleavage via acid- and base-catalyzed hydrolysis, making RNA more transient than DNA.[32] Additionally, the 2′-OH serves as a versatile hydrogen-bond donor and acceptor, facilitating the compact packing of RNA helices and enabling RNA to form complex architectures unavailable to DNA.[32,43-47]

Given the central and diverse roles of RNA, particularly in gene regulation, as well as the unique structural architectures adopted, RNA has become a promising target for therapeutic applications, especially through the design of chemically-modified small RNAs such as siRNAs. This thesis focuses on understanding how chemical modifications influence siRNA structure and function, an area important for the rational design of more effective RNA-based therapeutics. The next section examines the biological roles of various RNA modifications, setting the foundation for the subsequent discussion on the therapeutic potentials of siRNA.

1.3 RNA Modifications and Their Biological Relevance

RNA modifications are pivotal post-transcriptional modifications that influence the fate of RNA in regulating gene expression and various biological processes.[48] RNA are recognized and acted upon by specific "writers" (enzymes that add modifications), "erasers" (enzymes that remove modification), and "readers" (proteins that interpret the modifications).[49] As of 2024, about 170 modifications have been characterized in different

RNA and have been well documented.[48,50] The most extensive studies have been on tRNA, mRNA, and ribosomal RNA (rRNA). For instance, N^6-methyladenosine (m^6A) is one of the most prevalent mRNA modifications,[51-55] and is known to destabilize RNA duplexes by altering the pattern of hydrogen bond donors and acceptor at either the canonical or non-canonical positions, leading to locally unstructured regions. In contrast, N^1-methyladenosine or (m^1A) disrupts standard Watson-Crick base pairing and introduces a positive charge,[56-59] which can reshape local RNA structure and promote electrostatic interactions with the phosphate backbone. 5-methylcytosine (m^5C) is suggested to alter the overall helical structure, potentially making the RNA more rigid or compact,[60-63] depending on the modification position. Additionally, pseudouridine (Ψ) improves base stacking and favors a C3′-*endo* sugar pucker,[64-68] which enhances RNA rigidity and can affect both secondary structure and translation efficiency.

RNA modifications can modulate the expression of genes involved in metabolic pathways, thereby participating in the reprogramming of cellular metabolism in both healthy and disease states, such as cancer and metabolic disorders.[48] RNA modifications also play essential roles in immunometabolism, regulating how immune cells respond to various stimuli and pathogens.[48,60,69,70] Changes in RNA modification states can affect the activation, proliferation, and function of immune cells, highlighting their importance in both immune responses and immune-related diseases.[48,70] For example, m^6A-modified transcripts of key metabolic regulators can alter the metabolic pathways in cancers, enhancing their proliferation and survival.[71-73] Alterations in m^1A levels can have downstream effects on cellular growth and protein synthesis, crucial for metabolic homeostasis.[48,74,75] Similarly, m^5C modifications have been found to regulate the stability of certain long noncoding RNAs (lncRNAs), which in turn can control the expression of

metabolic enzymes and transcription factors critical for various metabolic processes.[76,77] Additionally, Ψ-modifications have been shown to be associated with renal function damage and the risk of terminal-stage hypertensive disease, and support the translation of mRNAs encoding metabolic enzymes, thereby influencing metabolic flux.[48,75,76]

In addition to the involvement in diseases, there are clinical implications of RNA modifications, where they can play a large role in treatment strategies.[1] Modified nucleotides can significantly improve the half-life and reduce the immunogenicity of therapeutic RNA, enhancing their efficacy in various treatments.[2,78] For example, the success of mRNA vaccines during the COVID-19 pandemic exposed the potential of using RNA modifications to enhance the stability and efficiency of mRNA therapeutics.[1] Also, drugs targeting the m^6A methylation machinery (e.g., FTO inhibitors) have shown promise in enhancing the efficacy of existing chemotherapies by improving the apoptosis of cancer cells in acute myeloid leukemia (AML).[79] Recently, the use of chemical modifications has presented opportunities to reduce off-target effects, increase pharmacokinetics and pharmacodynamics effects, and improve the precision of siRNA-based therapies used for treatment of several diseases.[7,9] These advancements underpin the transformative potential of RNA modifications in shaping the next-generation siRNA-based therapies. Therefore, the subsequent sections focus on the role of siRNA in gene regulation and how chemical modifications can optimize the therapeutic potential.

1.4 Overview of siRNA-Based Therapeutics

1.4.1 RNA Interference (RNAi)

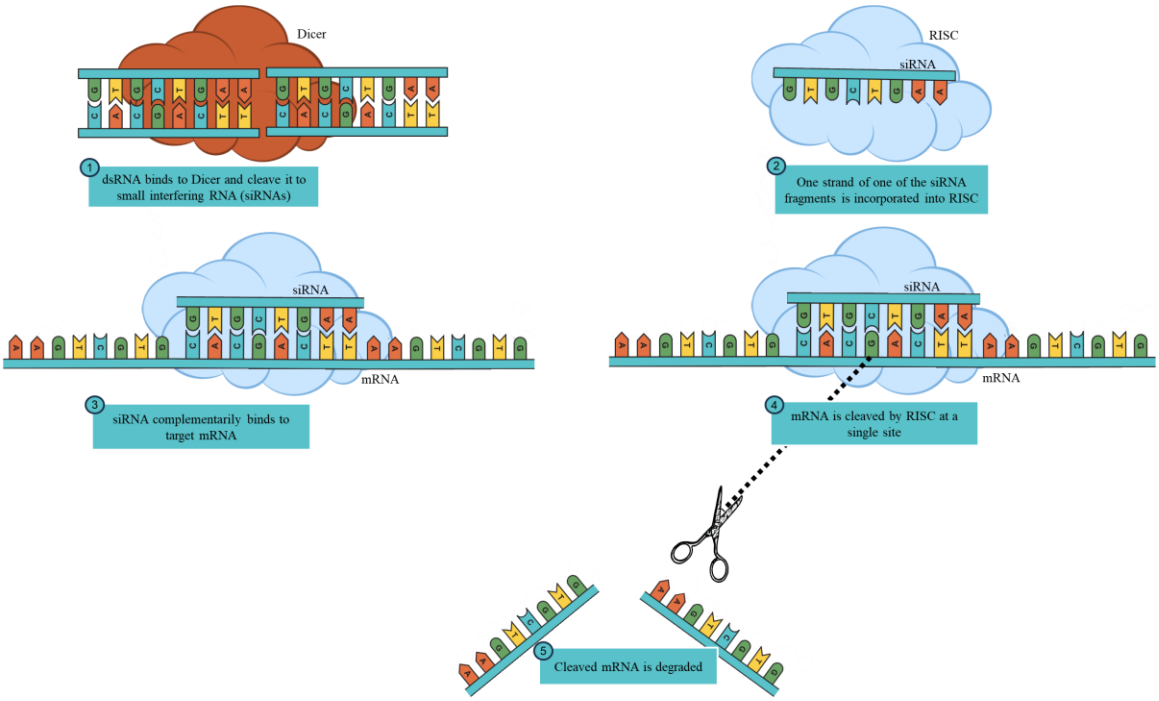

Figure 1.5: Schematic illustration of the RNAi mechanism.

siRNA is involved in RNAi, and RNAi is a highly conserved post-transcriptional gene regulation mechanism that plays a crucial role in cellular defense against external invasion by genetic elements.[6,9,28,29,31,43,80-86] The RNAi pathway is initiated in the cytoplasm by the endoribonuclease Dicer (Figure 1.5), which processes long, double-stranded RNA (dsRNA) or short hairpin RNA (shRNA) into mature siRNA duplexes of 21-23 nucleotides, typically bearing 3' overhangs. siRNA duplexes are then loaded into the RNA-induced silencing complex (RISC), a multiprotein assembly that includes human Argonaute-2 (hAgo2). Within RISC, RNA helicases assist strand separation of siRNA in an ATP-dependent manner.[30] The sense strand is discarded, while the antisense strand serves as a guide to direct sequence-specific binding to the target mRNA. This interaction

facilitates cleavage of the target transcript by hAgo2, leading to gene silencing.[29,30,84,87]

siRNA has innate advantages over small molecular therapeutics and monoclonal antibody drugs because of its reliance on Watson–Crick base pairing with mRNA rather than the need to recognize the complicated spatial conformation of a protein.[9] Indeed, small molecule and monoclonal antibody drugs require a high level of structural precision and therefore are complex and challenging to develop.[88] Theoretically, any gene of interest can be targeted by siRNA since only the correct nucleotide sequence of the targeting mRNA needs to be selected.[7] As a result, siRNA therapeutics have a shorter research and development span, and a wider therapeutic area than small molecule or antibody drugs. This affords the opportunity to selectively target and silence mRNA products of genes that were previously considered to be "undruggable" targets.[89,90] Over the past two decades, siRNA-based therapeutics have demonstrated significant potential for treating a range of diseases, including hypercholestomia, primary hyperoxaluria, hepatic porphyria.[7,9,91,92] This therapeutic potential of siRNA was ultimately realized through chemical modifications, which will be explored in greater detail in the next section.

1.4.2 Importance of siRNA Modifications in Therapeutic Applications

While unmodified siRNA serves in the natural RNAi pathway and siRNA has high therapeutical potential, clinical applications of siRNA pose several developmental challenges.[93-95] siRNAs have low bioavailability and are rapidly cleared, particularly by the kidneys due to their large size and anionic charge.[7,96] siRNAs are also highly susceptible to nuclease degradation, leading to a short half-life.[93] Once inside the target tissue, siRNAs must overcome cellular uptake barriers, as they do not naturally cross membranes, and endosomal trapping can further restrict their availability.[97,98] Additionally, siRNAs risk

being mistaken for viral RNA by immune sensors, such as toll-like receptors, potentially triggering an undesirable immune response.[7,99] These factors including poor stability, off-target effects, immunogenicity, and delivery difficulties significantly limit the therapeutic efficacy of siRNA and may lead to unintended toxicity.

There are two major solutions that have been curated to address these challenges associated with the clinical application of siRNA drugs: (1) using innovative delivery mechanisms and (2) introducing chemical modifications to siRNA. Currently, two major delivery mechanisms have been used: (i) formulation of the siRNA into nanocarriers that allow for transfection into target cells (e.g. lipid nanoparticle)[98,100] and (ii) conjugation of the siRNA to a targeting ligand that binds to a specific receptor of target cells (e.g., *N*-acetylgalactosamine, GalNac).[100-102] Meanwhile, chemical modifications have been shown to play a crucial role in improving the performance of siRNA drugs and various modifications have been implemented to enhance the stability and drug-like properties of siRNA.[83,103,104] The introduction of chemical modifications into siRNA may affect several structural and functional properties, including the susceptibility to ribonuclease degradation, recognition and processing by the RNAi machinery, toxicity, thermal stability (melting temperature), and maintenance of the A-form RNA helical structure.[83,105-107] This thesis focuses on elucidating how such chemical modifications impact siRNA structure and interactions.

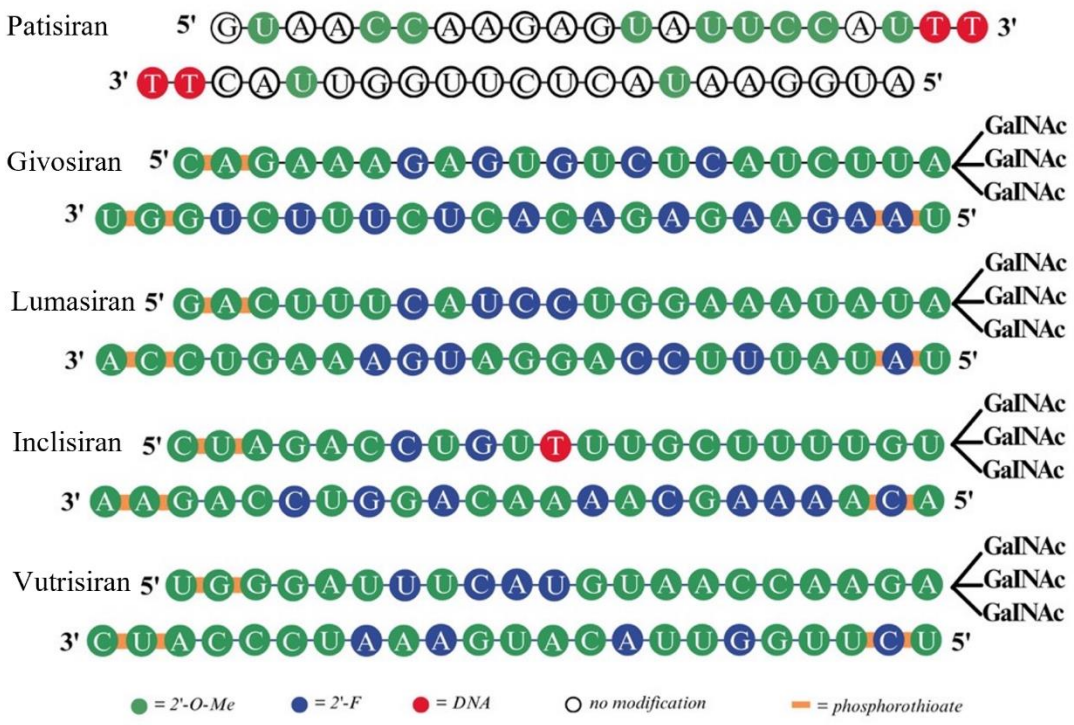

Figure 1.6: Sequence of the FDA approved siRNA therapeutics showing their modification patterns.

As a result of chemical modifications, several siRNA drugs have been approved by the United States Food and Drug Administration (FDA, Figure 1.6) and have been on the market since 2018,[108] twenty years after RNAi was discovered. The first siRNA drug, Patisiran, was approved in August 2018 for the treatment of Hereditary Transthyretin-Mediated Amyloidosis (hATTR).[108] This was followed by Givosiran (November 2019) for Acute Hepatic Porphyria (AHP),[109] Lumasiran (November 2020) for Primary Hyperoxaluria Type 1 (PH1),[110,111] Inclisiran (December 2021) for hypercholesterolemia,[112] and Vutrisiran (June 2022) as another treatment for hATTR.[7,113] Additional candidates, such as Fitusiran, Teprasiran, Cosdosiran, and Tivanisiran, are currently in various stages of clinical development.[9,114] The growing number of approved and emerging siRNA therapeutics highlights the role of chemical modifications in

enhancing siRNA performance and clinical viability. The next section reviews key experimental findings that shed light on the diverse impacts of these modifications.

1.5 Overview of Experimental Studies on siRNA Modifications

Among the chemical modifications to siRNA, ribose modifications (Figure 1.7) are the most used in the FDA-approved drugs, with the 2′-*O*-Me group at the 2′ position of the ribose being one of the most widely used and considered to be one of the most promising chemical strategies for the development of clinically viable siRNA-based drugs.[89,115,116] Experimental studies have demonstrated that the 2′-*O*-Me modification can significantly affect siRNA stability and function.[106,117] Ultraviolet and circular dichroism (CD) spectroscopic data have shown that methylation at the 2'-OH position of polyadenylic acid (poly A) enhances the thermal stability of the double-stranded structure, suggesting that the modification may confer subtle changes in the helical geometry, base stacking interactions, and backbone rigidity.[118] Another study conducted *in vitro* degradation assays, showing that 2′-*O*-Me-modified siRNAs exhibit enhanced resistance to ribonucleases compared to unmodified siRNAs.[119,120] This finding was supported by *in vivo* studies where siRNAs containing 2′-*O*-Me modifications showed increased nuclease stability and circulation time when used to silence targeted genes in human and mice cells.[107,121] In addition, other studies showed that introducing 2′-*O*-Me into siRNA reduced the activation of innate immune responses, highlighting its role in minimizing off-target immune responses.[122,123] In contrast to the known impact of the 2′-*O*-Me modification, excessive incorporation of 2′-*O*-Me into siRNAs, specifically modifying every nucleotide, completely abolishes gene silencing activity in cell-based assays.[81,124]

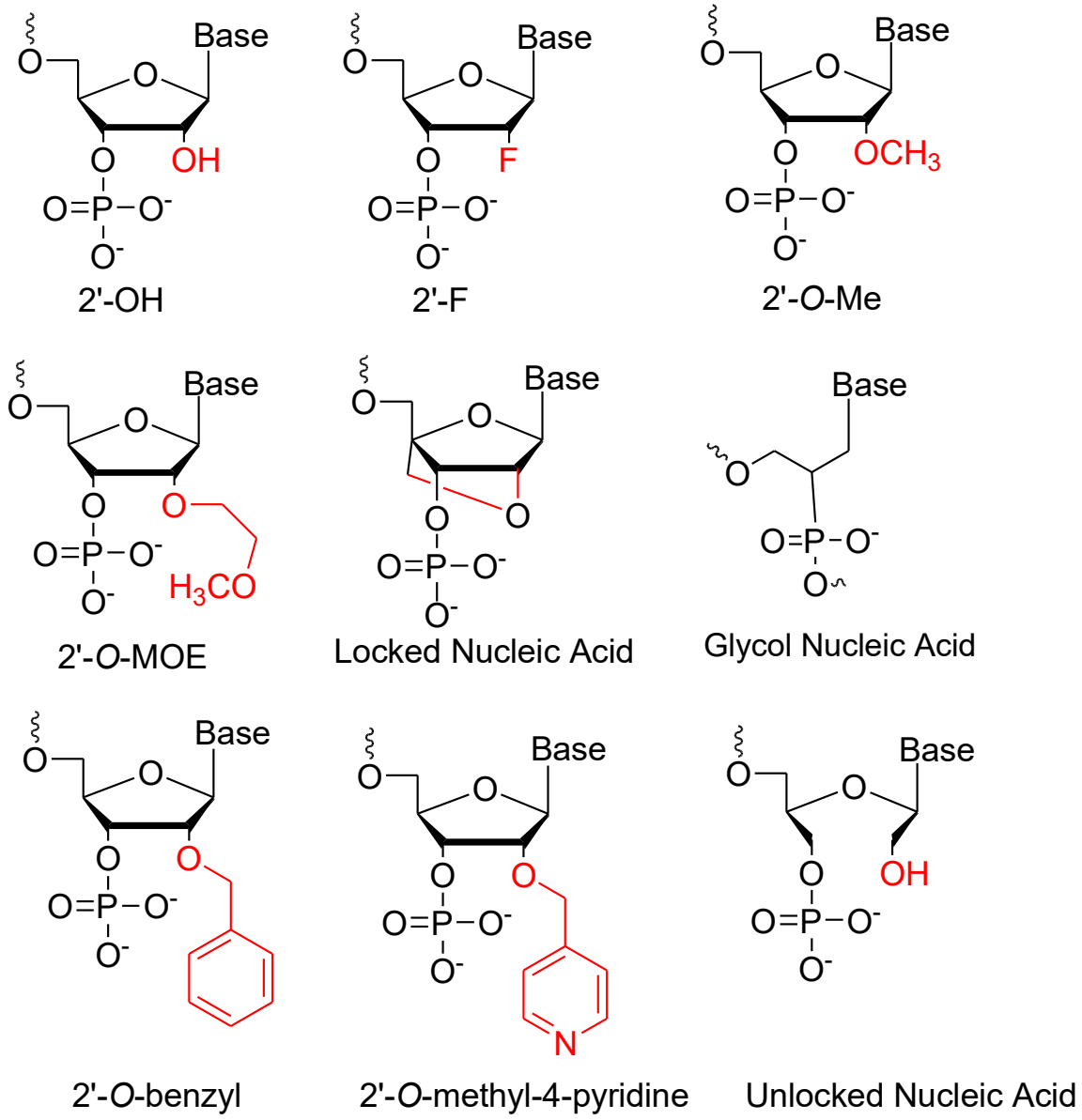

Figure 1.7: Examples of chemical modifications incorporated into ribose for potential use in siRNA-therapeutics.

The 2′-F modification has been widely investigated for its compatibility with siRNA function and its ability to enhance duplex stability.[125-128] Experimental studies demonstrate that incorporating 2′-F groups, particularly at pyrimidine positions, preserves siRNA silencing activity both *in vitro* and *in vivo*.[129,130] Additional studies have confirmed that siRNAs modified with 2′-F pyrimidines retain silencing efficiency *in vitro*,[131,132] with

similar efficacy *in vivo*.[95] Furthermore, combining 2′-F pyrimidines with 2′-*O*-Me purines yields RNA duplexes with enhanced nuclease resistance and longer half-life, leading to improved performance compared to unmodified siRNA *in vivo*.[133] UV melting analyses have also demonstrated that 2′-F modifications increase the thermal stability of RNA duplexes, as shown by higher melting temperatures in both fully and partially modified sequences.[127] Another previous study have reported successful crystallization of a fully 2′-F-modified RNA octamer duplex, and the crystallization of another octamer remained unsuccessful suggesting that extensive 2′-F substitution may impair the formation of high-quality, crystallizable helices.[127] Other chemical modifications like locked nucleic acid, 2′-*O*-methoxyethyl RNA, glycol nucleic acid etc., have also been tested for their enhanced thermal stability and nuclease resistance, meanwhile, they have not been incorporated into any FDA approved therapeutics yet.[83]

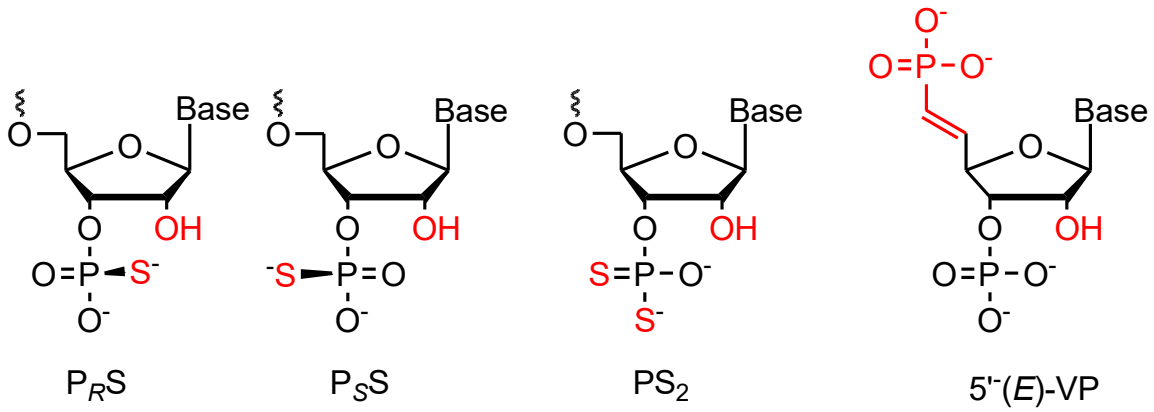

Figure 1.8: Examples of chemical modifications incorporated into the phosphate backbone for potential use in siRNA-therapeutics.

Substituting non-bridging oxygen in the phosphate of the siRNA backbone with sulfur, producing a PS linkage (Figure 1.8), enhances the stability of siRNA molecules.[106] This modification, originally introduced in 1967[134-136] by Eckstein and later expanded upon in their 2014 study,[137] has been experimentally demonstrated to protect siRNA from

nuclease degradation by promoting binding to carrier plasma both *in vitro* and *in vivo.* Another study found that systemically delivered PS-modified siRNA exhibited prolonged serum stability and resistance to enzymatic degradation, which translated to improved silencing efficacy in mice models.[138] However, another study revealed that when PS modifications are applied extensively across both strands of the siRNA duplex, RNAi efficiency can be impaired.[139] This study suggests that such modifications may interfere with strand separation or reduce affinity for argonaute proteins, thereby compromising the RISC assembly.[139] Using fluorescence microscopy and uptake assays, another experiment showed that PS-modified siRNA enters cells via clathrin-mediated endocytosis due to non-specific interactions with cell surface proteins, suggesting that PS modified oligonucleotides could enter cells without the aid of transfection agents, thereby enhancing cellular uptake of siRNA.[140]

Substitution of native nucleobases with chemically modified analogs (Figure 1.9) has been explored experimentally to enhance siRNA stability and modulate its biological properties.[103] Several analogs have been introduced, including pseudouridine, 2′-thiouridine, and dihydrouridine,[141,142] as well as synthetic bases like 5-nitroindole,[103,143] hypoxanthine,[144] 5-halouracil,[130] N-ethylpiperidine triazole-modified adenosine,[145,146] N^2alkyl-8-oxoguanine,[147,148] N^2-propyl/N2-cyclopentyl-2-aminopurines,[103] N^2-benzylguanine,[149] 2,6-diaminopurine,[130] and O^6-[2-(2-nitrophenyl)propyl]guanine.[150] These modifications have been shown to increase duplex thermal stability by enhancing hydrogen-bonding efficiency within base pairs. Notwithstanding these potential advantages, nucleobase modifications have not gained widespread application in therapeutic siRNA design. This could be because functional assays have demonstrated that extensive nucleobase substitutions interfere with effective RISC loading or target

recognition, leading to reduced gene silencing efficiency.[103]

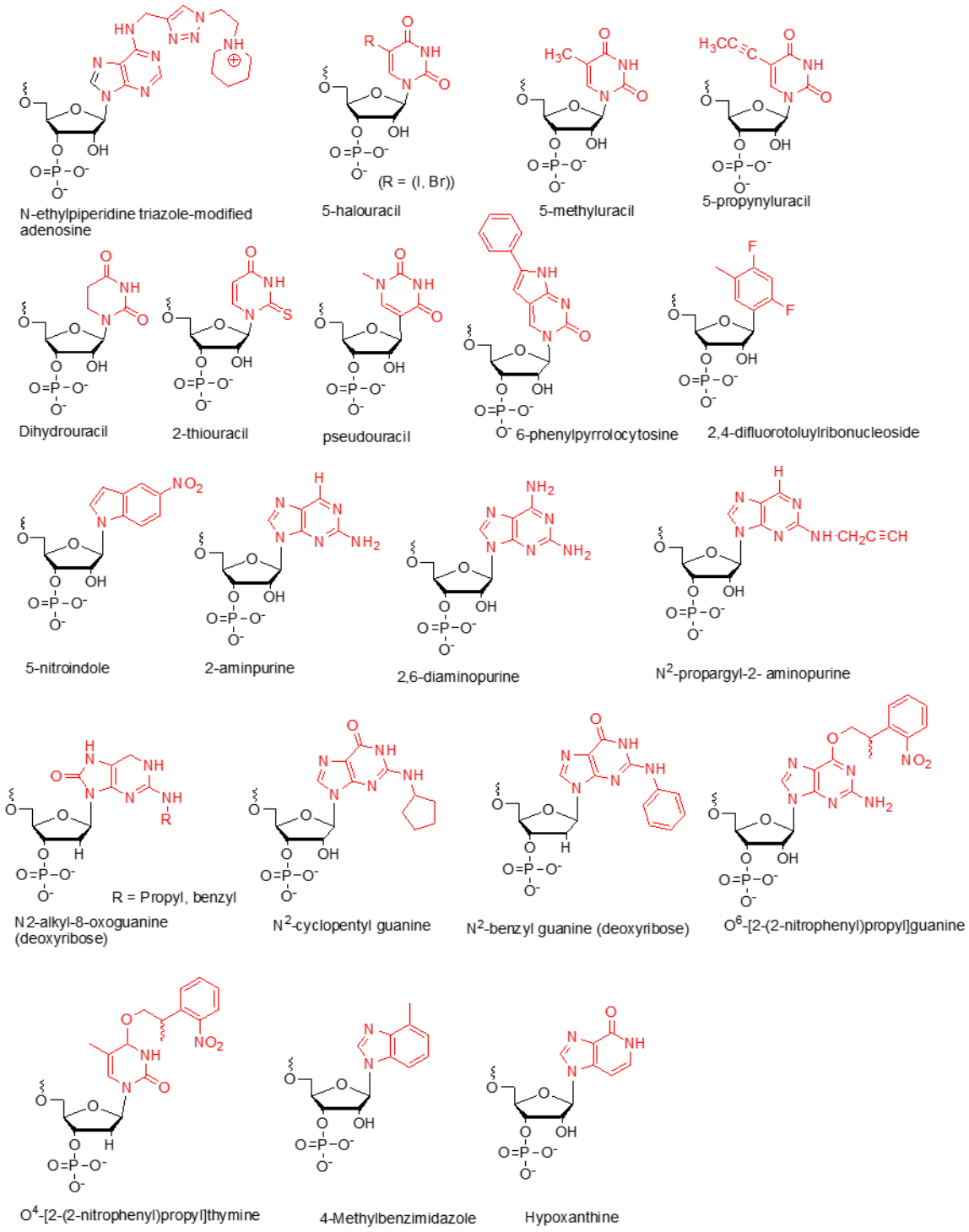

Figure 1.9: Examples of chemical modifications incorporated into a nucleobase for potential use in siRNA-therapeutics.

Despite significant advances in the field of siRNA therapeutics, several key gaps remain in our knowledge. In particular, structural insights into chemically modified siRNAs are limited. High-resolution atomic structures from X-ray crystallography and NMR have primarily focused on unmodified or minimally modified RNA duplex.[151,152] The crystal structure of the guide strand of siRNA in hAgo2 complex (PDB ID: 5JS2),[151] which contains alternating 2′-*O*-Me and 2′-F modifications, has been characterized to examine the binding mode and compatibility of the modifications with hAgo2. Nevertheless, fully-modified siRNA duplex, and fully-modified siRNA-hAgo2 complexes remain largely uncharacterized at atomic resolution. This scarcity of structural characterization impedes our ability to understand how these modifications alter duplex geometry and conformation. To the best of my knowledge, only one high-resolution X-ray crystallography structure exists for fully-modified siRNAs in complex with hAgo2,[151] making it difficult to assess how chemical changes affect siRNA recognition and dynamics within the RNAi machinery. While some studies have characterized modified siRNA interactions with hAgo2,[153,154] they do not include high-resolution crystal structures of such complexes. Finally, current experimental structural studies often provide only static snapshots, with limited information on the dynamic conformational behaviors of fully-modified siRNAs in solutions or in complex with proteins. These limitations underscore the need for computational approaches that can fill this gap in knowledge by providing atomic-level, time-resolved insight into the behavior of chemically-modified siRNAs. Computational chemistry offers a powerful framework to investigate how modifications affect siRNA structure, dynamics, and function. The next section provides an overview of computational strategies for modeling RNA structure and dynamics, laying the foundation for the methods applied in this thesis.

1.6 Overview of Computational Approaches for RNA Structure

Computational chemistry provides a robust mechanism for understanding molecular systems at an atomic level by simulating their behavior using the principles of quantum mechanics, classical mechanics, and statistical mechanics. Various computational techniques operate at different resolutions depending on the nature of the problem. Quantum mechanical (QM) methods, such as density functional theory (DFT) and Hartree-Fock theory, solve the Schrödinger equation and are used to study the electronic structure, reactivity, and energetics of molecules with high accuracy. Due to their computational intensity, these methods are typically applied to small molecules or localized regions of larger systems, such as enzymatic active sites, where detailed electronic information is most important. Molecular mechanics (MM) approaches used in molecular dynamics (MD) simulations apply classical mechanics techniques and empirical force fields to model the motions and interactions of large biomolecular systems over time, providing insights into conformational dynamics. These techniques are often integrated or used in multiscale modeling frameworks, enabling a comprehensive understanding of chemical and biological systems that is difficult to gain using more traditional experimental methods. MD simulations have evolved into an important and widely used computational tool that allows scientists to model the detailed microscopic dynamical behavior of many different types of systems.[155-158] By modelling the interactions between particles using classical mechanics, MD provides atomistic insights into the structural and dynamic behaviour of molecular systems, and thus serves as a practical and powerful alternative for investigating system properties such as conformational changes, protein folding, or binding based on the microscopic interactions and energetics that govern molecular behaviour.[32,159-161] These simulations have been pivotal in juxtaposing computational results with experimental

observations. Several advancements in MD methodologies have addressed limitations, including short time scales and inaccuracies in force fields,[162-164] leading to a remarkable agreement between computational predictions and experimental data.

Previous MD simulations have yielded in-depth analyses of structural intricacies, stability, sequence-dependent attributes, and functional characteristics of nucleic acids.[165] When combined with quantum mechanical (QM) approaches, MD simulations have successfully elucidated structure–function relationships in small-molecule therapeutics. For example, MD simulations and molecular orbital calculations revealed that, although both trifluorothymidine (FTD) and 5-fluorouracil can be incorporated into DNA, only FTD induces significant double-helix destabilization through enhanced dispersion and halogen-bonding interactions, particularly involving the trifluoromethyl group, thereby explaining its unique and potent anti-tumor effects.[166] MD simulations have further been used to understand the sequence-dependent structural behaviour of RNA structure and sensitivity to water and ion environments.[167-169] Advances in MD force fields have further improved the accurate representation of RNA conformational preferences.[32,165] Similarly, a combined DFT and MD simulations study analysed 33 sugar-modified uridine and cytidine nucleotides, revealing that sugar puckering influences Watson–Crick base pair stability, south-type sugars strengthen C:G and weaken U:A interactions, while most modifications minimally affect base stacking, except for glycol nucleic acids, which significantly disrupt stacking.[10]

While previous computational studies have advanced our understanding of modified RNA structural dynamics, most of the studies focused on unmodified or partially-modified RNA duplexes, on individual modifications in isolation, and modifications on nucleotides. There remains a substantial gap in our understanding how

fully-modified siRNA duplexes, especially those incorporating 2'-*O*-Me and 2'-F modifications in the FDA-approved drugs, affect RNA structure and dynamics. This thesis aims to address this gap by applying MD simulations to investigate the structural and dynamics implications of full chemical modifications in siRNA duplexes.

In addition to characterizing the structural properties of siRNA duplexes, it is equally important to investigate their interactions with key biological partners, most especially, hAgo2, which plays a central role in RNAi. There are relatively few computational studies focusing on the siRNA–hAgo2 complex. One study performed a single 1 μs MD simulation of hAgo2 complexes with guide strands, using bacteria argonaute structure as template to model hAgo2.[12] The study investigated the effects of individual chemical modifications such as 2′-*O*-Me, 2′-*O*-Benzyl, and 2′-*O*-methoxyethyl (2′-*O*-MOE) at guide strand positions 2, 3, 5, and 14, based on the hypothesis that these positions influence RNAi activity.[12] The computational analysis focused on how these modifications affect binding interactions and the conformational dynamics of the complex.[12] Building on this, another study combined molecular docking and a single 1 μs MD simulation to explore RNAi-based therapeutic strategies against SARS-CoV-2, using the above model without incorporating chemical modifications in the siRNA strands.[170] Additionally, 25 ns MD simulations have been used to examine seven unmodified siRNAs targeting tdp43 mutants in complex with hAgo2, observing notable conformational switching between "open" (the MID and PAZ domains move away from each other, while the PAZ and N-terminal domains come closer) and "closed" (PAZ domain moves closer to the MID domain) states, with high flexibility in the PAZ domain that anchors the 3′ end of the siRNA guide strand.[171] In addition to the lack of replica simulations in these studies, there is no computational study on a full chemically-modified or FDA-approved siRNA in

complex with hAgo2. The existing computational studies have only examined individual chemical modifications such as 2′-*O*-Me, 2′-F, or PS. Consequently, there exists a knowledge gap in the understanding of the structural impact of diverse ribose modifications on the interactions with hAgo2, including potential synergistic or antagonistic effects among binary modification patterns in the same siRNA duplex as seen in the FDA-approved siRNA therapeutics. Therefore, in addition to examining RNA duplexes, this thesis aims to address this gap by applying MD simulations to investigate how chemical modifications in siRNA duplexes influence the interactions with hAgo2.

1.7 Thesis Objectives

This thesis uses computational methods to investigate how full and diverse chemical modification patterns influence the structural properties of siRNAs and their interactions with hAgo2. Emphasis is placed on the modification patterns present in the first five FDA-approved siRNA therapeutics. Using long-timescale MD simulations, I will explore how differential sequence and modification patterns influence the siRNA duplex conformation, dynamics, and recognition by the key components of hAgo2. By systematically analyzing fully-modified siRNAs in isolation and in complex with hAgo2 at an atomic resolution, this work contributes to the broader literature by providing insights that are currently lacking due to the scarcity of high-resolution structural data.

In Chapter 2, I will investigate the structural properties of the duplexes of the first five FDA-approved siRNA therapeutics namely Patisiran, Givosiran, Lumasiran, Inclisiran, and Vutrisiran. Based on published sequences, I will model each drug in the original chemically-modified form, as well as generate corresponding canonical RNA, canonical DNA, full 2′-fluorinated, and full 2′-*O*-methylated analogs. These siRNA

duplexes will be subjected to long-timescale all-atom MD simulations in explicit solvent to capture their structural dynamics under physiological conditions. Given that the structural integrity of siRNA is critical for RNAi activity, [129, 130] my detailed analyses will evaluate the impact of chemical modifications on the local and global siRNA conformations, including the backbone geometry, sugar puckering, and overall helical structure.

In Chapter 3, I will investigate the siRNA–hAgo2 complexes. I will use one sequence examined for the duplex study namely, Givosiran, which is the first siRNA drug with full and diverse chemical modifications to be approved by FDA. This will involve constructing the modified siRNA-guide strand complexes and simulating their interactions with hAgo2 to assess how specific chemical modifications influence binding interactions and conformational dynamics within the RISC. This analysis will provide insight into how chemical modifications modulate siRNA–hAgo2 interactions critical for RNAi activity, complementing the duplex-level investigations in Chapter 2.

Finally, Chapter 4 presents the major conclusions drawn from this work and outlines potential directions for future research in this field. Collectively, this thesis addresses critical gaps in the understanding of the structural and dynamic of chemically-modified siRNA duplexes, with a particular emphasis on FDA-approved siRNA therapeutics. The findings are expected to inform rational design principles for next-generation siRNA therapeutics.

1.8 References

(1) Chavda, V. P.; Soni, S.; Vora, L. K.; Soni, S.; Khadela, A.; Ajabiya, J. mRNA-Based Vaccines and Therapeutics for COVID-19 and Future Pandemics. *Vaccines* **2022**, *10* (12), 2150.
(2) Liu, A.; Wang, X. The Pivotal Role of Chemical Modifications in mRNA Therapeutics. *Front. cell dev. biol* **2022**, *Volume 10 - 2022*, Review.

(3) Elkhalifa, D.; Rayan, M.; Negmeldin, A. T.; Elhissi, A.; Khalil, A. Chemically modified mRNA beyond COVID-19: Potential preventive and therapeutic applications for targeting chronic diseases. *Biomed. Pharmacother.* **2022**, *145*, 112385.
(4) Warminski, M.; Mamot, A.; Depaix, A.; Kowalska, J.; Jemielity, J. Chemical Modifications of mRNA Ends for Therapeutic Applications. *Acc. Chem. Res.* **2023**, *56* (20), 2814-2826.
(5) Rohner, E.; Yang, R.; Foo, K. S.; Goedel, A.; Chien, K. R. Unlocking the promise of mRNA therapeutics. *Nat. Biotechnol.* **2022**, *40* (11), 1586-1600.
(6) Setten, R. L.; Rossi, J. J.; Han, S.-p. The current state and future directions of RNAi-based therapeutics. *Nat. Rev. Drug Discov.* **2019**, *18* (6), 421-446.
(7) Zhang, M. M.; Bahal, R.; Rasmussen, T. P.; Manautou, J. E.; Zhong, X. B. The growth of siRNA-based therapeutics: Updated clinical studies. *Biochem. Pharmacol.* **2021**, *189*, 114432.
(8) Bennett, C. F. Therapeutic Antisense Oligonucleotides Are Coming of Age. *Annu. Rev. Med.* **2019**, *70*, 307-321.
(9) Hu, B.; Zhong, L.; Weng, Y.; Peng, L.; Huang, Y.; Zhao, Y.; Liang, X. J. Therapeutic siRNA: state of the art. *Signal Transduct. Target. Ther.* **2020**, *5* (1), 101.
(10) Das, G.; Harikrishna, S.; Gore, K. R. Investigating the Effect of Chemical Modifications on the Ribose Sugar Conformation, Watson-Crick Base Pairing, and Intrastrand Stacking Interactions: A Theoretical Approach. *J. Phys. Chem. B* **2024**, *128* (35), 8313-8331.
(11) Das, G.; Harikrishna, S.; Gore, K. R. Influence of Sugar Modifications on the Nucleoside Conformation and Oligonucleotide Stability: A Critical Review. *Chem. Rec.* **2022**, *22* (12), e202200174.
(12) Harikrishna, S.; Pradeepkumar, P. I. Probing the Binding Interactions between Chemically Modified siRNAs and Human Argonaute 2 Using Microsecond Molecular Dynamics Simulations. *J. Chem. Inf. Model.* **2017**, *57* (4), 883-896.
(13) Sim, A. Y.; Minary, P.; Levitt, M. Modeling nucleic acids. *Curr. Opin. Struct. Biol.* **2012**, *22* (3), 273-278.
(14) Minchin, S.; Lodge, J. Understanding biochemistry: structure and function of nucleic acids. *Essays Biochem.* **2019**, *63* (4), 433-456.
(15) Pauling, L.; Corey, R. B. A Proposed Structure For The Nucleic Acids. *PNAS* **1953**, *39* (2), 84-97.
(16) Crick, F. Central Dogma of Molecular Biology. *Nat.* **1970**, *227* (5258), 561-563.
(17) Sharp, S. J.; Jerone, S.; Lyan, C.; Johnson, B. D.; and Soil, D. Structure and Transcription of Eukaryotic tRNA Gene. *Crit. Rev. Biochem* **1985**, *19* (2), 107-144.
(18) Pereira, M. J. B. H., D. A.; Rueda, D.; Walter, N. G. Reaction pathway of the trans-acting hepatitis delta virus ribozyme: a conformational change accompanies catalysis. *Biochemistry* **2002**, *41*, 730−740.
(19) Schmitt, A. M.; Chang, H. Y. Long Noncoding RNAs in Cancer Pathways. *Cancer Cell.* **2016**, *29* (4), 452-463.
(20) Djebali, S.; Davis, C. A.; Merkel, A.; Dobin, A.; Lassmann, T.; Mortazavi, A.; Tanzer, A.; Lagarde, J.; Lin, W.; Schlesinger, F.; et al. Landscape of transcription in human cells. *Nat.* **2012**, *489* (7414), 101-108.
(21) Guttman, M.; Amit, I.; Garber, M.; French, C.; Lin, M. F.; Feldser, D.; Huarte, M.; Zuk, O.; Carey, B. W.; Cassady, J. P.; et al. Chromatin signature reveals over a thousand highly conserved large non-coding RNAs in mammals. *Nat.* **2009**, *458* (7235), 223-227.

(22) Pitchiaya, S.; Heinicke, L. A.; Custer, T. C.; Walter, N. G. Single molecule fluorescence approaches shed light on intracellular RNAs. *Chem Rev* **2014**, *114* (6), 3224-3265.
(23) Diederichs, S.; Bartsch, L.; Berkmann, J. C.; Frose, K.; Heitmann, J.; Hoppe, C.; Iggena, D.; Jazmati, D.; Karschnia, P.; Linsenmeier, M.; et al. The dark matter of the cancer genome: aberrations in regulatory elements, untranslated regions, splice sites, non-coding RNA and synonymous mutations. *EMBO Mol. Med.* **2016**, *8* (5), 442-457.
(24) Belinky, F.; Bahir, I.; Stelzer, G.; Zimmerman, S.; Rosen, N.; Nativ, N.; Dalah, I.; Iny Stein, T.; Rappaport, N.; Mituyama, T.; et al. Non-redundant compendium of human ncRNA genes in GeneCards. *Bioinformatics* **2013**, *29* (2), 255-261.
(25) Wilson, R. C.; Doudna, J. A. Molecular mechanisms of RNA interference. *Annu. Rev. Biophys.* **2013**, *42*, 217-239.
(26) Ghildiyal, M.; Seitz, H.; Horwich, M. D.; Li, C.; Du, T.; Lee, S.; Xu, J.; Kittler, E. L. W.; Zapp, M. L.; Weng, Z.; Zamore, P. D. Endogenous siRNAs Derived from Transposons and mRNAs in Drosophila Somatic Cells. *Science* **2008**, *320* (5879), 1077-1081.
(27) Tomari, Y.; Zamore, P. D. Perspective: machines for RNAi. *Genes Dev.* **2005**, *19* (5), 517-529.
(28) Hannon, G. J. RNA interference. *Nat.* **2002**, *418* (6894), 244-251.
(29) Kim, D.; Rossi, J. RNAi mechanisms and applications. *Biotechniques* **2008**, *44* (5), 613-616.
(30) Zamore, P. D.; Tuschl, T.; Sharp, P. A.; Bartel, D. P. RNAi: double-stranded RNA directs the ATP-dependent cleavage of mRNA at 21 to 23 nucleotide intervals. *Cell* **2000**, *101* (1), 25-33.
(31) Hannon, G. J.; Rossi, J. J. Unlocking the potential of the human genome with RNA interference. *Nat.* **2004**, *431* (7006), 371-378.
(32) Sponer, J.; Bussi, G.; Krepl, M.; Banas, P.; Bottaro, S.; Cunha, R. A.; Gil-Ley, A.; Pinamonti, G.; Poblete, S.; Jurecka, P.; et al. RNA Structural Dynamics As Captured by Molecular Simulations: A Comprehensive Overview. *Chem. Rev.* **2018**, *118* (8), 4177-4338.
(33) Saenger, W. *Principles of Nucleic Acid Structure*; Springer New York, 2013.
(34) Liu, B.; Baskin, R. J.; Kowalczykowski, S. C. DNA unwinding heterogeneity by RecBCD results from static molecules able to equilibrate. *Nat.* **2013**, *500* (7463), 482-485.
(35) Eschenmoser, A. Chemical Etiology of Nucleic Acid Structure. *Science* **1999**, *284* (5423), 2118-2124.
(36) Crick, F. H. Linking numbers and nucleosomes. *PNAS* **1976**, *73* (8), 2639-2643.
(37) Wilkins, M. H. F.; Stokes, A. R.; Wilson, H. R. Molecular Structure of Nucleic Acids: Molecular Structure of Deoxypentose Nucleic Acids. *Nat.* **1953**, *171* (4356), 738-740.
(38) Furberg, S., Jensen, M. B., & Faurholt, C. <on the structure of nucleic acid.pdf>. *Acta Chem. Scand.* **1952**, *6*, 634–640.
(39) Vesley, P. Molecular biology of the cell: A problems approach, 4th edition. By John Wilson and Tim Hunt, Pavel Vesely, Garland Sciences, New York, 2002, ISBN0-8153–3577–6; paperback; 550 pages; $35.95. *Scanning* **2004**, *26* (4), 206-206.
(40) Levitt, M. How many base-pairs per turn does DNA have in solution and in chromatin? Some theoretical calculations. *PNAS* **1978**, *75* (2), 640-644.
(41) Parsons, M. F.; Allan, M. F.; Li, S.; Shepherd, T. R.; Ratanalert, S.; Zhang, K.; Pullen, K. M.; Chiu, W.; Rouskin, S.; Bathe, M. 3D RNA-scaffolded wireframe origami. *Nat. Commun.* **2023**, *14* (1), 382.

(42) Rebek, J., Jr.; Askew, B.; Ballester, P.; Buhr, C.; Jones, S.; Nemeth, D.; Williams, K. Molecular recognition: hydrogen bonding and stacking interactions stabilize a model for nucleic acid structure. *J. Am. Chem. Soc.* **1987**, *109* (16), 5033-5035.
(43) Ku, S. H.; Jo, S. D.; Lee, Y. K.; Kim, K.; Kim, S. H. Chemical and structural modifications of RNAi therapeutics. *Adv. Drug Deliv. Rev.* **2016**, *104*, 16-28.
(44) Stombaugh, J.; Zirbel, C. L.; Westhof, E.; Leontis, N. B. Frequency and isostericity of RNA base pairs. *Nucleic Acids Res.* **2009**, *37* (7), 2294-2312.
(45) Leontis, N. B.; Westhof, E. Geometric nomenclature and classification of RNA base pairs. *RNA.* **2001**, *7* (4), 499-512.
(46) Leontis, N. B.; Stombaugh, J.; Westhof, E. The non-Watson–Crick base pairs and their associated isostericity matrices. *Nucleic Acids Res.* **2002**, *30* (16), 3497-3531.
(47) Šponer, J.; Šponer, J. E.; Petrov, A. I.; Leontis, N. B. Quantum Chemical Studies of Nucleic Acids: Can We Construct a Bridge to the RNA Structural Biology and Bioinformatics Communities? *J. Phys. Chem. B.* **2010**, *114* (48), 15723-15741.
(48) Liu, W. W.; Zheng, S. Q.; Li, T.; Fei, Y. F.; Wang, C.; Zhang, S.; Wang, F.; Jiang, G. M.; Wang, H. RNA modifications in cellular metabolism: implications for metabolism-targeted therapy and immunotherapy. *Signal Transduct. Target. Ther.* **2024**, *9* (1), 70.
(49) Moore, L. D.; Le, T.; Fan, G. DNA methylation and its basic function. *Neuropsychopharmacol.* **2013**, *38* (1), 23-38.
(50) Cappannini, A.; Ray, A.; Purta, E.; Mukherjee, S.; Boccaletto, P.; Moafinejad, S. N.; Lechner, A.; Barchet, C.; Klaholz, B. P.; Stefaniak, F.; Bujnicki, J. M. MODOMICS: a database of RNA modifications and related information. 2023 update. *Nucleic Acids Res.* **2024**, *52* (D1), D239-D244.
(51) Zhang, K.; Zhuang, X.; Dong, Z.; Xu, K.; Chen, X.; Liu, F.; He, Z. The dynamics of N(6)-methyladenine RNA modification in interactions between rice and plant viruses. *Genome Biol* **2021**, *22* (1), 189.
(52) Liu, Z.; Gao, L.; Cheng, L.; Lv, G.; Sun, B.; Wang, G.; Tang, Q. The roles of N6-methyladenosine and its target regulatory noncoding RNAs in tumors: classification, mechanisms, and potential therapeutic implications. *Exp. Mol. Med.* **2023**, *55* (3), 487-501.
(53) Xiao, C.-L.; Zhu, S.; He, M.; Chen, D.; Zhang, Q.; Chen, Y.; Yu, G.; Liu, J.; Xie, S.-Q.; Luo, F.; et al. N6-Methyladenine DNA Modification in the Human Genome. *Mol. Cell* **2018**, *71* (2), 306-318.e307.
(54) Desrosiers, R.; Friderici, K.; Rottman, F. Identification of Methylated Nucleosides in Messenger RNA from Novikoff Hepatoma Cells. *PNAS* **1974**, *71* (10), 3971-3975.
(55) Jia, G.; Fu, Y.; Zhao, X.; Dai, Q.; Zheng, G.; Yang, Y.; Yi, C.; Lindahl, T.; Pan, T.; Yang, Y.-G.; He, C. N6-Methyladenosine in nuclear RNA is a major substrate of the obesity-associated FTO. *Nat. Chem. Biol.* **2011**, *7* (12), 885-887.
(56) Dunn, D. B. The occurence of 1-methyladenine in ribonucleic acid. *Biochim. Biophys. Acta* **1961**, *46* (1), 198-200.
(57) Foo, M.; Frietze, L. R.; Enghiad, B.; Yuan, Y.; Katanski, C. D.; Zhao, H.; Pan, T. Prokaryotic RNA N1-Methyladenosine Erasers Maintain tRNA m1A Modification Levels in Streptomyces venezuelae. *ACS Chem. Biol.* **2024**, *19* (7), 1616-1625.
(58) Xiong, W.; Zhao, Y.; Wei, Z.; Li, C.; Zhao, R.; Ge, J.; Shi, B. N1-methyladenosine formation, gene regulation, biological functions, and clinical relevance. *Mol. Ther.* **2023**, *31* (2), 308-330.

(59) Wang, Y.; Wang, J.; Li, X.; Xiong, X.; Wang, J.; Zhou, Z.; Zhu, X.; Gu, Y.; Dominissini, D.; He, L.; et al. N(1)-methyladenosine methylation in tRNA drives liver tumourigenesis by regulating cholesterol metabolism. *Nat. Commun.* **2021**, *12* (1), 6314.
(60) Cui, L.; Ma, R.; Cai, J.; Guo, C.; Chen, Z.; Yao, L.; Wang, Y.; Fan, R.; Wang, X.; Shi, Y. RNA modifications: importance in immune cell biology and related diseases. *Signal Transduct. Target. Ther.* **2022**, *7* (1), 334.
(61) Breiling, A.; Lyko, F. Epigenetic regulatory functions of DNA modifications: 5-methylcytosine and beyond. *Epigenetics Chromatin* **2015**, *8* (1), 24.
(62) Ehrlich, M.; Gama-Sosa, M. A.; Huang, L.-H.; Midgett, R. M.; Kuo, K. C.; McCune, R. A.; Gehrke, C. Amount and distribution of 5-methylcytosine in human DNA from different types of tissues or cells. *Nucleic Acids Res.* **1982**, *10* (8), 2709-2721.
(63) Wang, T.; Fowler, J. M.; Liu, L.; Loo, C. E.; Luo, M.; Schutsky, E. K.; Berríos, K. N.; DeNizio, J. E.; Dvorak, A.; Downey, N.; et al. Direct enzymatic sequencing of 5-methylcytosine at single-base resolution. *Nat. Chem. Biol.* **2023**, *19* (8), 1004-1012.
(64) Morais, P.; Adachi, H.; Yu, Y.-T. The Critical Contribution of Pseudouridine to mRNA COVID-19 Vaccines. *Front. cell dev. biol* **2021**, *9*, Mini Review.
(65) Spenkuch, F.; Yuri, M.; and Helm, M. Pseudouridine: Still mysterious, but never a fake (uridine)! *RNA Biol.* **2014**, *11* (12), 1540-1554.
(66) Herridge, R. P.; Dolata, J.; Migliori, V.; de Santis Alves, C.; Borges, F.; Schorn, A. J.; van Ex, F.; Lin, A.; Bajczyk, M.; Parent, J. S.; et al. Pseudouridine guides germline small RNA transport and epigenetic inheritance. *Nat. Struct. Mol. Biol* **2025**, *32* (2), 277-286.
(67) Carlile, T. M.; Rojas-Duran, M. F.; Zinshteyn, B.; Shin, H.; Bartoli, K. M.; Gilbert, W. V. Pseudouridine profiling reveals regulated mRNA pseudouridylation in yeast and human cells. *Nat.* **2014**, *515* (7525), 143-146.
(68) Cerneckis, J.; Cui, Q.; He, C.; Yi, C.; Shi, Y. Decoding pseudouridine: an emerging target for therapeutic development. *Trends Pharmacol. Sci.* **2022**, *43* (6), 522-535.
(69) Hu, T.; Liu, C. H.; Lei, M.; Zeng, Q.; Li, L.; Tang, H.; Zhang, N. Metabolic regulation of the immune system in health and diseases: mechanisms and interventions. *Signal Transduct. Target. Ther.* **2024**, *9* (1), 268.
(70) Zhang, Y.; Hu, W.; Li, H. B. RNA modification-mediated translational control in immune cells. *RNA Biol.* **2023**, *20* (1), 603-613.
(71) Han, X.; Wang, L.; Han, Q. Advances in the role of m(6)A RNA modification in cancer metabolic reprogramming. *Cell biosci.* **2020**, *10*, 117.
(72) He, J.; Liu, F.; Zhang, Z. Functions of N6-methyladenosine in cancer metabolism: from mechanism to targeted therapy. *Biomark. Res.* **2023**, *11* (1), 40.
(73) Xi, J. F.; Liu, B. D.; Tang, G. R.; Ren, Z. H.; Chen, H. X.; Lan, Y. L.; Yin, F.; Li, Z.; Cheng, W. S.; Wang, J.; et al. m(6)A modification regulates cell proliferation via reprogramming the balance between glycolysis and pentose phosphate pathway. *Commun. Biol.* **2025**, *8* (1), 496.
(74) Ali, A. T.; Idaghdour, Y.; Hodgkinson, A. Analysis of mitochondrial m1A/G RNA modification reveals links to nuclear genetic variants and associated disease processes. *Commun. Biol.* **2020**, *3* (1), 147.
(75) Qiu, L.; Jing, Q.; Li, Y.; Han, J. RNA modification: mechanisms and therapeutic targets. *Mol. Biomed.* **2023**, *4* (1), 25.
(76) Yin, L.; Zhu, X.; Novák, P.; Zhou, L.; Gao, L.; Yang, M.; Zhao, G.; Yin, K. The epitranscriptome of long noncoding RNAs in metabolic diseases. *Clin. Chim. Acta* **2021**, *515*, 80-89.

(77) Zheng, L.; Duan, Y.; Li, M.; Wei, J.; Xue, C.; Chen, S.; Wei, Q.; Tang, F.; Xiong, W.; Zhou, M.; Deng, H. Deciphering the vital roles and mechanism of m5C modification on RNA in cancers. *Am. J. Cancer Res.* **2023**, *13* (12), 6125-6146.
(78) Kang, H.; Ga, Y. J.; Kim, S. H.; Cho, Y. H.; Kim, J. W.; Kim, C.; Yeh, J.-Y. Small interfering RNA (siRNA)-based therapeutic applications against viruses: principles, potential, and challenges. *J. Biomed. Sci.* **2023**, *30* (1), 88.
(79) Feng, G.; Wu, Y.; Hu, Y.; Shuai, W.; Yang, X.; Li, Y.; Ouyang, L.; Wang, G. Small molecule inhibitors targeting m6A regulators. *J. Hematol. Oncol.* **2024**, *17* (1), 30.
(80) Fire, A., Xu, SiQun, Montgomery, Mary K., Kostas, Steven A., Driver, Samuel E., Mello, Craig C. Potent and specific genetic interference by double-stranded RNA in Caenorhabditis elegans. *Nat.* **1998**, *391* (6669), 806-811.
(81) Czauderna, F.; Fechtner, M.; Dames, S.; Aygun, H.; Klippel, A.; Pronk, G. J.; Giese, K.; Kaufmann, J. Structural variations and stabilising modifications of synthetic siRNAs in mammalian cells. *Nucleic Acids Res.* **2003**, *31* (11), 2705-2716.
(82) Napoli, C.; Lemieux, C.; Jorgensen, R. Introduction of a Chimeric Chalcone Synthase Gene into Petunia Results in Reversible Co-Suppression of Homologous Genes in trans. *The Plant Cell.* **1990**, *2* (4), 279-289.
(83) Behlke, M. A. Chemical modification of siRNAs for in vivo use. *Oligonucleotides* **2008**, *18* (4), 305-319.
(84) Elbashir, S. M.; Lendeckel, W.; Tuschl, T. RNA interference is mediated by 21- and 22-nucleotide RNAs. *Genes Dev.* **2001**, *15* (2), 188-200.
(85) Dykxhoorn, D. M.; Novina, C. D.; Sharp, P. A. Killing the messenger: short RNAs that silence gene expression. *Nat. Rev. Mol. Cell Biol.* **2003**, *4* (6), 457-467.
(86) Elbashir, S., Harborth, J., Lendeckel, W., Yalcin, A., Weber, K., Tuschl, T. Duplexes of 21-nucleotide RNAs mediate RNA interference in cultured mammalian cells. *Nat.* **2001**, *411* (6836), 494-498.
(87) Ketting, R. F.; Fischer, S. E.; Bernstein, E.; Sijen, T.; Hannon, G. J.; Plasterk, R. H. Dicer functions in RNA interference and in synthesis of small RNA involved in developmental timing in C. elegans. *Genes Dev.* **2001**, *15* (20), 2654-2659.
(88) Quinteros, D. A.; Bermúdez, J. M.; Ravetti, S.; Cid, A.; Allemandi, D. A.; Palma, S. D. Chapter 25 - Therapeutic use of monoclonal antibodies: general aspects and challenges for drug delivery. In *Nanostructures for Drug Delivery*, Andronescu, E., Grumezescu, A. M. Eds.; Elsevier, 2017; pp 807-833.
(89) Tang, Q.; Khvorova, A. RNAi-based drug design: considerations and future directions. *Nat. Rev. Drug Discov.* **2024**, *23* (5), 341-364.
(90) Yu, A.-M.; Choi, Y. H.; Tu, M.-J. RNA Drugs and RNA Targets for Small Molecules: Principles, Progress, and Challenges. *Pharmacol. Rev.* **2020**, *72* (4), 862-898.
(91) Lundin, K. E.; Gissberg, O.; Smith, C. I. Oligonucleotide Therapies: The Past and the Present. *Hum. Gene. Ther.* **2015**, *26* (8), 475-485.
(92) Un Jan Contreras, S.; Redfern, L. K.; Maguire, L. W.; Promi, S. I.; Gardner, C. M. Small Interfering RNAs (siRNAs) Negatively Impact Growth and Gene Expression of Environmentally Relevant Bacteria in In Vitro Conditions. *Environ. Sci. Technol.* **2024**, *58* (31), 13856-13865.
(93) Sajid, M. I.; Moazzam, M.; Kato, S.; Yeseom Cho, K.; Tiwari, R. K. Overcoming Barriers for siRNA Therapeutics: From Bench to Bedside. *Pharmaceuticals* **2020**, *13* (10), 294.

(94) Hickerson, R. P.; Vlassov, A. V.; Wang, Q.; Leake, D.; Ilves, H.; Gonzalez-Gonzalez, E.; Contag, C. H.; Johnston, B. H.; Kaspar, R. L. Stability Study of Unmodified siRNA and Relevance to Clinical Use. *Oligonucleotides* **2008**, *18* (4), 345-354.
(95) Layzer, J. M.; McCaffrey, A. P.; Tanner, A. K.; Huang, Z.; Kay, M. A.; Sullenger, B. A. In vivo activity of nuclease-resistant siRNAs. *RNA.* **2004**, *10* (5), 766-771.
(96) Naeem, S.; Zhang, J.; Zhang, Y.; Wang, Y. Nucleic acid therapeutics: Past, present, and future. *Mol. Ther. Nucleic Acids* **2025**, *36* (1), 102440.
(97) Ali Zaidi, S. S.; Fatima, F.; Ali Zaidi, S. A.; Zhou, D.; Deng, W.; Liu, S. Engineering siRNA therapeutics: challenges and strategies. *J. Nanobiotechnology* **2023**, *21* (1), 381.
(98) Dowdy, S. F. Overcoming cellular barriers for RNA therapeutics. *Nat. Biotechnol.* **2017**, *35* (3), 222-229.
(99) Idres, Y. M.; Idris, A.; Gao, W. Preclinical testing of antiviral siRNA therapeutics delivered in lipid nanoparticles in animal models - a comprehensive review. *Drug Deliv. Transl. Res* **2025**.
(100) Crooke, S. T.; Witztum, J. L.; Bennett, C. F.; Baker, B. F. RNA-Targeted Therapeutics. *Cell Metab.* **2018**, *27* (4), 714-739.
(101) Nair, J. K.; Attarwala, H.; Sehgal, A.; Wang, Q.; Aluri, K.; Zhang, X.; Gao, M.; Liu, J.; Indrakanti, R.; Schofield, S.; et al. Impact of enhanced metabolic stability on pharmacokinetics and pharmacodynamics of GalNAc–siRNA conjugates. *Nucleic Acids Res.* **2017**, *45* (19), 10969-10977.
(102) Janas, M. M.; Schlegel, M. K.; Harbison, C. E.; Yilmaz, V. O.; Jiang, Y.; Parmar, R.; Zlatev, I.; Castoreno, A.; Xu, H.; Shulga-Morskaya, S.; et al. Selection of GalNAc-conjugated siRNAs with limited off-target-driven rat hepatotoxicity. *Nat. Commun.* **2018**, *9* (1), 723.
(103) Peacock, H.; Kannan, A.; Beal, P. A.; Burrows, C. J. Chemical modification of siRNA bases to probe and enhance RNA interference. *J. Org. Chem.* **2011**, *76* (18), 7295-7300.
(104) Deleavey, G. F.; Damha, M. J. Designing chemically modified oligonucleotides for targeted gene silencing. *Chem. Biol.* **2012**, *19* (8), 937-954.
(105) Manoharan, M. RNA interference and chemically modified small interfering RNAs. *Curr. Opin. Chem. Biol.* **2004**, *8* (6), 570-579.
(106) Chernikov, I. V.; Vlassov, V. V.; Chernolovskaya, E. L. Current Development of siRNA Bioconjugates: From Research to the Clinic. *Front. Pharmacol.* **2019**, *10*, 444.
(107) Chernikov, I. V.; Gladkikh, D. V.; Meschaninova, M. I.; Ven'yaminova, A. G.; Zenkova, M. A.; Vlassov, V. V.; Chernolovskaya, E. L. Cholesterol-Containing Nuclease-Resistant siRNA Accumulates in Tumors in a Carrier-free Mode and Silences MDR1 Gene. *Mol. Ther. Nucleic Acids* **2017**, *6*, 209-220.
(108) Zhang, X.; Goel, V.; Robbie, G. J. Pharmacokinetics of Patisiran, the First Approved RNA Interference Therapy in Patients With Hereditary Transthyretin-Mediated Amyloidosis. *J. Clin. Pharmacol.* **2020**, *60* (5), 573-585.
(109) Scott, L. J. Givosiran: First Approval. *Drugs* **2020**, *80* (3), 335-339.
(110) Garrelfs Sander, F.; Frishberg, Y.; Hulton Sally, A.; Koren Michael, J.; O'Riordan William, D.; Cochat, P.; Deschênes, G.; Shasha-Lavsky, H.; Saland Jeffrey, M.; van't Hoff William, G.; et al. Lumasiran, an RNAi Therapeutic for Primary Hyperoxaluria Type 1. *N. Engl. J. Med.* **2021**, *384* (13), 1216-1226.
(111) Scott, L. J.; Keam, S. J. Lumasiran: First Approval. *Drugs* **2021**, *81* (2), 277-282.
(112) Mullard, A. 2022 FDA approvals. *Nat. Rev. Drug Discov.* **2023**, *22* (2), 83-88.

(113) Gangopadhyay, S.; Gore, K. R. Advances in siRNA therapeutics and synergistic effect on siRNA activity using emerging dual ribose modifications. *RNA Biol.* **2022**, *19* (1), 452-467.
(114) Egli, M.; Manoharan, M. Re-Engineering RNA Molecules into Therapeutic Agents. *Acc. Chem. Res.* **2019**, *52* (4), 1036-1047.
(115) Khvorova, A. Oligonucleotide Therapeutics — A New Class of Cholesterol-Lowering Drugs. *N. Engl. J. Med.* **2017**, *376* (1), 4-7.
(116) Ray, K. K.; Landmesser, U.; Leiter, L. A.; Kallend, D.; Dufour, R.; Karakas, M.; Hall, T.; Troquay, R. P.; Turner, T.; Visseren, F. L.; et al. Inclisiran in Patients at High Cardiovascular Risk with Elevated LDL Cholesterol. *N. Engl. J. Med.* **2017**, *376* (15), 1430-1440.
(117) Choung, S.; Kim, Y. J.; Kim, S.; Park, H.-O.; Choi, Y.-C. Chemical modification of siRNAs to improve serum stability without loss of efficacy. *Biochem. Biophys. Res. Commun.* **2006**, *342* (3), 919-927.
(118) Bobst, A. M.; Rottman, F.; Cerutti, P. A. Effect of the methylation of the 2′-hydroxyl groups in polyadenylic acid on its structure in weakly acidic and neutral solutions and on its capability to form ordered complexes with polyuridylic acid. *J. Mol. Biol.* **1969**, *46* (2), 221-234.
(119) Takahashi, M.; Nagai, C.; Hatakeyama, H.; Minakawa, N.; Harashima, H.; Matsuda, A. Intracellular stability of 2'-OMe-4'-thioribonucleoside modified siRNA leads to long-term RNAi effect. *Nucleic Acids Res.* **2012**, *40* (12), 5787-5793.
(120) Volkov, A. A.; Kruglova, N. y. S.; Meschaninova, M. I.; Venyaminova, A. G.; Zenkova, M. A.; Vlassov, V. V.; Chernolovskaya, E. L. Selective Protection of Nuclease-Sensitive Sites in siRNA Prolongs Silencing Effect. *Oligonucleotides* **2009**, *19* (2), 191-202.
(121) Liu, X.; Wang, W.; Samarsky, D.; Liu, L.; Xu, Q.; Zhang, W.; Zhu, G.; Wu, P.; Zuo, X.; Deng, H.; et al. Tumor-targeted in vivo gene silencing via systemic delivery of cRGD-conjugated siRNA. *Nucleic Acids Res.* **2014**, *42* (18), 11805-11817.
(122) Judge, A. D.; Bola, G.; Lee, A. C.; MacLachlan, I. Design of noninflammatory synthetic siRNA mediating potent gene silencing in vivo. *Mol. Ther.* **2006**, *13* (3), 494-505.
(123) Jackson, A. L.; Burchard, J.; Leake, D.; Reynolds, A.; Schelter, J.; Guo, J.; Johnson, J. M.; Lim, L.; Karpilow, J.; Nichols, K.; et al. Position-specific chemical modification of siRNAs reduces "off-target" transcript silencing. *RNA.* **2006**, *12* (7), 1197-1205.
(124) Sun, Y.; Zhao, Y.; Zhao, X.; Lee, R. J.; Teng, L.; Zhou, C. Enhancing the Therapeutic Delivery of Oligonucleotides by Chemical Modification and Nanoparticle Encapsulation. *Molecules* **2017**, *22* (10).
(125) Egli, M.; Manoharan, M. Chemistry, structure and function of approved oligonucleotide therapeutics. *Nucleic Acids Res.* **2023**, *51* (6), 2529-2573.
(126) Egli, M.; Pallan, P. S. Crystallographic studies of chemically modified nucleic acids: a backward glance. *Chem. Biodivers.* **2010**, *7* (1), 60-89.
(127) Pallan, P. S.; Greene, E. M.; Jicman, P. A.; Pandey, R. K.; Manoharan, M.; Rozners, E.; Egli, M. Unexpected origins of the enhanced pairing affinity of 2'-fluoro-modified RNA. *Nucleic Acids Res.* **2011**, *39* (8), 3482-3495.
(128) Manoharan, M.; Akinc, A.; Pandey, R. K.; Qin, J.; Hadwiger, P.; John, M.; Mills, K.; Charisse, K.; Maier, M. A.; Nechev, L.; et al. Unique gene-silencing and structural properties of 2'-fluoro-modified siRNAs. *Angew. Chem. Int. Ed. Engl.* **2011**, *50* (10), 2284-2288.

(129) Ya-Lin Chiu, T. M. R. RNAi in Human Cells: Basic Structural and Functional Features of Small Interfering RNA. *Mol. Cell* **2002**, *Volume 10* (Issue 3), Pages 549-561.
(130) Chiu, Y. L.; Rana, T. M. siRNA function in RNAi: a chemical modification analysis. *RNA.* **2003**, *9* (9), 1034-1048.
(131) Allerson CR, S. N., Jarres R, Prakash TP, Naik N, Berdeja A, Wanders L, Griffey RH, Swayze EE, Bhat B. <allerson-et-al-2005-fully-2-modified-oligonucleotide-duplexes-with-improved-in-vitro-potency-and-stability-compared-to.pdf>. **2005**.
(132) Prakash, T. P.; Allerson, C. R.; Dande, P.; Vickers, T. A.; Sioufi, N.; Jarres, R.; Baker, B. F.; Swayze, E. E.; Griffey, R. H.; Bhat, B. Positional Effect of Chemical Modifications on Short Interference RNA Activity in Mammalian Cells. *J. Med. Chem.* **2005**, *48* (13), 4247-4253.
(133) Morrissey, D. V.; Lockridge, J. A.; Shaw, L.; Blanchard, K.; Jensen, K.; Breen, W.; Hartsough, K.; Machemer, L.; Radka, S.; Jadhav, V.; et al. Potent and persistent in vivo anti-HBV activity of chemically modified siRNAs. *Nat. Biotechnol.* **2005**, *23* (8), 1002-1007.
(134) Eckstein, F.; Gindl, H. Polyribonucleotides containing a phosphorothioate backbone. *Eur. J. Biochem.* **1970**, *13* (3), 558-564.
(135) Volk, D. E.; Lokesh, G. L. R. Development of Phosphorothioate DNA and DNA Thioaptamers. *Biomedicines* **2017**, *5* (3), 41.
(136) Eckstein, F. A dinucleoside phosphorothioate. *Tetrahedron Letters* **1967**, *8* (13), 1157-1160.
(137) Eckstein, F. Phosphorothioates, Essential Components of Therapeutic Oligonucleotides. *Nucleic Acid Ther.* **2014**, *24* (6), 374-387.
(138) Soutschek, J.; Akinc, A.; Bramlage, B.; Charisse, K.; Constien, R.; Donoghue, M.; Elbashir, S.; Geick, A.; Hadwiger, P.; Harborth, J.; et al. Therapeutic silencing of an endogenous gene by systemic administration of modified siRNAs. *Nat.* **2004**, *432* (7014), 173-178.
(139) Schwarz, D. S.; Tomari, Y.; Zamore, P. D. The RNA-induced silencing complex is a Mg2+-dependent endonuclease. *Curr Biol* **2004**, *14* (9), 787-791.
(140) Wang, S.; Allen, N.; Vickers, T. A.; Revenko, A. S.; Sun, H.; Liang, X. H.; Crooke, S. T. Cellular uptake mediated by epidermal growth factor receptor facilitates the intracellular activity of phosphorothioate-modified antisense oligonucleotides. *Nucleic Acids Res.* **2018**, *46* (7), 3579-3594.
(141) Sipa, K.; Sochacka, E.; Kazmierczak-Baranska, J.; Maszewska, M.; Janicka, M.; Nowak, G.; Nawrot, B. Effect of base modifications on structure, thermodynamic stability, and gene silencing activity of short interfering RNA. *RNA.* **2007**, *13* (8), 1301-1316.
(142) Agris, P. F.; Sierzputowska-Gracz, H.; Smith, W.; Malkiewicz, A.; Sochacka, E.; Nawrot, B. Thiolation of uridine carbon-2 restricts the motional dynamics of the transfer RNA wobble position nucleoside. *J. Am. Chem. Soc.* **1992**, *114* (7), 2652-2656.
(143) Zhang, J.; Zheng, J.; Lu, C.; Du, Q.; Liang, Z.; Xi, Z. Modification of the siRNA passenger strand by 5-nitroindole dramatically reduces its off-target effects. *ChemBioChem* **2012**, *13* (13), 1940-1945.
(144) Addepalli, H.; Meena; Peng, C. G.; Wang, G.; Fan, Y.; Charisse, K.; Jayaprakash, K. N.; Rajeev, K. G.; Pandey, R. K.; Lavine, G.; et al. Modulation of thermal stability can enhance the potency of siRNA. *Nucleic Acids Res.* **2010**, *38* (20), 7320-7331.

(145) Valenzuela, R. A.; Suter, S. R.; Ball-Jones, A. A.; Ibarra-Soza, J. M.; Zheng, Y.; Beal, P. A. Base modification strategies to modulate immune stimulation by an siRNA. *ChemBioChem* **2015**, *16* (2), 262-267.
(146) Phelps, K. J.; Ibarra-Soza, J. M.; Tran, K.; Fisher, A. J.; Beal, P. A. Click modification of RNA at adenosine: structure and reactivity of 7-ethynyl- and 7-triazolyl-8-aza-7-deazaadenosine in RNA. *ACS Chem. Biol.* **2014**, *9* (8), 1780-1787.
(147) Kannan, A.; Fostvedt, E.; Beal, P. A.; Burrows, C. J. 8-Oxoguanosine switches modulate the activity of alkylated siRNAs by controlling steric effects in the major versus minor grooves. *J. Am. Chem. Soc.* **2011**, *133* (16), 6343-6351.
(148) Kannan, A.; Fostvedt, E.; Beal, P. A.; Burrows, C. J. 8-Oxoguanosine Switches Modulate the Activity of Alkylated siRNAs by Controlling Steric Effects in the Major versus Minor Grooves. *J. Am. Chem. Soc.* **2011**, *133* (16), 6343-6351.
(149) Puthenveetil, S.; Whitby, L.; Ren, J.; Kelnar, K.; Krebs, J. F.; Beal, P. A. Controlling activation of the RNA-dependent protein kinase by siRNAs using site-specific chemical modification. *Nucleic Acids Res.* **2006**, *34* (17), 4900-4911.
(150) Mikat, V.; Heckel, A. Light-dependent RNA interference with nucleobase-caged siRNAs. *RNA.* **2007**, *13* (12), 2341-2347.
(151) Schirle, N. T.; Kinberger, G. A.; Murray, H. F.; Lima, W. F.; Prakash, T. P.; MacRae, I. J. Structural Analysis of Human Argonaute-2 Bound to a Modified siRNA Guide. *J. Am. Chem. Soc.* **2016**, *138* (28), 8694-8697.
(152) Sheu-Gruttadauria, J.; Xiao, Y.; Gebert, L. F.; MacRae, I. J. Beyond the seed: structural basis for supplementary microRNA targeting by human Argonaute2. *EMBO J.* **2019**, *38* (13), e101153.
(153) Allerson, C. R.; Sioufi, N.; Jarres, R.; Prakash, T. P.; Naik, N.; Berdeja, A.; Wanders, L.; Griffey, R. H.; Swayze, E. E.; Bhat, B. Fully 2'-modified oligonucleotide duplexes with improved in vitro potency and stability compared to unmodified small interfering RNA. *J. Med. Chem.* **2005**, *48* (4), 901-904.
(154) Suter, S. R.; Sheu-Gruttadauria, J.; Schirle, N. T.; Valenzuela, R.; Ball-Jones, A. A.; Onizuka, K.; MacRae, I. J.; Beal, P. A. Structure-Guided Control of siRNA Off-Target Effects. *J. Am. Chem. Soc.* **2016**, *138* (28), 8667-8669.
(155) Alder, B. J.; Wainwright, T. E. Phase Transition for a Hard Sphere System. *J. Chem. Phys.* **1957**, *27* (5), 1208-1209.
(156) Alder, B. J.; Wainwright, T. E. Studies in Molecular Dynamics. I. General Method. *J. Chem. Phys.* **1959**, *31* (2), 459-466.
(157) Rahman, A. Correlations in the Motion of Atoms in Liquid Argon. *Phys. Rev.* **1964**, *136* (2A), A405-A411.
(158) Verlet, L. Computer "Experiments" on Classical Fluids. I. Thermodynamical Properties of Lennard-Jones Molecules. *Phys. Rev.* **1967**, *159* (1), 98-103.
(159) Bottaro, S.; Lindorff-Larsen, K. Biophysical experiments and biomolecular simulations: A perfect match? *Science* **2018**, *361* (6400), 355-360.
(160) Sadeghi, A.; Mohammad Jasour, A.; Kowsari, E.; Gheibi, M.; Hadi Ghasemi, M.; Ramakrishna, S. Comprehensive viewpoint on ionic liquids applications in sustainable pharmaceutical technology (experiments, simulations, and managerial insights). *J. Mol. Liq.* **2024**, *404*, 124991.
(161) Frenkel, D.; Smit, B. Chapter 4 - Molecular Dynamics simulations. In *Understanding Molecular Simulation (Third Edition)*, Frenkel, D., Smit, B. Eds.; Academic Press, 2023; pp 97-124.

(162) Auffinger, P. Molecular Dynamics Simulations of RNA Systems. In *Handbook of RNA Biochemistry*, 2014; pp 687-718.
(163) McDowell, S. E.; Spackova, N.; Sponer, J.; Walter, N. G. Molecular dynamics simulations of RNA: an in silico single molecule approach. *Biopolymers* **2007**, *85* (2), 169-184.
(164) D'Esposito, R. J.; Myers, C. A.; Chen, A. A.; Vangaveti, S. Challenges with Simulating Modified RNA: Insights into Role and Reciprocity of Experimental and Computational Approaches. *Genes.* **2022**, *13* (3).
(165) Bernetti, M.; Bussi, G. Integrating experimental data with molecular simulations to investigate RNA structural dynamics. *Curr. Opin. Struct. Biol.* **2023**, *78*, 102503.
(166) Koseki, J.; Konno, M.; Asai, A.; Horie, N.; Tsunekuni, K.; Kawamoto, K.; Obika, S.; Doki, Y.; Mori, M.; Ishii, H. Theoretical analyses and experimental validation of the effects caused by the fluorinated substituent modification of DNA. *Scientific Reports* **2020**, *10* (1).
(167) Battistini, F.; Sala, A.; Hospital, A.; Orozco, M. Sequence-Dependent Properties of the RNA Duplex. *J. Chem. Inf. Model.* **2023**, *63* (16), 5259-5271.
(168) Kuhrova, P.; Mlynsky, V.; Otyepka, M.; Sponer, J.; Banas, P. Sensitivity of the RNA Structure to Ion Conditions as Probed by Molecular Dynamics Simulations of Common Canonical RNA Duplexes. *J. Chem. Inf. Model.* **2023**, *63* (7), 2133-2146.
(169) Kuhrova, P.; Otyepka, M.; Sponer, J.; Banas, P. Are Waters around RNA More than Just a Solvent? - An Insight from Molecular Dynamics Simulations. *J. Chem. Theory Comput.* **2014**, *10* (1), 401-411.
(170) Uppuladinne, M. V. N.; Koulgi, S.; Jani, V.; Sonavane, U.; Joshi, R. Unlocking the potential of RNAi as a therapeutic strategy against infectious viruses: an in-silico study. *Chem. Pap.* **2023**, *78* (3), 1537-1552.
(171) Bhandare, V.; Ramaswamy, A. Structural Dynamics of Human Argonaute2 and Its Interaction with siRNAs Designed to Target Mutant tdp43. *Adv. Bioinformatics* **2016**, *2016*, 8792814.

CHAPTER 2: IMPACT OF CHEMICAL MODIFICATIONS ON siRNA DUPLEXES

2.1 Introduction

As discussed in Chapter 1, RNA interference (RNAi) is a highly conserved post-transcriptional gene regulation mechanism that plays a crucial role in cellular defense against external invasion by genetic elements.[1-13] The RNAi pathway is initiated in the cytoplasm by the endoribonuclease Dicer (Figure 1.5), which processes long dsRNA or short hairpin RNA (shRNA) into mature siRNA duplexes of 19–25 nucleotides, typically bearing 3' overhangs. siRNA duplexes are then loaded into the RNA-induced silencing complex (RISC), a multiprotein assembly that includes human Argonaute-2 (hAgo2). Within RISC, RNA helicases assist siRNA to undergo strand separation in an ATP-dependent manner.[14] The sense strand is discarded, while the antisense strand serves as a guide to direct sequence-specific binding to the target mRNA. This interaction facilitates cleavage of the target transcript by hAgo2, leading to gene silencing.[4,11,14,15]

Over the past two decades, siRNA-based therapeutics have demonstrated significant potential for treating a range of diseases, including hereditary transthyretin mediated amyloidosis, acute hepatic porphyria, primary hyperoxaluria, and high cholesterol.[9,16-18] While unmodified siRNA serves in the natural RNAi pathway, clinical applications are hindered by the short half-life (rapid degradation) of canonical RNA in biological environments.[19-21] To enhance siRNA stability and drug-like properties, chemical modifications have been introduced to the canonical nucleotides.[10,22,23] One of the most common modifications used to improve siRNA function is the replacement of one non-bridging oxygen atom of each phosphate group(s) in the backbone with sulfur atom(s).[24] This phosphorothioate (PS) modification has been reported to significantly

increase hydrophobicity and resistance to nuclease and phosphodiesterase activity, which promotes siRNA binding to carrier plasma proteins.[9,25,26] Ribose modifications at the 2'-position have also been widely reported to improve nuclease resistance since ribonucleases require the 2'-OH group for RNA hydrolysis, but the 2'-OH group is not essential for the silencing effect of siRNA.[2,6,19,23,27-43] Among sugar modifications, the 2'-*O*-methyl (2'-*O*-Me) modification, a naturally occurring RNA modification in mammalian cells,[10] is frequently employed in siRNA therapeutics due to its low toxicity and compatibility with both the sense and antisense strands.[36] However, experimental investigations have shown extensive incorporation of 2'-*O*-Me can reduce or even abolish RNAi activity.[42,44] In contrast, alternating 2'-*O*-Me modifications with unmodified RNA nucleotides generally preserves siRNA functionality while providing substantial resistance to nuclease degradation.[2,10,36,42-44] The 2'-fluoro (2'-F) modification has also been studied, demonstrating siRNA functionality while enhancing duplex resistance to nuclease activity.[39,45,46] The incorporation of 2'-F modifications in the canonical residues makes the modified ribose adopt the C3′-*endo* conformation, increases thermal stability, and preserves siRNA activity *in vitro* and *in vivo*.[21,45,46] Additionally, combining 2'-F modifications at pyrimidines with 2'-*O*-Me modifications at purines has been shown to result in remarkable resistance to serum nucleases and significantly improve biological performance *in vivo*.[42,43,47] Several other modifications, such as glycol nucleic acid (GNA),[48] locked nucleic acid (LNA),[49-51] ethyl-bridged nucleic acid (ENAs),[52] and 2′-*O*-methoxyethyl RNA (2′-*O*-MOE)[53] have also been experimentally explored (Figure 2.1). While heavy modification of siRNA with any single type of chemical modifications generally results in decreased activity, the limited introduction or alternation of modifications with other modification types helps retain RNAi efficiency.[2,10,51,54-57]

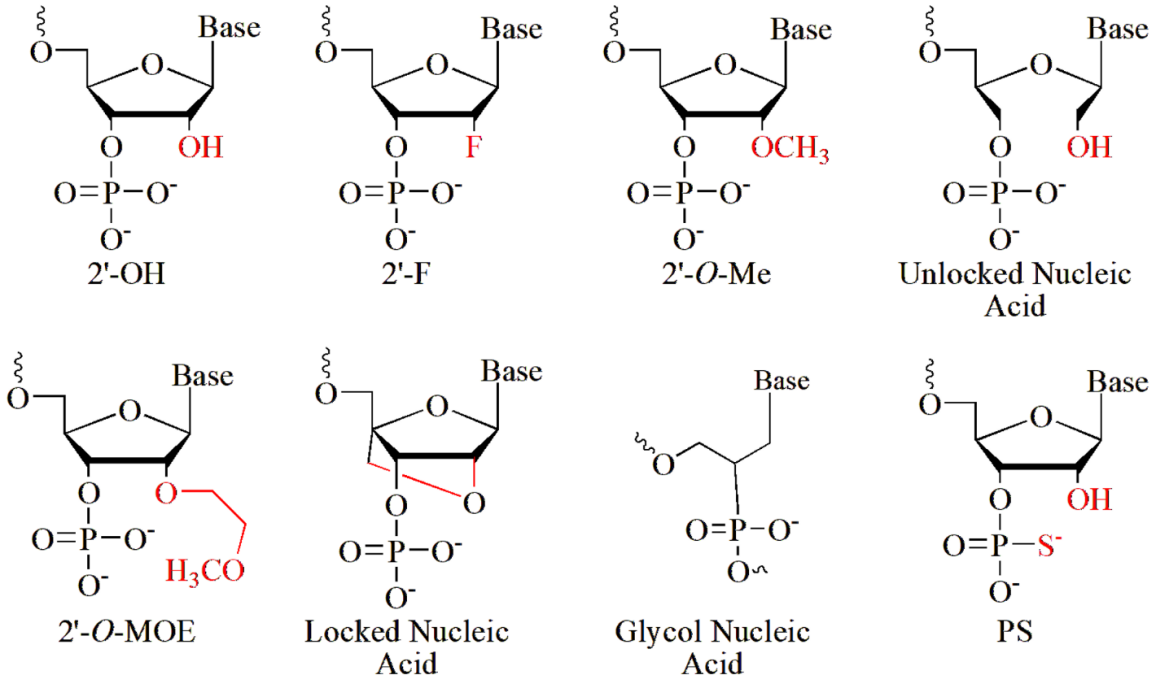

Figure 2.1: Structures of chemically-modified RNA components designed for use in siRNA therapeutics

As previously discussed in Chapter 1, five siRNA drugs have been approved by the United States Food and Drug Administration (FDA, Figure 1.6). Despite advancements in siRNA therapeutics design and use, no experimentally resolved structure exists for any FDA-approved siRNA drug to the best of our knowledge. While some properties of siRNA, like the thermal stability and nuclease resistance have been studied,[39,40,46] detailed atomic-level characterization remains limited. Specifically, it was found that maintaining an A-form helical conformation is crucial for siRNA function, with deviations in the A-form structure disrupting RNAi activity.[42] Experiments have shown that modifications like 2'-*O*-Me and 2'-F reinforce A-form geometry and enhances the thermal stability (melting temperature) without abolishing RNAi efficiency.[37-40,42,44,58,59] Given the structural dependence of RNAi activity,[42] further structural analyses are essential for the rational design of next-generation siRNA therapeutics.

While various experimental techniques have been employed to determine RNA structures, each method presents inherent limitations. X-ray crystallography is a powerful tool, but the inherent flexibility of RNA makes crystal contacts harder to come by at a sufficient resolution.[60] Cryo-electron microscopy (cryo-EM) requires highly-specialized and expensive equipment and usually less suitable for small molecules like siRNA.[61] Small-angle scattering (SAS) offers only low-resolution information on RNA structure,[62] while nuclear magnetic resonance (NMR) spectroscopy is laborious and constrained by spectral overcrowding.[63] Consequently, significant gaps remain in our understanding of how chemical modifications influence the structures of siRNA. Computational approaches like molecular dynamics (MD) simulations can offer atomic-level insights by using molecular mechanics (MM) force fields to capture the time-dependent behavior of molecular systems, which could enable a detailed understanding of how modifications influence siRNA dynamics and interactions. While previous MD studies have explored ribose conformation of the modifications like 2'-*O*-Me, 2'-*O*-MOE and 2'-F used in siRNA,[32-34] modification of siRNA bases and their effect on the duplex melting temperature,[22] and modified siRNA-hAgo2 complexes,[64-66] systematic investigations of full chemically-modified FDA approved siRNA drugs are lacking. Furthermore, these studies either use short timescales (25 – 500 ns) or lack replicas, limiting the usefulness of the information obtained. Therefore, a broader, systematic analysis of chemically-modified siRNA drugs is still needed to understand the impacts of the modifications on the conformation and dynamics of siRNA.

This study employs MD simulations to examine the impact of chemical modifications on siRNA structure using the nucleobase sequences of the first five FDA-approved siRNA drugs (Figure 1.6). For each drug nucleobase sequence, five models were

constructed that vary in the 2'-ribose substituents throughout the strand. Specifically, each nucleotide was modeled in the canonical RNA form, the canonical DNA form, fully 2'-*O*-Me substituted (OMeNA), fully 2'-F substituted (FNA), or the sugar modification pattern found in the original drug. By comparing these differentially 2'-substituted duplexes, we reveal how the structural dynamics of RNA are differentially influenced by the sugar modification pattern, addressing key gaps in the atomic-level understanding of how modifications impact RNA structure, and providing insights necessary for the rational design of improved siRNA therapeutics.

2.2 Computational Methods

To generate the modification sequences investigated in the present study, the unmodified A-form and B-form duplexes were first constructed for the nucleobase sequences corresponding to each of the 5 FDA-approved drugs (Figure 1.6) using the Build Structure tool implemented in UCSF Chimera.[67] The 2'-*O*-Me and 2'-F nucleotide modifications were then introduced using GaussView 6.0.16.[68] Although synthetic siRNAs are commonly designed with 2-nucleotide 3' overhangs to mimic natural Dicer-generated siRNAs, experimental studies have demonstrated that the absence of the 3' overhangs does not impact siRNA function,[2,43] and may instead offer greater resistance to exonucleolytic degradation.[2] Therefore, the 3' overhangs were not included in the sense or antisense strand in the present work. Additional models were generated using the nucleobase sequence of Patisiran and the modification pattern of the remaining four drugs (denoted Pati-Vutri, Pati-Incli, Pati-Luma, or Pati-Givo).

Amber force fields were implemented, with RNA nucleotides modelled using χOL3 and DNA nucleotides using OL15.[69,70] The partial charges for the modified nucleotides

were acquired using geometries optimized with the HF/6-31G(d) level of theory and the PyRED online RESP charge fitting server.[71,72] Generalized Amber Force Field (GAFF2)[73] parameters were produced for the modified nucleotides using parmchk2 from AmberTools21.[74] Each system was solvated in a truncated-octahedral TIP3P[75-77] water box such that the solute is at least 12 Å from the edge of a box face in any direction, neutralized with Na^+, and NaCl added to 150 mM to mimic physiological conditions. The number of ions added was determined using the SLTCAP calculator.[78]

Each system was minimized, heated, and equilibrated. Specifically, the minimization of the solvent, hydrogen atoms of the solute, solute, and all atoms was performed sequentially in four stages each involving 11,000 steps using the steepest descent (4,000 steps) and conjugate gradient (7,000 steps) methods, and a 100 $kcal \cdot mol^{-1} Å^{-2}$ restraint on the relevant atoms. Next, each system was heated in 6 increments from 10 K to 310 K in 50K increments over the course of 120,000 simulation steps and then equilibrated using 5 x 10,000 step segments while applying decreasing restraints on the solvent from 25 to 1.5 $kcal \cdot mol^{-1} Å^{-2}$ to ensure gradual relaxation at the desired temperature and pressure of 1 bar.

Finally, 1 μs unrestrained MD simulations using the NPT ensemble were carried out in quintuplicate on each system using AMBER20.[74] The temperature was held at 310 K using the Langevin thermostat,[79,80] with a collision frequency of 3 ps^{-1}. A Berendsen barostat[81] was employed to maintain the pressure at 1 bar with a relaxation interval of 2 ps. The periodic boundary condition was applied, and the non-bonded interactions were calculated using the particle mesh Ewald method[82,83] with a cutoff distance of 10 Å. The SHAKE algorithm[84] was used to constrain the bonds involving hydrogen atoms to allow for two femtosecond timesteps. The coordinates were saved every 50 ps for analysis,

generating 100,000 frames total per system over all replicas. During the initial MD simulations, the FNA duplex exhibited extensive fraying, which contributed to duplex destabilization. Given our interest in characterizing a fully fluorinated duplex, we applied distance restraints between all heavy atoms involved in Watson–Crick base pairing (1.80 Å and 3.90 Å for the lower and upper bounds, respectively). To validate this approach, we compared helical parameters between the unrestrained and restrained FNA duplexes (Appendix A, Figure A.1d). The analysis revealed no significant deviations in regions of the duplex that remained unfrayed. To further justify this strategy, we compared the restrained FNA duplex to the canonical RNA duplex. The insignificant differences in the FNA and RNA structural parameters predicted from our simulations is consistent with previous experimental findings showing that fully 2′-F-modified RNA octamers adopt structures similar to native RNA for the same nucleobase sequence.[45] Nevertheless, although crystallization of a fully 2′-F-modified RNA octamer was successful, another octamer of a different sequence (f(CCCCGGGG)) yielded only low-resolution diffraction, and attempts to improve crystal quality or obtain alternative crystal forms were unsuccessful.[45] This suggests that extensive 2′-F substitution may impair crystallization.

The cpptraj[85] module of AmberTools21[74] was used to analyze the MD trajectories averaged over all datasets. Root-mean-square deviation (RMSD) was carried out to ensure system convergence (Appendix A, Figure A.11). Clustering was carried out to obtain representative structures based on the RMSD of atomic positions of all heavy atoms and we evaluated the duplex flexibility by analyzing the root-mean-square-fluctuation (RMSF). The sugar puckering of the canonical and modified nucleotides was evaluated using Barnaba.[86] Helical parameters were also evaluated using the nastruct command and in-house scripts, which utilize the same algorithms, definitions, and units for helical

parameters, and groove sizes as X3DNA.[85,87-90] To assess helical width, we analyzed intra and interstrand backbone distances, specifically monitoring O5'···O3' distances both between strands and adjacent nucleotides along the same strand throughout the simulation. Terminal base pairs and base pair steps were excluded from structural analyses to avoid artifacts arising from the increased fluctuations typically observed at the termini during MD simulations.[87,91-93] The average measurements across datasets and across replicas are reported to produce a single value for each duplex. The calculations of standard deviations and standard errors of the mean were performed to assess the measure of observed differences. To ensure the reliability of the reported means, estimated errors for the calculated structural parameters were determined, which are within a 95% confidence interval and are provided in Appendix A, thereby confirming the statistical relevance and reliability of the results.

2.3 Results

2.3.1 2'-*O*-Me, 2'-F, and Patisiran Modification Patterns Induce A-form Helices

Patisiran stands out among FDA-approved siRNA drugs due to its distinctive pattern of nucleoside modifications.[94] Specifically, among the 19-base pairs, 2'-*O*-Me modifications occur in all pyrimidine nucleotides in the sense strand and two uridines in the antisense strand, while the remaining nucleotides in the duplex are unmodified and additional TT DNA overhangs exist on both 3'-ends. Thus, containing eleven modifications, this is the only partially-modified siRNA drug currently approved. Furthermore, unlike other siRNA therapeutics, Patisiran does not contain 2'-fluoro or phosphorothioate modifications.

To understand the impact of the Patisiran modification pattern on the structure of

RNA duplexes, MD simulations were initially performed on 19-mer canonical RNA and DNA duplexes with the same nucleobase sequence context as the drug. As widely reported throughout the nucleic acid literature,[33,34,95-97] the RNA duplex exhibits 11 base pairs per turn, an average rise per base pair of 2.6 ± 0.2 Å, and a predominant C3'-*endo* sugar pucker throughout the simulations (Table 2.1), structural features that are characteristic of an A-form duplex. In contrast, the DNA duplex contains 10 base pairs per turn, an average rise per base pair of 3.2 ± 0.1 Å, and a predominant C2'-*endo* sugar pucker (Table 2.1), key features of a B-form duplex. Furthermore, consistent with A-form nucleic acids being wider and shorter than their B-form counterparts,[95,96,98] the average interstrand distance is slightly larger for RNA (16.4 ± 0.1 Å) compared to DNA (16.1 ± 0.2 Å, Table 2.1), while the average intrastrand distance is smaller for RNA (3.9 ± 0.05 Å) than DNA (4.3 ± 0.03 Å; Table 2.1).

Table 2.1: Average (and standard deviation) of structural parameters of canonical and chemically-modified nucleic acids from 5 replicas of 1 μs MD simulations.

Feature	**Canonical**	**DNA**	**OMeNA**	**FNA**	**Patisiran**
Sugar Pucker	C3'-endo	C2'-endo	C3'-endo	C3'-endo	C3'-endo
Rise/Base Pair	2.62 (0.15) Å	3.24 (0.11) Å	2.16 (0.12) Å	2.68 (0.14) Å	2.18 (0.25) Å
Base Pairs/Turn	11	10	11	11	11
Intrastrand Distance	3.90 (0.03) Å	4.27 (0.03) Å	3.91 (0.09) Å	3.91 (0.06) Å	3.95 (0.05) Å
Interstrand Distance	16.42 (0.05) Å	16.12 (0.16) Å	16.54 (0.13) Å	16.44 (0.21) Å	16.62 (0.14) Å

Upon complete duplex modification to 2'-*O*-Me (OMeNA) or 2'-F (FNA) nucleotides or the introduction of the ribose modification pattern of Patisiran, 11 base pairs per turn, an average rise per base pair of 2.2 Å – 2.7 Å, and a dominant C3'-*endo* sugar conformation are observed throughout the simulations (Table 2.1). Furthermore, the

average interstrand distances falls between 16.4 Å and 16.6 Å, while the average intrastrand distance is 3.9 ± 0.01 Å. Thus, our simulations highlight that all modified duplexes retain the general A-form structural characteristics of canonical RNA, as previously described by experiments.[88,90]

2.3.2 2'-*O*-Me, 2'-F, and Patisiran Modification Patterns Fine-Tune the Structure of the Canonical RNA Duplex

Although the ribose modifications promote global properties consistent with an A-form helical conformation, the structural dynamics must be investigated to determine whether 2'-*O*-Me, 2'-F, and Patisiran modification patterns impart any distinct structural features to the duplex. First, we consider the distribution and equilibrium of the sugar conformations across the modified duplexes. The pseudorotation phase angles (P), which is the parameter that describes the conformation of five-membered sugar rings in nucleic acids, sampled by ribose during MD simulations on canonical RNA span a broad range of values in the northern region of the plot (0–72° and 288–360°; Figure 2.2a). Although (unmodified) ribose favors the C3'-*endo* pucker (0–36°), the structural dynamics permits sampling of alternative conformations, such as C4'-*exo* (36–72°), C1'-*endo* (288–324°), and C2'-*exo* (324–360°). In contrast, FNA displays a more diverse puckering distribution than RNA, with clusters appearing at multiple angular orientations (P = 0–72°, 108–180°, and 288–360°; Figure 2.2c), suggesting that the 2'-F modification enables sampling of both C2'-*endo* (144–180°) and C1'-*exo* (108–144°) in addition to the conformations sampled by RNA. There is a pronounced effect of 2'-*O*-Me substitution on the sugar pucker, with the modification restricting the conformational variability (i.e., P falls between 0–50° and 300–360°; Figure 2.2b) and tight clustering sugar conformations around C3'-*endo* and C2'-*exo*.

Finally, Patisiran exhibits a strong preference for the C3'-*endo* sugar pucker, displaying conformational variability similar to RNA, yet occasional flexibility, as indicated by minor sampling of the C2'-*endo* conformation (Figure 2.2d). These observations demonstrate that chemical modification type and pattern can markedly influence sugar pucker dynamics in RNA, either restricting or enhancing conformational flexibility.

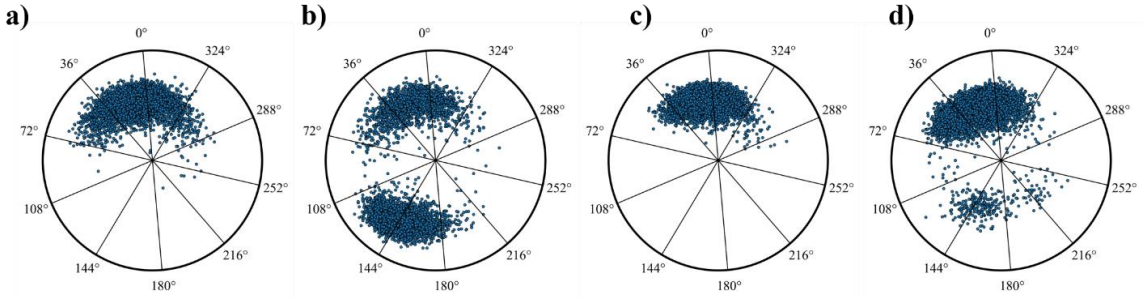

Figure 2.2: Distribution of the pseudorotation phase angle (P) sampled by the ribose of (a) canonical RNA, (b) FNA, (c) OMeNA, and (d) Patisiran across 5 replicas of 1 μs MD simulations.

To understand how differences in the sugar puckering dynamics associated with modification type and pattern influence nucleotide flexibility, we analyzed the RMSF over the course of the simulations (Figure 2.3a). Patisiran and OMeNA exhibit a similar pattern of lower RMSF values compared to RNA, FNA and DNA across both strands, indicating more rigid duplexes relative to the others. In contrast, canonical RNA, FNA, and DNA show relatively higher RMSF values, suggesting greater flexibility. This infers that the differences in the dynamics of the sugar puckering are propagated throughout the entire duplex.

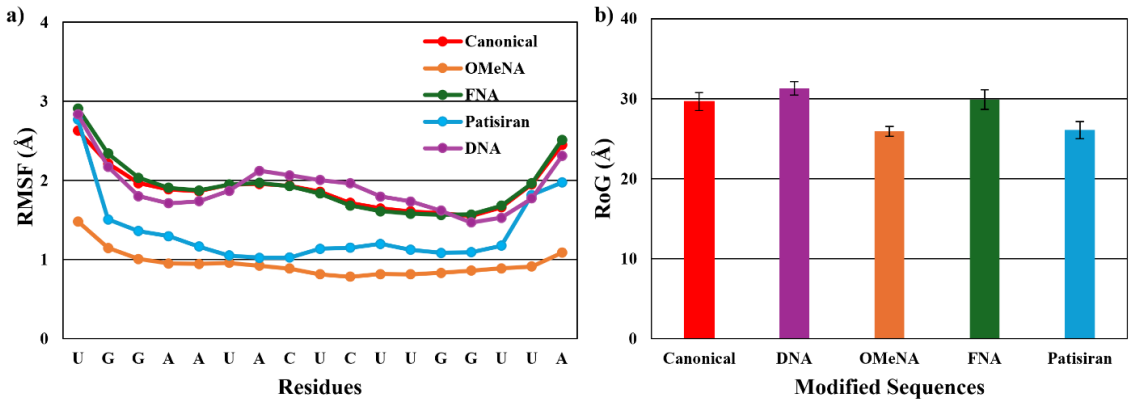

Figure 2.3: (a) Root-Mean-Square fluctuations (RMSF in Å) and (b) radius of gyration (RoG in Å) for canonical and chemically-modified nucleic acids across 5 replicas of 1 μs MD simulations.

To further assess the impact of chemical modifications on the structure of the nucleic acid duplex, the nucleic acid structural parameters (base pair, base pair step, and helical parameters) were evaluated across all residues in the duplexes. Heatmaps illustrating the deviations in structural parameters of modified nucleic acids relative to canonical RNA are presented in (Figure 2.4 and Appendix A; Figure A.5). Each column represents the deviation in average structural parameters between RNA and the modified duplexes, with color gradients indicating the magnitude of the difference. Blue denotes RNA parameter average values are larger, while red shows that the average value of the modified duplexes are greater than canonical RNA, with the intensity of each color reflecting the extent of the variation. Among the parameters evaluated, roll, inclination, and x-displacement exhibited the most pronounced deviations, and are the focus of the discussion below.

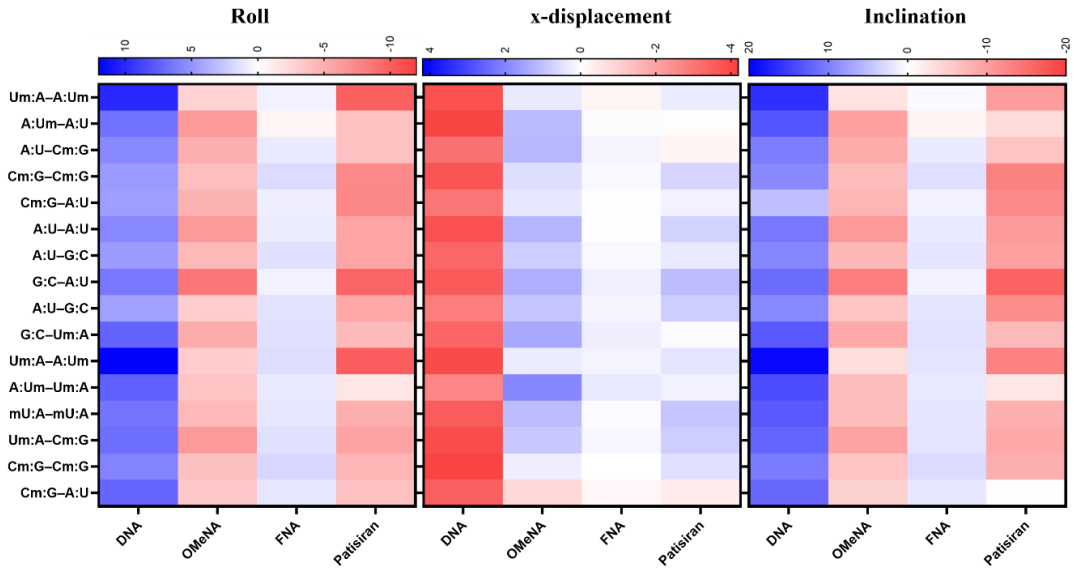

Figure 2.4: Heatmaps of the deviations in the key structural parameters of modified nucleic acids relative to canonical RNA of Patisiran nucleobase sequence. Each row represents the difference between RNA and the modified nucleic acids in the columns. Blue shows a positive value difference, while red shows a negative value difference.

RNA can be distinguished from DNA by higher roll and inclination, and lower x-displacement values,[99] which is evident in the heatmap (i.e., the DNA column exhibits an intense blue or red color in the case of x-displacement). Among the modified duplexes, FNA demonstrates the smallest deviations from RNA in all parameters as indicated by minimal color gradient. Specifically, FNA exhibits deviations less than –1.3° to 2.8° for inclination, –0.3 Å to 0.3 Å for x-displacement, and –0.8° to 1.9° for roll. This also occurs throughout all other parameters (see Appendix, Figures A.7 – A.9). In contrast, OMeNA displays more pronounced structural deviations from RNA as shown by the increased intensity in the color gradient, with values ranging from –13.7° to –3.0° for inclination, –0.9 Å to 2.0 Å for x-displacement, and –8.6° to –2.9° for roll. OMeNA consistently shows the greatest deviation across all parameters compared to other modified RNA duplexes (see Appendix, Figures A.7 – A.9). Similarly, Patisiran showed significant differences from canonical RNA, with deviations spanning –16.4° to –0.2° for inclination, –0.4 Å to 1.1 Å

for x-displacement, and –10.2° to –1.6° for roll. Overall, OMeNA and Patisiran exhibit similar structural deviations from RNA, with increased base pair inclination and roll and reduced x-displacement. The more pronounced global distortions observed upon the introduction of 2'-*O*-Me modifications into canonical RNA compared to the effects of 2'-F modifications, reinforce the differential structural dynamics (RMSF and sugar pucker) discussed earlier.

To understand how differences in structural dynamics and parameters impact the overall shape of the duplexes, RoG was compared (Figure 2.3b). Canonical RNA and FNA exhibit a comparable average RoG (29.6 ± 1.1 Å and 29.9 ± 1.2 Å, respectively) and no substantial structural deviations were observed between canonical RNA and FNA (Figure 2.3b). Previous comparisons between RNA and partially or fully 2′-F–modified RNA duplexes using X-ray crystallography have shown minimal differences in both local and overall helical geometry. [45] While minor differences are observed across multiple metrics, including rise per base pair (Table 2.1), RMSF (Figure 2.3a), helical parameters (Figure 2.4), and RoG values (Figure 2.3b), they are not sufficient to impact the global RNA structure.

Patisiran and OMeNA display similar average RoG (26.1 ± 1.1 Å and 25.9 ± 0.6 Å, respectively). Indeed, OMeNA and Patisiran exhibit a similar increased roll and inclination relative to RNA, which results in a smaller RoG than for RNA that reflects a more compact helix than RNA and FNA. As a result, the global conformations of Patisiran and OMeNA closely resemble each other (Figure 2.5), but are structurally distinct from RNA. Indeed, although both Patisiran and OMeNA share structural similarities with canonical (A-form) RNA, the modifications induce a slightly thicker (smaller interstrand backbone distances) and shorter duplex (smaller rise per base pair values, Table 2.1). These subtle differences

at each base pair step have a large impact on the global helical structure.

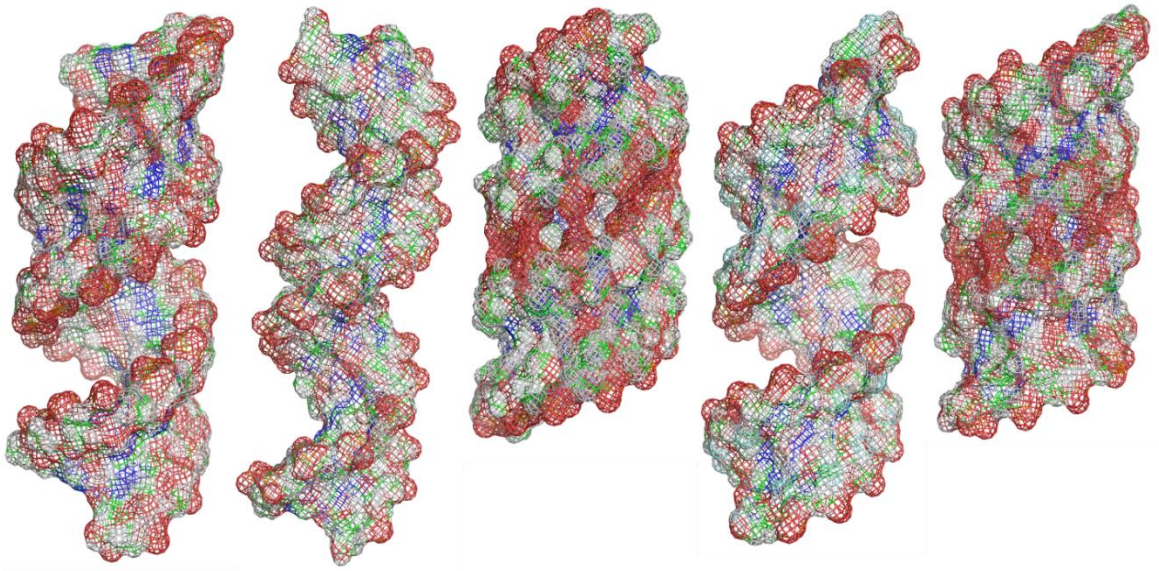

Figure 2.5: Global structure of RNA, DNA, OMeNA, FNA, and Patisiran (L-R).

Together, these findings demonstrate that while all modified duplexes adopt an A-form conformation, the type and pattern of chemical modification fine-tunes the structural properties of the canonical duplex. While FNA and RNA have similar structural features, OMeNA is distinct from RNA. Therefore, Patisiran, which has several 2'-*O*-Me, but no F modifications, looks more like OMeNA than RNA.

2.3.3 2'-F and 2'-*O*-Me Modifications Have Synergistic Effects on RNA Structure, Highlighting their Importance for Givosiran, Lumasiran, Inclisiran, and Vutrisiran

Givosiran is the second FDA-approved siRNA therapeutic and exhibits a distinct chemical modification pattern compared to Patisiran. Unlike Patisiran, all nucleotides in Givosiran are chemically modified, with a combination of 2'-*O*-Me and 2'-F modifications distributed throughout the duplex.[9,18] Among the 21-base pairs, twenty-six nucleotides are 2'-*O*-Me modified and sixteen nucleotides are 2'-F modified, with the majority of the 2'-F alterations existing on the antisense strand. Both the sense and antisense strands of the

Givosiran duplex contain phosphorothioate linkages at the 5' terminal ends on the first 2 linkages, and the antisense strand contains phosphorothioate linkages at the 3'-terminal overhangs, making Givosiran the first fully modified siRNA drug approved for treatment of disease.

To assess the structural properties of Givosiran, key conformational parameters distinguishing A-form and B-form nucleic acids were analyzed as done for Patisiran (Table 2.2). Despite the presence of full or mixed chemical modifications, the canonical Givosiran-based duplexes including OMeNA, FNA, and Givosiran consistently retain key A-form structural features,[33,34,95,98] similar to those observed for Patisiran (Table 2.2). These include 11 base pairs per turn, a dominant C3'-*endo* sugar pucker conformation throughout the simulations, and an average rise per base pair ranging from 2.1 to 2.7 Å. The interstrand and intrastrand backbone distances also remained comparable to canonical RNA, with values between 16.4–16.5 Å and 3.8–3.9 Å, respectively.

Table 2.2: Average (and standard deviation) of structural parameters of canonical and chemically modified nucleic acids from 5 replicas of 1 μs MD simulations.

Feature	**Canonical**	**DNA**	**OMeNA**	**FNA**	**Givosiran**
Sugar Pucker	C3'-endo	C2'-endo	C3'-endo	C3'-endo	C3'-endo
Rise/Base Pair	2.65 (0.09) Å	3.27 (0.07) Å	2.14 (0.11) Å	2.73 (0.10) Å	2.51 (0.17) Å
Base Pairs/Turn	11	10	11	11	11
Intrastrand Distance	3.90 (0.02) Å	4.27 (0.03) Å	3.90 (0.03) Å	3.91 (0.06) Å	3.84 (0.02) Å
Interstrand Distance	16.41 (0.07) Å	16.10 (0.20) Å	16.49 (0.10) Å	16.41 (0.26) Å	16.41 (0.10) Å

Similar to the analysis conducted for Patisiran, we next investigated how distinct chemical modification patterns in Givosiran, OMeNA, and FNA influence the structural dynamics of RNA duplexes by examining the distribution and equilibrium of the sugar

conformations. Both FNA and OMeNA modifications influence the ribose pucker to varying extents (Figure 2.6a–c). The conformational flexibility observed in FNA for Patisiran is similarly seen in Givosiran, indicating a consistent effect across different sequences. In contrast, OMeNA shows a more confined pucker distribution predominantly in the northern region, mirroring the behavior previously observed in Patisiran. However, OMeNA occasionally samples sugar conformation in the southern region. In contrast, the Givosiran modification pattern displays the most conformationally restricted sugar conformational distribution among the four modification sequences. Specifically, the pseudorotation phase angles of Givosiran are tightly clustered around the C3'-*endo* region (P = 0–50° and 324–360°; Figure 2.6d), reflecting a pronounced bias toward the C3-*endo* conformation. This highlights how different chemical modification types and patterns can significantly modulate the sugar conformational dynamics in RNA.

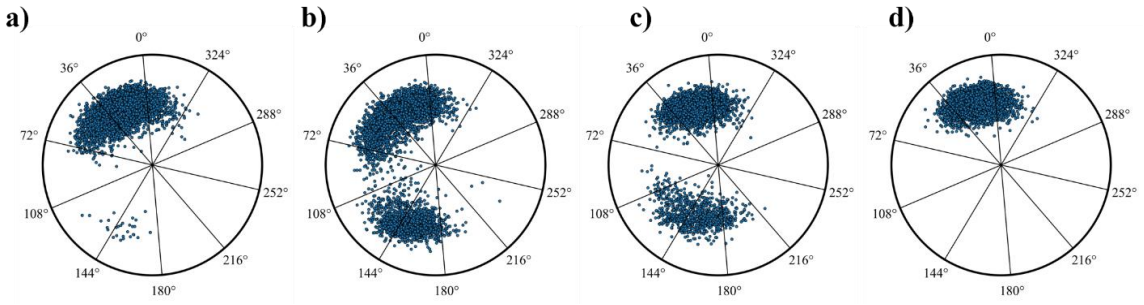

Figure 2.6: Distribution of the pseudorotation phase angle (P) sampled by the ribose of (a) canonical RNA, (b) FNA, (c) OMeNA, and (d) Givosiran across 5 replicas of 1 µs MD simulations.

The RMSF was evaluated over the course of the simulations (Figure 2.7a, and Appendix, Figure A.10). To understand how differences in sugar conformational dynamics associated with modification patterns influence nucleotide flexibility, in contrast to what we observed for Patisiran, canonical RNA, FNA and Givosiran show comparable nucleotide fluctuations in both strands throughout the simulation (i.e. higher RMSF values).

However, as discussed for Patisiran, OMeNA exhibits distinct fluctuations (lower RMSF values) from those observed in other modified duplexes. This suggests 2'-F is playing a role in moderating how OMe modification differentially influences the dynamics of the entire nucleotide in a duplex with the Givosiran modification pattern.

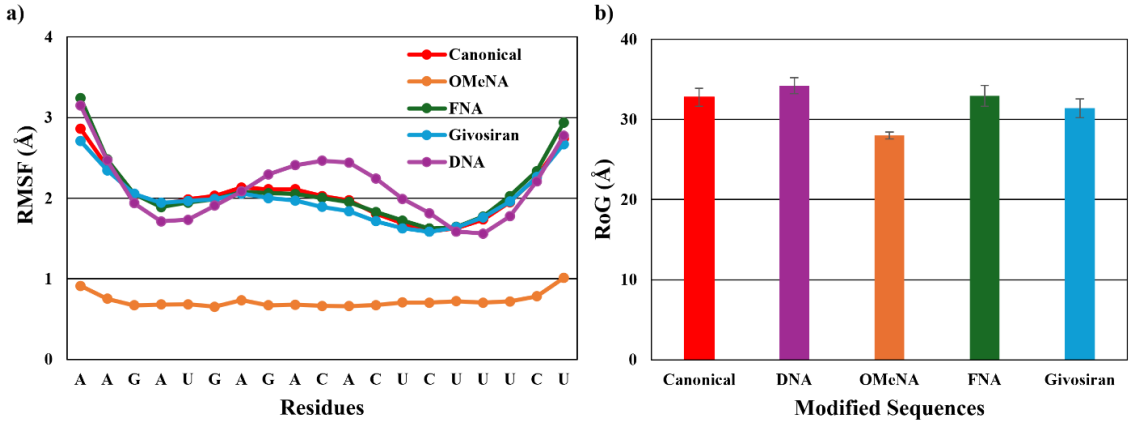

Figure 2.7: (a) Root-Mean-Square fluctuations (RMSF in Å) and (b) radius of gyration (RoG in Å) for canonical and chemically modified nucleic acids across 5 replicas of 1 μs MD simulations.

Among the base pair, base pair step, and helical structural parameters, roll, inclination, and x-displacement still exhibit the most pronounced trend. FNA exhibits the smallest structural deviation relative to canonical RNA (Figure 2.8, and see Appendix, Figures A.7–A.9). Specifically, FNA displays deviations ranging from –0.3° to 4.0° for inclination, –0.2 Å to 0.4 Å for x-displacement, and –0.1° to 1.8° for roll. In contrast, OMeNA demonstrates significantly greater deviations from RNA, spanning –15.3° to –2.3° for inclination, 0.5 Å to 2.2 Å for x-displacement, and –9.4° to –1.1° for roll. This trend is similar to that observed in Patisiran nucleobase sequence. These findings shows that while 2'-*O*-Me substitutions introduce significant global base pair distortions, 2'-F modifications in FNA result in minimal perturbation of global structural parameters. Difference in the Givosiran structural parameters from canonical RNA vary at each base pair and step

throughout the helix, with deviations ranging from –6.6° to 4.8° for inclination, 0.02 Å to 1.3 Å for x-displacement, and –4.3° to 3.2° for roll. Also, the effect of the sugar modification type is evident at the level of the individual base pairs and steps. This gives rise to a distinct fingerprint in the heatmap. The color variation corresponds to the presence of either 2′-F or 2′-*O*-Me modifications at specific positions. For example, in the Givosiran column in Figure 2.8, the last three rows show consecutive 2′-F modifications in the sugar of the 2nd, 3rd, and 4th nucleotides from the 5′-end of the antisense strand. Additionally, alternate rows contain 2′-F modifications, which is clearly reflected in the Givosiran color scheme. Interestingly, the intensity of the red/blue colour associated with the 2'-*O*-Me modifications appears attenuated in the Givosiran modification sequence compared to OMeNA. This reduced colour intensity likely reflects the interplay between different sugar modifications within the same sequence context, suggesting a modulation of structural or dynamic properties due to the combination of 2'-F and 2'-*O*-Me substitutions.

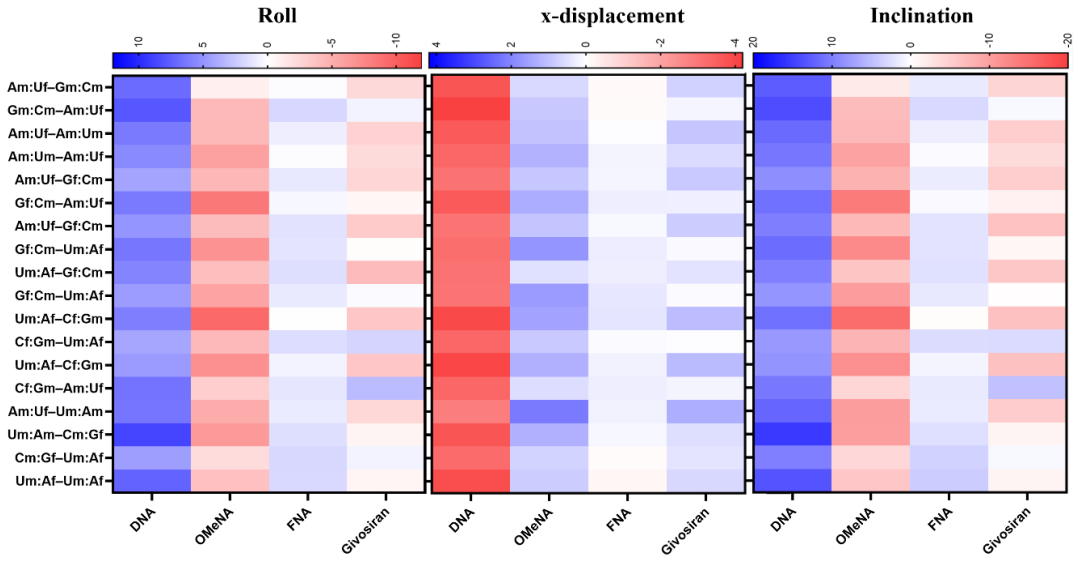

Figure 2.8: Heatmaps of the deviations in the key structural parameters of modified nucleic acids relative to canonical RNA of Givosiran nucleobase sequence. Each row represents the difference between RNA and the modified nucleic acids in the columns. Blue shows a positive value difference, while red shows a negative value difference.

This is supported by a previous experiment that suggested that a 21-nt siRNA with alternating 2'-*O*-Me/2'-F modification is an attractive design for creating functionally active duplexes.[42,43] The simulation data highlights that the presence of diverse modifications better fine-tunes the duplex structure than unmodified duplex, leading to overall structural parameters distinct from OMeNA (unlike Patisiran). In fact, as shown in Table 2.2, the rise per base pair of the FNA duplex is higher than that of the canonical RNA duplex, while the OMeNA duplex has a lower value. The rise per base pair for the Givosiran duplex falls between those of OMeNA and FNA, and most closely resembles that of canonical RNA than either modified duplex. This observation is consistent with the heat map patterns described above, which reflects the local structural influences of sugar modifications.

To further investigate how differences in nucleotide flexibility and local helical parameters affect the global conformation of the duplexes, we evaluated the RoG as a measure of the overall structural compactness (Figure 2.7b). The canonical RNA, FNA, and Givosiran duplexes exhibit comparable RoG values of 32.8 ± 1.1 Å, 33.0 ± 1.3 Å, and 31.4 ± 1.2 Å, respectively, indicating similar global structural compactness. In contrast, the OMeNA duplex shows a markedly lower RoG (28.0 ± 0.4 Å), consistent with a more compact helical structure as observed for the Patisiran nucleobase sequence context. Hence, the RoG of Givosiran again falls between those of FNA and OMeNA, supporting the conclusion that the combined effects of 2'-*O*-Me and 2'-F modifications result in local and global structural properties that are intermediate to those for either fully modified duplex.

The above analysis suggests that since Givosiran incorporates both 2'-*O*-Me and 2'-F modifications, the drug does not attain the same level of structural compaction as OMeNA. This must be attributed to the presence of the 2'-F residues, which modulate the local flexibility and prevent rigidity associated with a uniform 2'-*O*-Me substitution pattern.

This observation is further supported by the RMSF (Figure 2.7a), where Givosiran exhibits nucleotide fluctuation patterns more closely aligned with canonical RNA and FNA than OMeNA, reflecting the dynamic influence of the 2'-F modifications. Additionally, representative structures from the MD simulations reinforce this conclusion (Figure 2.9), showing high structural similarity between Givosiran and canonical RNA. Canonical RNA and FNA also show striking similarities, whereas OMeNA retains a distinct, more condensed conformation. These observations are corroborated by multiple structural metrics, including the rise per base pair (Table 2.2), RMSF (Figure 2.7a), and RoG (Figure 2.7b), which collectively demonstrate that Givosiran adopts a more RNA-like global conformation despite containing 2'-*O*-Me chemical modifications, largely due to the simultaneous presence of 2'-F substitutions.

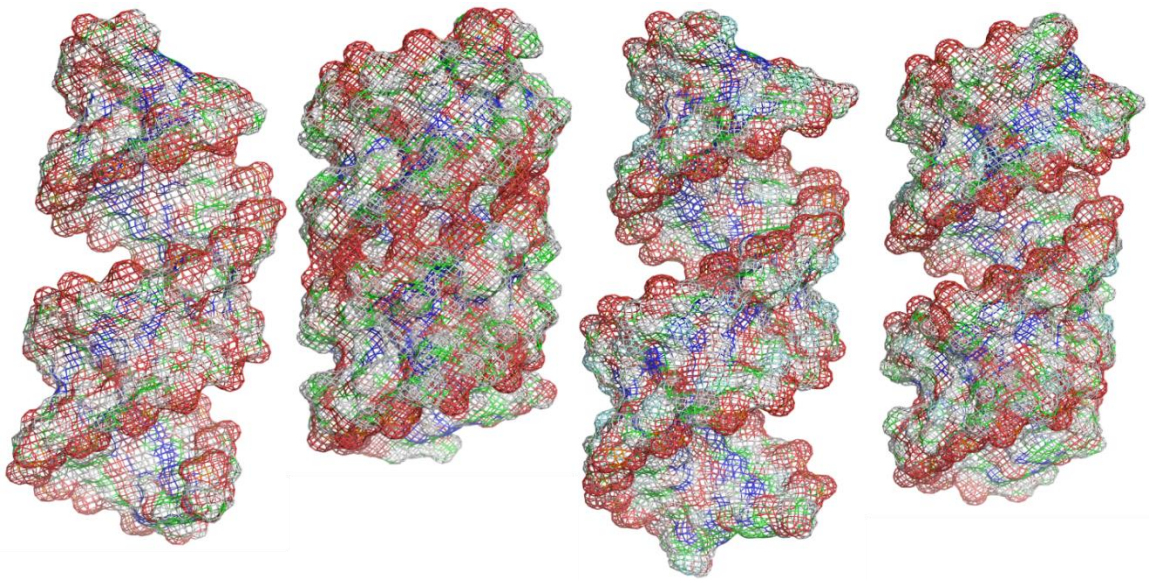

Figure 2.9: Global structure of RNA, OMeNA, FNA, and Givosiran (L-R).

Similar analyses of Lumasiran, Inclisiran, and Vutrisiran support the conclusions drawn for Givosiran (Figure 2.10), primarily due to their modification patterns involving a combination of 2'-*O*-Me and 2'-F substitutions. Among the siRNA drug sequences

analyzed, the modification patterns associated with the drugs exhibit the most conformationally confined sugar puckers, indicating a stronger preference for the C3'-*endo* conformation compared to duplexes containing only 2'-*O*-Me or 2'-F modifications (Appendix, Figure A.3). OMeNA remains structurally distinct from all other modified analogues (Appendix, Figure A.4), whereas there are no substantial structural differences among canonical RNA, drugs, and FNA (Appendix, Figure A.3). Furthermore, the chemical modification patterns impart distinct structural fingerprints in the heatmaps (Figure 2.10 and Appendix, Figure A.5), which are characteristic of each drug sequence, as seen for Givosiran. For instance, the roll parameter of Lumasiran in Figure 2.10 highlights the impact of 2′-F modifications at specific positions from the 5′-end of the antisense strand such as positions 2, 6, and 8, which correspond to the bottom rows moving upward in the Lumasiran column.

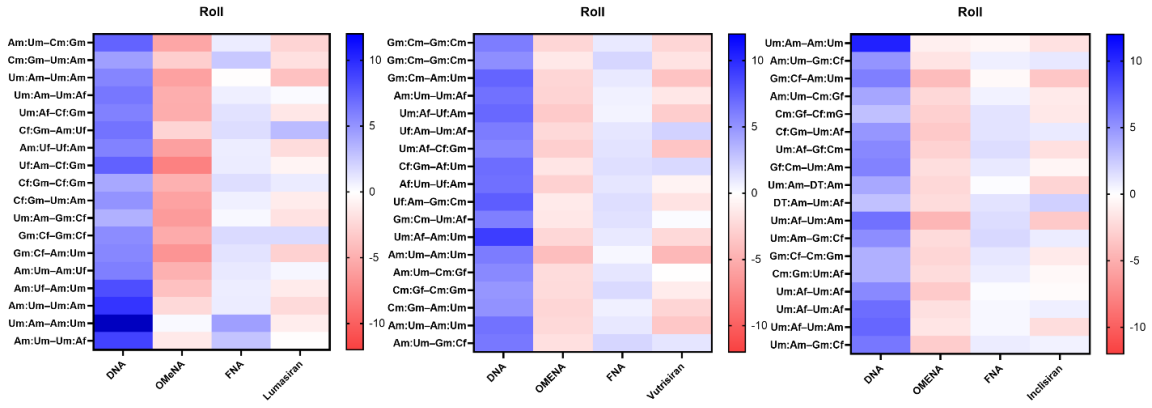

Figure 2.10: Representative heatmaps of the deviations in the key structural parameters of modified nucleic acids relative to canonical RNA for Lumasiran, Vutrisiran and Inclisiran. Each row represents the difference between RNA and the modified nucleic acids in the columns. Blue shows a positive value difference, while red shows a negative value difference.

The primary difference between Patisiran and the other FDA approved drugs is the absence of 2'-F modifications, which are a significant feature in the modification sequence of the remaining four approved drugs. The heatmaps reveal that the color gradients for these

drug sequences are generally less intense than those for Patisiran, indicating reduced deviations in roll, x-displacement, and inclination from the RNA baseline across many base pairs. This further underscores that there is a synergistic effect between 2'-*O*-Me and 2'-F modifications in Givosiran, Lumasiran, Inclisiran, and Vutrisiran that reduces the structural deviation from canonical RNA arising from the 2'-*O*-Me modifications. Indeed, 2'-F appears to counterbalance the rigidity introduced by 2'-*O*-Me into the structural features of RNA, resulting in a global structure closer to the RNA baseline.

2.3.4 Structural Impacts of 2'-*O*-Me and 2'-F Modifications on Canonical Duplex are Nucleobase Sequence Independent

To validate the consistency and significance of the combined effects of 2'-*O*-Me and 2'-F and the unique structural fingerprints observed in the structural parameter heatmaps for Givosiran, Lumasiran, Inclisiran, and Vutrisiran, which we hypothesise is due to modification pattern, we evaluated the impact of different sugar modification patterns across various nucleobase sequence contexts. Specifically, the structural parameters of Patisiran, which is the only FDA-approved siRNA drug lacking 2′-F modifications were compared to those of duplexes, that retain the nucleobase sequence of Patisiran but adopt the modification patterns of Givosiran, Lumasiran, Inclisiran, and Vutrisiran, respectively (denoted Pati-Givo, Pati-Luma, Pati-Incli, and Pati-Vutri). The resulting heatmaps of the deviations in structural parameters of the modified nucleic acids relative to canonical RNA demonstrate that combinations of 2'-*O*-Me and 2'-F modifications induce characteristic and reproducible structural changes that are largely sugar modification dependent, but sequence independent (Figures 2.11 and 2.12). Interestingly, the deviation in structural parameters from RNA for Patisiran are very different from those of its analogs (Pati-Givo, Pati-Luma,

Pati-Incli, and Pati-Vutri), where the nucleobase sequence remains constant, but the modification pattern differs (Figure 2.11). In contrast, each Patisiran variant exhibits changes in the RNA structural parameter that closely resemble those of the clinically-approved drug that shares the identical modification pattern (Figure 2.12). This reinforces the previous conclusion that the specific structural impacts of 2'-*O*-Me and 2'-F modifications on the canonical RNA duplex are primarily driven by the modification pattern, generating a distinct fingerprint that is independent of the underlying nucleotide sequence.

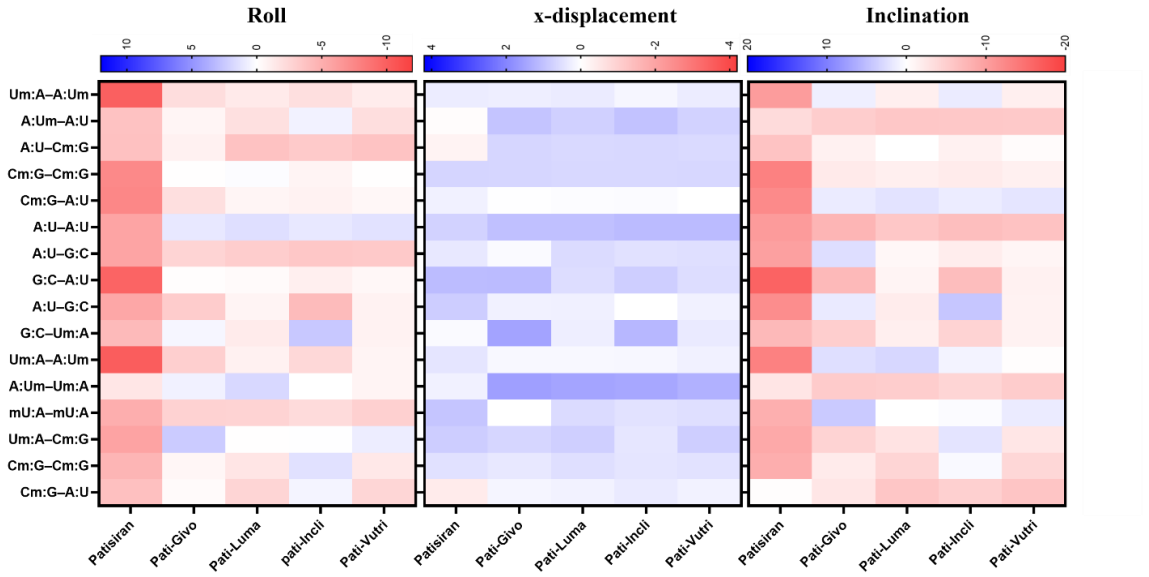

Figure 2.11: Heatmaps of the deviations in the key structural parameters of Patisiran analogs relative to Patisiran. Each row represents the difference between RNA and the Patisiran analogs in the columns. Blue shows a positive value difference, while red shows a negative value difference.

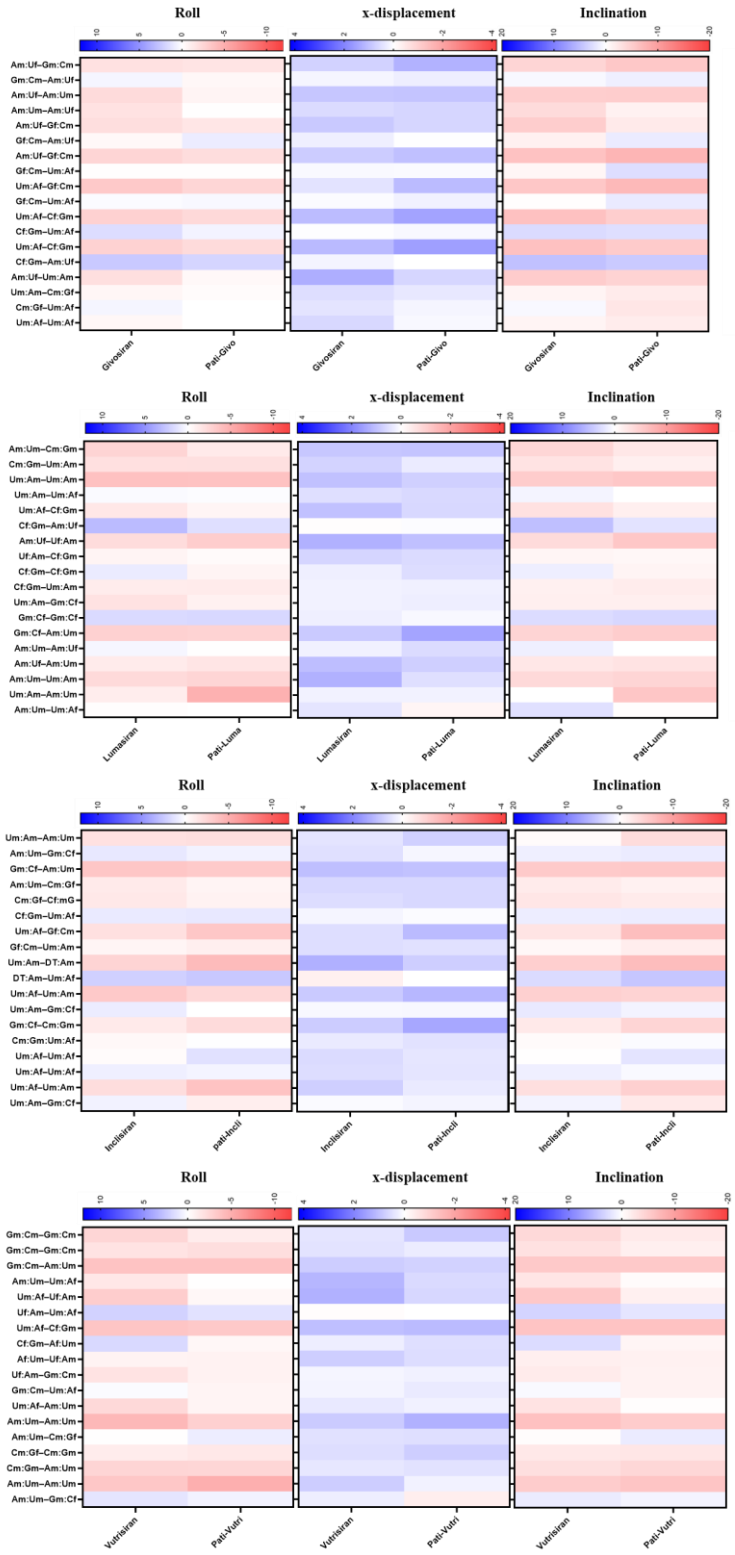

Figure 2.12: Heatmaps of the deviations in the key structural parameters of Patisiran analogs relative to the drugs. Each row represents the difference between RNA and the Patisiran analog in the columns. Blue shows a positive value difference, while red shows a negative value difference.

2.4 Discussion

Our results indicate that the 2'-*O*-Me and 2'-F modifications considered in this study result in A-form helices with differentially altered structural characteristics compared to RNA duplexes. This finetuning of RNA structure can be critical for interactions with the RISC to effectively mediate RNAi.[4,6,42,44,100] The full 2'-*O*-Me modification in OMeNA induces a more rigid structure (Figure 2.3, 2.5, 2.7 and 2.9), effectively "squishing" the RNA duplex into a more compact conformation. Previous experiments showed that 2'-*O*-methylation may confer some subtle changes in the helix geometry, the stacking interactions and the rigidity of the backbone of polyadenine.[101] This rigidity could reduce the conformational flexibility that is necessary for RISC recognition and activity, thereby could impair RNAi functionality. This observation is supported by prior experimental findings showing that incorporation of 2'-*O*-Me nucleotides into either the sense or antisense strand of siRNA significantly reduced Enhanced Green Fluorescent Protein (EGFP) gene silencing to ~25% or ~16%, respectively, while fully 2'-*O*-Me-modified siRNA duplexes completely abolished RNAi activity. [10, 42, 44]

In contrast, FNA introduces a degree of fluctuation in the sugar pucker distribution of the RNA duplex and disrupts the helical geometry. Our simulations demonstrated that FNA exhibits a more diverse distribution of sugar pucker conformations, sampling both C2'-*endo* and C3'-*endo* puckers, which may increase the structural instability of the duplex However, when distance restraints were applied to maintain base pairing during molecular dynamics (MD) simulations (see Methods and Appendix A.1), the structural properties of the FNA duplex closely resembled those of a canonical RNA duplex. Supporting this observation, previous studies have shown that fully 2′-F-modified RNA octamers can adopt structures similar to native RNA.[45] Although crystallization of a fully 2′-F-modified RNA

octamer was reported, the crystallization of another octamer diffracted only to low resolution, and attempts to improve crystal quality or obtain alternative crystal forms were unsuccessful.[45] Notably, while 2′-F modifications have been shown to enhance siRNA duplex efficacy in cells,[46] such studies typically involved only partial modifications, unlike the fully modified FNA duplex investigated here.

Interestingly, we observed synergistic structural effects when a mixture of 2'-F and 2'-*O*-Me modifications are included in a duplex. It was found that siRNA duplex with a mixture of 2'-F and 2'-*O*-Me modifications can have greater stability in serum and improved *in vivo* performance.[42,43,47] In fact, the heatmaps provide a striking visual representation of the structural fingerprints associated with 2'-F and 2'-*O*-Me modifications. Each modification results in distinct deviations from the canonical RNA baseline, allowing the structural influence of these modifications to be tracked in a quantitative manner. The heatmap for FNA showed minimal deviation from RNA, suggesting that the 2'-F modification alone preserves much of the duplex characteristics of RNA. This is supported by previous experiments that proposed no structural differences between canonical RNA and 2'-F-modified RNA.[40,45] This finding was particularly evident in the roll, x-displacement and inclination parameters, which are crucial for defining the helical structure of nucleic acids. In contrast, the heatmap for OMeNA displays a more pronounced effect on the RNA baseline in roll, x-displacement and inclination parameters, indicating that the 2'-*O*-Me more significantly alters the duplex structure. In addition, the introduction of 2'-*O*-Me into the RNA duplex confers structural rigidity to the duplex.

Since Patisiran contains only 2'-*O*-Me modifications and canonical RNA nucleotides, the Patisiran heatmap showed similarity to that of OMeNA. In contrast, the combination of 2'-*O*-Me and 2'-F modifications in siRNA therapeutics like Givosiran,

Lumasiran, Inclisiran and Vutrisiran fine-tunes the duplex structure in a way that more closely preserves RNA-like structural properties than duplexes containing only a single type of modification. This suggests that the 2'-F modification moderates the structural alteration (increased conformational rigidity and compactness) and the larger deviations in key structural parameters induced by 2'-*O*-Me. This, in turn, may enhance the ability of the duplex to interact with RISC and contribute to the conformational flexibility required for effective RNAi.[34,43] Most importantly, the combination of 2'-*O*-Me and 2'-F modified nucleotides leads to a unique structural fingerprint for each modification pattern. This distinction in the heatmaps for each drug underscores the subtle, but critical differences between the modifications and their combined effects on RNA structure.

A particularly interesting aspect of our study is the sequence independence of the structural changes induced by the 2'-*O*-Me and 2'-F modifications. By comparing different RNA duplexes with varying nucleobase sequences but enforcing the same modification patterns, we found that the structural changes observed for a given drug, particularly in parameters such as roll, inclination and x-displacement, were primarily driven by the sequence of chemical modifications. This sequence independence highlights the robustness of modifications to influence RNA structure. This finding is important for the design of siRNA therapeutics, as it suggests that the effectiveness of 2'-*O*-Me and 2'-F modifications may be generalized across various nucleobase sequences. This insight could streamline the design of future RNA therapeutics by focusing on the modification pattern rather than individual sequence variations.

2.5 Conclusion

Our study highlights the significant structural consequences of 2'-*O*-Me and 2'-F

modifications and modification patterns on RNA duplexes, including the synergistic influences. The uniform modification of RNA duplexes with 2'-*O*-Me or 2'-F has a clear impact on structural features such as sugar puckers and helical parameters, which can either enhance or diminish structural dynamics of RNA. Importantly, the distinct fingerprint observed in the duplex structural features according to the 2'-modification pattern provides a valuable tool to predict how specific modifications and modification patterns influence RNA structure and function, paving the way for the design of more effective siRNA-based therapeutics. Finally, the sequence independence of these structural changes suggests that these modifications have broad applicability across different siRNA sequences, pointing to a simplified design process for RNA therapeutics.

2.6 References

(1) Fire, A., Xu, SiQun, Montgomery, Mary K., Kostas, Steven A., Driver, Samuel E., Mello, Craig C. Potent and specific genetic interference by double-stranded RNA in Caenorhabditis elegans. *Nature* **1998**, *391* (6669), 806-811.
(2) Czauderna, F.; Fechtner, M.; Dames, S.; Aygun, H.; Klippel, A.; Pronk, G. J.; Giese, K.; Kaufmann, J. Structural variations and stabilising modifications of synthetic siRNAs in mammalian cells. *Nucleic Acids Res.* **2003**, *31* (11), 2705-2716.
(3) Hannon, G. J.; Rossi, J. J. Unlocking the potential of the human genome with RNA interference. *Nature* **2004**, *431* (7006), 371-378.
(4) Kim, D.; Rossi, J. RNAi mechanisms and applications. *Biotechniques* **2008**, *44* (5), 613-616.
(5) Setten, R. L.; Rossi, J. J.; Han, S.-p. The current state and future directions of RNAi-based therapeutics. *Nat. Rev. Drug Discov.* **2019**, *18* (6), 421-446.
(6) Ku, S. H.; Jo, S. D.; Lee, Y. K.; Kim, K.; Kim, S. H. Chemical and structural modifications of RNAi therapeutics. *Adv. Drug Deliv. Rev.* **2016**, *104*, 16-28.
(7) Hannon, G. J. RNA interference. *Nature* **2002**, *418* (6894), 244-251.
(8) Napoli, C.; Lemieux, C.; Jorgensen, R. Introduction of a Chimeric Chalcone Synthase Gene into Petunia Results in Reversible Co-Suppression of Homologous Genes in trans. *The Plant Cell.* **1990**, *2* (4), 279-289.
(9) Hu, B.; Zhong, L.; Weng, Y.; Peng, L.; Huang, Y.; Zhao, Y.; Liang, X. J. Therapeutic siRNA: state of the art. *Signal Transduct. Target. Ther.* **2020**, *5* (1), 101.
(10) Behlke, M. A. Chemical modification of siRNAs for in vivo use. *Oligonucleotides* **2008**, *18* (4), 305-319.
(11) Elbashir, S. M.; Lendeckel, W.; Tuschl, T. RNA interference is mediated by 21- and 22-nucleotide RNAs. *Genes Dev.* **2001**, *15* (2), 188-200.

(12) Dykxhoorn, D. M.; Novina, C. D.; Sharp, P. A. Killing the messenger: short RNAs that silence gene expression. *Nat. Rev. Mol. Cell Biol.* **2003**, *4* (6), 457-467.
(13) Elbashir, S., Harborth, J., Lendeckel, W., Yalcin, A., Weber, K., Tuschl, T. Duplexes of 21-nucleotide RNAs mediate RNA interference in cultured mammalian cells. *Nature* **2001**, *411* (6836), 494-498.
(14) Zamore, P. D.; Tuschl, T.; Sharp, P. A.; Bartel, D. P. RNAi: double-stranded RNA directs the ATP-dependent cleavage of mRNA at 21 to 23 nucleotide intervals. *Cell* **2000**, *101* (1), 25-33.
(15) Ketting, R. F.; Fischer, S. E.; Bernstein, E.; Sijen, T.; Hannon, G. J.; Plasterk, R. H. Dicer functions in RNA interference and in synthesis of small RNA involved in developmental timing in C. elegans. *Genes Dev.* **2001**, *15* (20), 2654-2659.
(16) Lundin, K. E.; Gissberg, O.; Smith, C. I. Oligonucleotide Therapies: The Past and the Present. *Hum. Gene. Ther.* **2015**, *26* (8), 475-485.
(17) Un Jan Contreras, S.; Redfern, L. K.; Maguire, L. W.; Promi, S. I.; Gardner, C. M. Small Interfering RNAs (siRNAs) Negatively Impact Growth and Gene Expression of Environmentally Relevant Bacteria in In Vitro Conditions. *Environ. Sci. Technol.* **2024**, *58* (31), 13856-13865.
(18) Zhang, M. M.; Bahal, R.; Rasmussen, T. P.; Manautou, J. E.; Zhong, X. B. The growth of siRNA-based therapeutics: Updated clinical studies. *Biochem. Pharmacol.* **2021**, *189*, 114432.
(19) Sajid, M. I.; Moazzam, M.; Kato, S.; Yeseom Cho, K.; Tiwari, R. K. Overcoming Barriers for siRNA Therapeutics: From Bench to Bedside. *Pharmaceuticals* **2020**, *13* (10), 294.
(20) Hickerson, R. P.; Vlassov, A. V.; Wang, Q.; Leake, D.; Ilves, H.; Gonzalez-Gonzalez, E.; Contag, C. H.; Johnston, B. H.; Kaspar, R. L. Stability Study of Unmodified siRNA and Relevance to Clinical Use. *Oligonucleotides* **2008**, *18* (4), 345-354.
(21) Layzer, J. M.; McCaffrey, A. P.; Tanner, A. K.; Huang, Z.; Kay, M. A.; Sullenger, B. A. In vivo activity of nuclease-resistant siRNAs. *RNA.* **2004**, *10* (5), 766-771.
(22) Peacock, H.; Kannan, A.; Beal, P. A.; Burrows, C. J. Chemical modification of siRNA bases to probe and enhance RNA interference. *J. Org. Chem.* **2011**, *76* (18), 7295-7300.
(23) Deleavey, G. F.; Damha, M. J. Designing chemically modified oligonucleotides for targeted gene silencing. *Chem. Biol.* **2012**, *19* (8), 937-954.
(24) Bennett, C. F. Therapeutic Antisense Oligonucleotides Are Coming of Age. *Annu. Rev. Med.* **2019**, *70*, 307-321.
(25) Yu, R. Z.; Kim, T.-W.; Hong, A.; Watanabe, T. A.; Gaus, H. J.; Geary, R. S. Cross-Species Pharmacokinetic Comparison from Mouse to Man of a Second-Generation Antisense Oligonucleotide, ISIS 301012, Targeting Human Apolipoprotein B-100. *Drug Metabolism and Disposition* **2007**, *35* (3), 460.
(26) Geselowitz, D. A.; Neckers, L. M. Bovine Serum Albumin Is a Major Oligonucleotide-Binding Protein Found on the Surface of Cultured Cells. *Antisense Research and Development* **1995**, *5* (3), 213-217.
(27) Epanchintseva, A. V.; Poletaeva, J. E.; Dome, A. S.; Dovydenko, I. S.; Pyshnaya, I. A.; Ryabchikova, E. I. Chemical Modifications Influence the Number of siRNA Molecules Adsorbed on Gold Nanoparticles and the Efficiency of Downregulation of a Target Protein. *Nanomaterials (Basel)* **2022**, *12* (24).

(28) Varley, A. J.; Hammill, M. L.; Salim, L.; Desaulniers, J. P. Effects of Chemical Modifications on siRNA Strand Selection in Mammalian Cells. *Nucleic Acid Ther.* **2020**, *30* (4), 229-236.
(29) Kraynack, B. A.; Baker, B. F. Small interfering RNAs containing full 2'-O-methylribonucleotide-modified sense strands display Argonaute2/eIF2C2-dependent activity. *RNA.* **2006**, *12* (1), 163-176.
(30) Sponer, J.; Bussi, G.; Krepl, M.; Banas, P.; Bottaro, S.; Cunha, R. A.; Gil-Ley, A.; Pinamonti, G.; Poblete, S.; Jurecka, P.; et al. RNA Structural Dynamics As Captured by Molecular Simulations: A Comprehensive Overview. *Chem. Rev.* **2018**, *118* (8), 4177-4338.
(31) Vandelli, A.; Broglia, L.; Armaos, A.; Delli Ponti, R.; Tartaglia, G. G. Rationalizing the effects of RNA modifications on protein interactions. *Mol. Ther. Nucleic Acids* **2024**, *35* (4), 102391.
(32) Koseki, J.; Konno, M.; Asai, A.; Horie, N.; Tsunekuni, K.; Kawamoto, K.; Obika, S.; Doki, Y.; Mori, M.; Ishii, H. Theoretical analyses and experimental validation of the effects caused by the fluorinated substituent modification of DNA. *Scientific Reports* **2020**, *10* (1).
(33) Das, G.; Harikrishna, S.; Gore, K. R. Investigating the Effect of Chemical Modifications on the Ribose Sugar Conformation, Watson-Crick Base Pairing, and Intrastrand Stacking Interactions: A Theoretical Approach. *J. Phys. Chem. B* **2024**, *128* (35), 8313-8331.
(34) Das, G.; Harikrishna, S.; Gore, K. R. Influence of Sugar Modifications on the Nucleoside Conformation and Oligonucleotide Stability: A Critical Review. *Chem. Rec.* **2022**, *22* (12), e202200174.
(35) Gangopadhyay, S.; Gore, K. R. Advances in siRNA therapeutics and synergistic effect on siRNA activity using emerging dual ribose modifications. *RNA Biol.* **2022**, *19* (1), 452-467.
(36) Sahoo, A.; Gupta, S.; Das, G.; Ghosh, A.; Bagale, S. S.; Sinha, S.; Gore, K. R. 2'-O-Alkyl-N (3)-Methyluridine Functionalized Passenger Strand Improves RNAi Activity by Modulating the Thermal Stability. *ACS Med. Chem. Lett.* **2024**, *15* (8), 1250-1259.
(37) Shukla, S.; Sumaria, C. S.; Pradeepkumar, P. I. Exploring chemical modifications for siRNA therapeutics: a structural and functional outlook. *ChemMedChem* **2010**, *5* (3), 328-349.
(38) Egli, M.; Manoharan, M. Re-Engineering RNA Molecules into Therapeutic Agents. *Acc. Chem. Res.* **2019**, *52* (4), 1036-1047.
(39) Egli, M.; Manoharan, M. Chemistry, structure and function of approved oligonucleotide therapeutics. *Nucleic Acids Res.* **2023**, *51* (6), 2529-2573.
(40) Egli, M.; Pallan, P. S. Crystallographic studies of chemically modified nucleic acids: a backward glance. *Chem. Biodivers.* **2010**, *7* (1), 60-89.
(41) Sun, Y.; Zhao, Y.; Zhao, X.; Lee, R. J.; Teng, L.; Zhou, C. Enhancing the Therapeutic Delivery of Oligonucleotides by Chemical Modification and Nanoparticle Encapsulation. *Molecules* **2017**, *22* (10).
(42) Chiu, Y. L.; Rana, T. M. siRNA function in RNAi: a chemical modification analysis. *RNA.* **2003**, *9* (9), 1034-1048.
(43) Allerson, C. R.; Sioufi, N.; Jarres, R.; Prakash, T. P.; Naik, N.; Berdeja, A.; Wanders, L.; Griffey, R. H.; Swayze, E. E.; Bhat, B. Fully 2'-modified oligonucleotide duplexes with improved in vitro potency and stability compared to unmodified small interfering RNA. *J. Med. Chem.* **2005**, *48* (4), 901-904.

(44) Ya-Lin Chiu, T. M. R. RNAi in Human Cells: Basic Structural and Functional Features of Small Interfering RNA. *Mol. Cell* **2002**, *Volume 10* (Issue 3), Pages 549-561.
(45) Pallan, P. S.; Greene, E. M.; Jicman, P. A.; Pandey, R. K.; Manoharan, M.; Rozners, E.; Egli, M. Unexpected origins of the enhanced pairing affinity of 2'-fluoro-modified RNA. *Nucleic Acids Res.* **2011**, *39* (8), 3482-3495.
(46) Manoharan, M.; Akinc, A.; Pandey, R. K.; Qin, J.; Hadwiger, P.; John, M.; Mills, K.; Charisse, K.; Maier, M. A.; Nechev, L.; et al. Unique gene-silencing and structural properties of 2'-fluoro-modified siRNAs. *Angew. Chem. Int. Ed. Engl.* **2011**, *50* (10), 2284-2288.
(47) Morrissey, D. V.; Lockridge, J. A.; Shaw, L.; Blanchard, K.; Jensen, K.; Breen, W.; Hartsough, K.; Machemer, L.; Radka, S.; Jadhav, V.; et al. Potent and persistent in vivo anti-HBV activity of chemically modified siRNAs. *Nat. Biotechnol.* **2005**, *23* (8), 1002-1007.
(48) Janas, M. M.; Schlegel, M. K.; Harbison, C. E.; Yilmaz, V. O.; Jiang, Y.; Parmar, R.; Zlatev, I.; Castoreno, A.; Xu, H.; Shulga-Morskaya, S.; et al. Selection of GalNAc-conjugated siRNAs with limited off-target-driven rat hepatotoxicity. *Nat. Commun.* **2018**, *9* (1), 723.
(49) Elmen, J.; Lindow, M.; Schutz, S.; Lawrence, M.; Petri, A.; Obad, S.; Lindholm, M.; Hedtjarn, M.; Hansen, H. F.; Berger, U.; et al. LNA-mediated microRNA silencing in non-human primates. *Nature* **2008**, *452* (7189), 896-899.
(50) Doessing, H.; Vester, B. Locked and unlocked nucleosides in functional nucleic acids. *Molecules* **2011**, *16* (6), 4511-4526.
(51) Mook, O. R.; Baas, F.; de Wissel, M. B.; Fluiter, K. Evaluation of locked nucleic acid–modified small interfering RNA in vitro and in vivo. *Mol. Cancer Ther.* **2007**, *6* (3), 833-843.
(52) Morita, K.; Hasegawa, C.; Kaneko, M.; Tsutsumi, S.; Sone, J.; Ishikawa, T.; Imanishi, T.; Koizumi, M. 2′-O, 4′-C-Ethylene-bridged nucleic acids (ENA) with nuclease-resistance and high affnity for RNA. *Nucleic Acids Symposium Series* **2001**, *1* (1), 241-242.
(53) Prakash, T. P.; Allerson, C. R.; Dande, P.; Vickers, T. A.; Sioufi, N.; Jarres, R.; Baker, B. F.; Swayze, E. E.; Griffey, R. H.; Bhat, B. Positional Effect of Chemical Modifications on Short Interference RNA Activity in Mammalian Cells. *J. Med. Chem.* **2005**, *48* (13), 4247-4253.
(54) Braasch, D. A.; Jensen, S.; Liu, Y.; Kaur, K.; Arar, K.; White, M. A.; Corey, D. R. RNA Interference in Mammalian Cells by Chemically-Modified RNA. *Biochemistry* **2003**, *42* (26), 7967-7975.
(55) Santel, A.; Aleku, M.; Keil, O.; Endruschat, J.; Esche, V.; Fisch, G.; Dames, S.; Löffler, K.; Fechtner, M.; Arnold, W.; et al. A novel siRNA-lipoplex technology for RNA interference in the mouse vascular endothelium. *Gene Therapy* **2006**, *13* (16), 1222-1234.
(56) Choung, S.; Kim, Y. J.; Kim, S.; Park, H.-O.; Choi, Y.-C. Chemical modification of siRNAs to improve serum stability without loss of efficacy. *Biochem. Biophys. Res. Commun.* **2006**, *342* (3), 919-927.
(57) Grünweller, A.; Wyszko, E.; Bieber, B.; Jahnel, R.; Erdmann, V. A.; Kurreck, J. Comparison of different antisense strategies in mammalian cells using locked nucleic acids, 2′-O-methyl RNA, phosphorothioates and small interfering RNA. *Nucleic Acids Res.* **2003**, *31* (12), 3185-3193.
(58) Ali Zaidi, S. S.; Fatima, F.; Ali Zaidi, S. A.; Zhou, D.; Deng, W.; Liu, S. Engineering siRNA therapeutics: challenges and strategies. *J. Nanobiotechnology* **2023**, *21* (1), 381.

(59) Chernikov, I. V.; Ponomareva, U. A.; Chernolovskaya, E. L. Structural Modifications of siRNA Improve Its Performance In Vivo. *Int. J. Mol. Sci.* **2023**, *24* (2).
(60) Jackson, R. W.; Smathers, C. M.; Robart, A. R. General Strategies for RNA X-ray Crystallography. *Molecules* **2023**, *28* (5), 2111.
(61) Bonilla, S. L.; Jang, K. Challenges, advances, and opportunities in RNA structural biology by Cryo-EM. *Curr. Opin. Struct. Biol.* **2024**, *88*, 102894.
(62) Tants, J. N.; Schlundt, A. Advances, Applications, and Perspectives in Small-Angle X-ray Scattering of RNA. *ChemBioChem* **2023**, *24* (17), e202300110.
(63) Zhang, H.; Keane, S. C. Advances that facilitate the study of large RNA structure and dynamics by nuclear magnetic resonance spectroscopy. *Wiley Interdiscip Rev RNA* **2019**, *10* (5), e1541.
(64) Harikrishna, S.; Pradeepkumar, P. I. Probing the Binding Interactions between Chemically Modified siRNAs and Human Argonaute 2 Using Microsecond Molecular Dynamics Simulations. *J. Chem. Inf. Model.* **2017**, *57* (4), 883-896.
(65) Matsuda, S.; Bala, S.; Liao, J. Y.; Datta, D.; Mikami, A.; Woods, L.; Harp, J. M.; Gilbert, J. A.; Bisbe, A.; Manoharan, R. M.; et al. Shorter Is Better: The alpha-(l)-Threofuranosyl Nucleic Acid Modification Improves Stability, Potency, Safety, and Ago2 Binding and Mitigates Off-Target Effects of Small Interfering RNAs. *J. Am. Chem. Soc.* **2023**, *145* (36), 19691-19706.
(66) Uppuladinne, M. V. N.; Koulgi, S.; Jani, V.; Sonavane, U.; Joshi, R. Unlocking the potential of RNAi as a therapeutic strategy against infectious viruses: an in-silico study. *Chem. Pap.* **2023**, *78* (3), 1537-1552.
(67) Pettersen, E. F.; Goddard, T. D.; Huang, C. C.; Couch, G. S.; Greenblatt, D. M.; Meng, E. C.; Ferrin, T. E. UCSF Chimera--a visualization system for exploratory research and analysis. *J. Comput. Chem.* **2004**, *25* (13), 1605-1612.
(68) *GaussView, Version 6.0.16*; 2019. (accessed.
(69) Kuhrova, P.; Mlynsky, V.; Zgarbova, M.; Krepl, M.; Bussi, G.; Best, R. B.; Otyepka, M.; Sponer, J.; Banas, P. Improving the Performance of the Amber RNA Force Field by Tuning the Hydrogen-Bonding Interactions. *J. Chem. Theory. Comput.* **2019**, *15* (5), 3288-3305.
(70) Zgarbova, M.; Sponer, J.; Otyepka, M.; Cheatham, T. E., 3rd; Galindo-Murillo, R.; Jurecka, P. Refinement of the Sugar-Phosphate Backbone Torsion Beta for AMBER Force Fields Improves the Description of Z- and B-DNA. *J. Chem. Theory Comput.* **2015**, *11* (12), 5723-5736.
(71) Vanquelef, E.; Simon, S.; Marquant, G.; Garcia, E.; Klimerak, G.; Delepine, J. C.; Cieplak, P.; Dupradeau, F. Y. R.E.D. Server: a web service for deriving RESP and ESP charges and building force field libraries for new molecules and molecular fragments. *Nucleic Acids Res.* **2011**, *39* (Web Server issue), W511-517.
(72) Dupradeau, F. Y.; Pigache, A.; Zaffran, T.; Savineau, C.; Lelong, R.; Grivel, N.; Lelong, D.; Rosanski, W.; Cieplak, P. The R.E.D. tools: advances in RESP and ESP charge derivation and force field library building. *Phys. Chem. Chem. Phys.* **2010**, *12* (28), 7821-7839.
(73) Wang, J.; Wolf, R. M.; Caldwell, J. W.; Kollman, P. A.; Case, D. A. Development and testing of a general amber force field. *J. Comput. Chem.* **2004**, *25* (9), 1157-1174.
(74) Case, D. A. B., K.; Ben-Shalom, I. Y.; Brozell, S. R.; Cerutti, D. S.; Cheatham III, T. E.; Cruzeiro, V. W. D.; Darden, T. A.; Duke, R. E.; Giambasu, G.; Gilson, M. K.; Gohlke, H.; Goetz, A. W.; Harris, R.; Izadi, S.; Izmailov, S. A.; Kasavajhala, K.; Kovalenko, A.;

Krasny, R.; Kurtzman, T.; Lee, T. S.; LeGrand, S.; Li, P.; Lin, C.; Liu, J.; Luchko, T.; Machado, M.; Man, V.; Merz, K. M.; Miao, Y.; Mikhailovskii, O.; Monard, G.; Nguyen, H.; Onufriev, A.; Pan, F.; Pantano, S.; Qi, R.; Rahaman, O.; Roitberg, A.; Sagui, C.; Schott-Verdugo, S.; Shajan, A.; Shen, J.; Simmerling, C. L.; Skrynnikov, N. R.; Smith, J.; Swails, J.; Walker, R. C.; Wang, J.; Wilson, L.; Wolf, R. M.; Wu, X.; Xue, Y.; York, D. M.; Zhu, Y. Amber 2021. *University of California, San Francisco.* **2021**.
(75) Jorgensen, M. A five-site model for liquid water and the reproduction of the density anomaly by rigid, nonpolarizable potential functions. *J. Chem. Phys.* **2000**, *112*, 8910-8922.
(76) Jorgensen, W. L.; Chandrasekhar, J.; Madura, J. D.; Impey, R. W.; Klein, M. L. Comparison of simple potential functions for simulating liquid water. *J. Chem. Phys.* **1983**, *79* (2), 926-935.
(77) Mark, P.; Nilsson, L. Structure and Dynamics of the TIP3P, SPC, and SPC/E Water Models at 298 K. *J. Phys. Chem. A.* **2001**, *105* (43), 9954-9960.
(78) Schmit, J.; Kariyawasam, N.; Needham, V.; Smith, P. SLTCAP: A simple method for calculating the number of ions needed for MD simulation. *J. Chem. Theory Comput.* **2018**, *14*.
(79) Pastor, R. W.; Brooks, B. R.; Szabo, A. An analysis of the accuracy of Langevin and molecular dynamics algorithms. *Mol. Phys.* **1988**, *65* (6), 1409-1419.
(80) Schneider, T.; Stoll, E. Molecular-dynamics study of a three-dimensional one-component model for distortive phase transitions. *Phys. Rev. B* **1978**, *17* (3), 1302-1322.
(81) Berendsen, H. J. C.; Postma, J. P. M.; van Gunsteren, W. F.; DiNola, A.; Haak, J. R. Molecular dynamics with coupling to an external bath. *J. Chem. Phys.* **1984**, *81* (8), 3684-3690.
(82) Essmann, U.; Perera, L.; Berkowitz, M. L.; Darden, T.; Lee, H.; Pedersen, L. G. A smooth particle mesh Ewald method. *J. Chem. Phys.* **1995**, *103* (19), 8577-8593.
(83) Darden, T.; York, D.; Pedersen, L. Particle mesh Ewald: An N·log(N) method for Ewald sums in large systems. *J. Chem. Phys.* **1993**, *98* (12), 10089-10092.
(84) Macuglia, D. SHAKE and the exact constraint satisfaction of the dynamics of semi-rigid molecules in Cartesian coordinates, 1973–1977. *Archive for History of Exact Sciences* **2023**, *77* (4), 345-371.
(85) Roe, D. R.; Cheatham, T. E., 3rd. PTRAJ and CPPTRAJ: Software for Processing and Analysis of Molecular Dynamics Trajectory Data. *J. Chem. Theory Comput.* **2013**, *9* (7), 3084-3095.
(86) Bottaro, S.; Bussi, G.; Pinamonti, G.; Reisser, S.; Boomsma, W.; Lindorff-Larsen, K. Barnaba: software for analysis of nucleic acid structures and trajectories. *RNA.* **2019**, *25* (2), 219-231.
(87) Knappeova, B.; Mlynsky, V.; Pykal, M.; Sponer, J.; Banas, P.; Otyepka, M.; Krepl, M. Comprehensive Assessment of Force-Field Performance in Molecular Dynamics Simulations of DNA/RNA Hybrid Duplexes. *J. Chem. Theory. Comput.* **2024**, *20* (15), 6917-6929.
(88) Lu, X. J.; Olson, W. K. 3DNA: a software package for the analysis, rebuilding and visualization of three-dimensional nucleic acid structures. *Nucleic Acids Res.* **2003**, *31* (17), 5108-5121.
(89) Babcock, M. S.; Pednault, E. P. D.; Olson, W. K. Nucleic Acid Structure Analysis: Mathematics for Local Cartesian and Helical Structure Parameters That Are Truly Comparable Between Structures. *J. Mol. Biol.* **1994**, *237* (1), 125-156.

(90) Olson, W. K.; Bansal, M.; Burley, S. K.; Dickerson, R. E.; Gerstein, M.; Harvey, S. C.; Heinemann, U.; Lu, X. J.; Neidle, S.; Shakked, Z.; et al. A standard reference frame for the description of nucleic acid base-pair geometry. *J. Mol. Biol.* **2001**, *313* (1), 229-237.
(91) Galindo-Murillo, R.; Roe, D. R.; Cheatham, T. E. On the absence of intrahelical DNA dynamics on the μs to ms timescale. *Nat. Commun.* **2014**, *5* (1), 5152.
(92) Anosova, I.; Kowal, E. A.; Sisco, N. J.; Sau, S.; Liao, J.-y.; Bala, S.; Rozners, E.; Egli, M.; Chaput, J. C.; Van Horn, W. D. Structural Insights into Conformation Differences between DNA/TNA and RNA/TNA Chimeric Duplexes. *ChemBioChem* **2016**, *17* (18), 1705-1708.
(93) Lavery, R.; Zakrzewska, K.; Beveridge, D.; Bishop, T. C.; Case, D. A.; Cheatham, T., III; Dixit, S.; Jayaram, B.; Lankas, F.; Laughton, C.; et al. A systematic molecular dynamics study of nearest-neighbor effects on base pair and base pair step conformations and fluctuations in B-DNA. *Nucleic Acids Res.* **2009**, *38* (1), 299-313.
(94) Zhang, X.; Goel, V.; Robbie, G. J. Pharmacokinetics of Patisiran, the First Approved RNA Interference Therapy in Patients With Hereditary Transthyretin-Mediated Amyloidosis. *J. Clin. Pharmacol.* **2020**, *60* (5), 573-585.
(95) Levitt, M. How many base-pairs per turn does DNA have in solution and in chromatin? Some theoretical calculations. *PNAS* **1978**, *75* (2), 640-644.
(96) Vesley, P. Molecular biology of the cell: A problems approach, 4th edition. By John Wilson and Tim Hunt, Pavel Vesely, Garland Sciences, New York, 2002, ISBN0-8153–3577–6; paperback; 550 pages; $35.95. *Scanning* **2004**, *26* (4), 206-206.
(97) Minchin, S.; Lodge, J. Understanding biochemistry: structure and function of nucleic acids. *Essays Biochem.* **2019**, *63* (4), 433-456.
(98) Parsons, M. F.; Allan, M. F.; Li, S.; Shepherd, T. R.; Ratanalert, S.; Zhang, K.; Pullen, K. M.; Chiu, W.; Rouskin, S.; Bathe, M. 3D RNA-scaffolded wireframe origami. *Nat. Commun.* **2023**, *14* (1), 382.
(99) Ng, H.-L.; Kopka, M. L.; Dickerson, R. E. The structure of a stable intermediate in the A ↔ B DNA helix transition. *PNAS* **2000**, *97* (5), 2035-2039.
(100) Miyoshi, T.; Ito, K.; Murakami, R.; Uchiumi, T. Structural basis for the recognition of guide RNA and target DNA heteroduplex by Argonaute. *Nat. Commun.* **2016**, *7*, 11846.
(101) Bobst, A. M.; Rottman, F.; Cerutti, P. A. Effect of the methylation of the 2′-hydroxyl groups in polyadenylic acid on its structure in weakly acidic and neutral solutions and on its capability to form ordered complexes with polyuridylic acid. *J. Mol. Biol.* **1969**, *46* (2), 221-234.

CHAPTER 3: IMPACT OF CHEMICAL MODIFICATIONS ON siRNA INTERACTIONS WITH hAGO2

3.1 Introduction

Argonaute proteins are the central effectors of RNA-induced silencing complexes (RISCs) that use the sequence information of small regulatory RNAs (typically 21 to 23 nucleotides in length) to recognize, bind, and silence complementary target RNAs.[1-9] Argonaute proteins are part of a highly conserved gene family found across plant and animal genomes. They are especially amplified in the nematode C*aenorhabditis elegans*, which encode at least 26 distinct genes belonging to the Argonaute family.[10] Among the Argonaute family, Argonaute-2 (Ago2) is the only member with endonucleolytic activity, making it a critical target for therapeutic siRNA design.[11-14]

The Argonaute protein architecture is highly conserved and consists of four characteristic domains: N-terminal, PAZ (PIWI-Argonaute-Zwille), MID (middle), and PIWI.[11, 15] The N-terminal and PAZ domains are connected by the L1 linker, while the PAZ and MID domains are linked via L2.[16] siRNA binding occurs within a cleft formed between the N–PAZ and MID–PIWI lobes (Figure 3.1), with the guide strand being positioned and the mRNA target recognition occurring in this channel.[17]

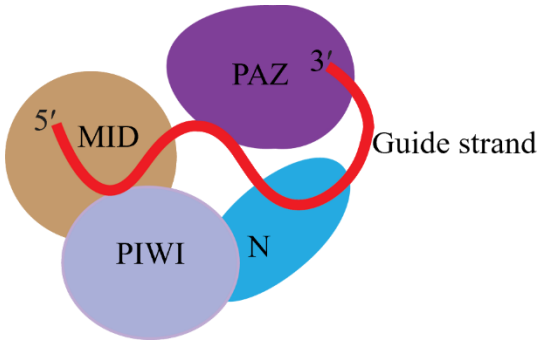

Figure 3.1: Schematic illustration of siRNA guide strand anchored in hAgo2 before complementary binding to target mRNA.

Functionally, the MID domain recognizes the 5'-end of the guide RNA,[18-25] while the PAZ

domain anchors the 3'-end and releases the 3'-end post-target cleavage.[14, 26, 27] Additionally, the N-terminal domain facilitates duplex unwinding,[4,28] while the PIWI domain harbors the catalytic site responsible for target mRNA cleavage.[13,14,22,29] Structural and biochemical studies have shown that the seed region of the guide strand (nucleotides 2–8) is critical for target recognition and binding.[20,29-37] Furthermore, experiments have emphasized that maintaining an A-form helical structure of the siRNA duplex is essential for efficient RNAi activity.[17,32,38,39]

Given the therapeutic promise of siRNA, chemical modifications have been widely applied to enhance the drug-like properties of siRNA.[40-46] For instance, modifications at the 2'-position of ribose (e.g., 2'-*O*-methyl, 2'-fluoro) are commonly found in FDA-approved siRNA therapeutics.[40,47-58] These modifications have been proposed to alter the structural dynamics of siRNA, including duplex geometry, and interactions with RNA-binding proteins, like hAgo2.[40,49,50,52,59-64] However, despite the growing number of FDA-approved siRNA drugs incorporating modifications at the 2'-position of the sugar, the dynamic and structural effects of such modifications on hAgo2–siRNA complexes remain poorly understood.

Molecular dynamics (MD) simulations have emerged as a powerful tool for exploring the structural dynamics of proteins and nucleic acids, and RNA–protein complexes, including those involving chemically-modified nucleic acids,[65-67] thereby providing atomistic insights that complement experimental methods such as X-ray crystallography, NMR, and cryo-EM. In this light, MD simulations have been used to provide an enhanced understanding of the structural dynamics and functional mechanisms of prokaryotic Argonaute proteins, such as *Thermus thermophilus* Argonaute (TtAgo).[68-71] For instance, MD simulations performed using the AMBER force field and SPC water

model with GROMACS revealed that the interdomain motions of the PAZ, MID, and PIWI domains, along with the arginine-rich RNA-binding channel, play essential roles in stabilizing guide RNA interactions and enhancing catalytic activity.[68] All-atom MD simulations conducted with the CHARMM force field and TIP3P water model using the NAMD software package demonstrated that TtAgo can accommodate G:U wobble base pairs and allow seed region mismatches without major structural disruption.[69] The conformational flexibility of the PAZ domain was identified as a key factor in enabling this tolerance. Using MD simulations (CHARMM and implicit solvation, Generalized Born (GB) Model), another study showed that varying Mg^{2+} concentrations modulate the structural flexibility of Ago2.[70] Lower Mg^{2+} levels were found to increase protein dynamics and destabilize the RNA duplex, conditions that favor RNA slicing activity. Furthermore, all-atom MD simulations using the AMBER99SB force field and TIP3P water model performed with GROMACS revealed that guide-strand loading in TtAgo follows an induced-fit mechanism, driven by the flexibility of the L1-PAZ hinge.[71]

In contrast, there are relatively few computational studies focusing on the siRNA–hAgo2 complex. Molecular docking combined with a single 1 μs all-atom MD simulation (without replicas) using the Amber software, χOL3 and FF12SB force fields, and the TIP3P water model was used to investigate RNAi–based therapeutic strategies against SARS-CoV-2.[72] This approach was based on a previously established model of the hAgo2–siRNA complex.[73] However, in contrast to the original study, the siRNA strands in this work were not chemically modified. The simulations aimed to assess the binding stability and structural compatibility of native siRNAs within the hAgo2 complex, providing insights into the feasibility of unmodified siRNA constructs for antiviral RNAi applications. Using MM-GBSA free energy analysis, they proposed the siRNA–hAgo2 construct with the most

stable binding that warrants further experimental exploration. Additionally, a single short (25 ns) all-atom MD simulation using GROMACS with the AMBER99-ILDN force field and TIP3P water model was used to examine the structural dynamics of hAgo2 in complex with seven unmodified siRNAs targeting mRNA corresponding to mutant TDP-43.[74] The simulation revealed conformational switching between the "open" (the MID and PAZ domains move away from each other, while the PAZ and N-terminal domains come closer) and "closed" (PAZ domain moves closer to the MID domain) states, with flexibility in the PAZ domain being responsible for anchoring the 3′ end of the guide strand. These findings underscore the role of domain dynamics in siRNA recognition and binding stability. Furthermore, a single 1 μs all-atom MD simulation (without replicas) using Amber software, χOL3 and FF12SB force fields, and the TIP3P water model was used to investigate how chemical modifications such as 2′-*O*-Me, 2′-*O*-Benzyl, and 2′-methoxyethyl (2′-MOE) at positions 2, 3, 5, and 14 of the siRNA guide strand influence conformational dynamics and binding interactions with hAgo2.[73] The hAgo2 was computationally modeled from the TtAgo structure.[73] Both the full trajectory and a truncated 500 ns segment were analyzed to conclude that more bulky modifications interfere with the key siRNA−hAGO2 noncovalent interactions, while less bulky modifications have no significant impact.

As described above, these studies all lacked simulation replicas that have been shown to be required for adequate sampling to produce reliable results for proteins[75] and nucleic acids.[76] Additionally, no study to date has investigated fully chemically-modified siRNAs or FDA-approved siRNA drugs in complex with hAgo2 at an atomic resolution. Furthermore, no experimentally-resolved structural model currently exists for FDA-approved drug complexes with hAgo2, highlighting a gap in the structural understanding

of clinically-relevant RNAi therapeutics that must be filled to aid the design of improved therapeutics.

To bridge current gaps in our understanding regarding the structural properties of FDA-approved siRNA drugs in complex with critical cellular machinery, this study aims to construct a novel hAgo2 model bound to a fully-modified seed region of Givosiran guide strand and conduct extensive MD simulations. Givosiran, as the first FDA-approved siRNA drug with complete chemical modifications, including both 2'-*O*-methyl (2'-*O*-Me) and 2'-fluoro (2'-F) substitutions, will be used in this study. This is important because the previous chapter has demonstrated a synergistic effect of these modifications on siRNA structural dynamics. The work in this chapter specifically aims to elucidate how 2'-*O*-Me and 2'-F chemical modifications alter the structure, dynamics, and binding interactions within the siRNA–hAgo2 complex. The findings will provide critical insights into the structural and functional effects of chemical modifications, aiding the rational design of next-generation siRNA therapeutics.

3.2 Computational Details

3.2.1 Model Preparation

The initial protein coordinates were obtained from a high-resolution X-ray crystal structure of hAgo2 bound to a nucleic acid duplex (comprising a 21-nt guide strand and 9-nt target mRNA, PDB ID: 4W5O, 1.80 Å resolution).[33] To ensure structural completeness, missing amino acid residues within flexible loops (residues 1–21, 89, 90, 119–126, 270–275, 297–305, and 822–835) were reconstructed using homology modeling with MODELLER[77] to generate energetically favorable conformations consistent with the crystallographic backbone. All non-protein crystallographic entities, such as solvent

molecules and co-crystallized small ligands (phosphate ions, phenol, and isopropyl alcohol) were removed. The refined hAgo2 model was then structurally aligned to the original crystal structure with the resulting C_α RMSD being less than 2.0 Å, indicating that the modeled residues preserved the overall structural integrity of the protein.

Because the seed region is essential for target recognition and binding specificity,[78,79] the bound nucleic acid duplex present in PDB ID: 4W5O was excluded from the computational model due to its poorly arranged base pairs within this key region. Instead, the coordinates for a well-resolved RNA duplex were extracted from a separate siRNA–hAgo2 complex with a lower resolution (PDB ID: 6N4O, 2.90 Å resolution),[80] wherein the guide strand and mRNA exhibit proper base pairing throughout the seed region. The two crystal structures were superimposed, and the misaligned RNA duplex from PDB ID:4W5O was replaced with the duplex from PDB ID:6N4O, which contains 21-nt guide strand and 8-nt target mRNA. The corresponding 8-nt of the guide strand was kept while the remaining nucleotides were truncated.

The guide strand sequence from the PDB ID:6N4O crystal structure was modified using UCSF Chimera[81] to generate the Givosiran guide strand. First, the native nucleobase sequence was mutated to match the canonical Givosiran sequence. This sequence was then systematically altered to introduce specific 2'-chemical modifications, generating fully 2'-*O*-Me substituted (OMeNA), fully 2'-F substituted (FNA), and the exact ribose modification pattern present in Givosiran (Drug). Thus, three distinct modified duplexes alongside an unmodified version were considered for comparison. To minimize structural deviations, residues were replaced while maintaining the original phosphodiester linkages, thereby preserving the backbone conformation to ensure the starting models remained close to the experimentally-determined crystal structure.

The Amber force field was implemented, with RNA nucleotides modelled using χOL3[82] and protein residues with FF19SB.[83] The partial charges for the modified nucleotides were acquired using geometries optimized at the HF/6-31G(d) level of theory and the PyRED online RESP charge fitting server.[84,85] Generalized Amber Force Field (GAFF2)[86] parameters were produced for the modified nucleotides using parmchk2 from AmberTools21.[87] The protonation states of the histidine residues were determined at pH 7.0 using H++.[88] Each system was solvated in a truncated-octahedral TIP3P[89-91] water box such that the solute is at least 16 Å from the edge of a box face in any direction, neutralized with Na^+, and NaCl added to 150 mM to mimic physiological intracellular conditions. The number of ions added was determined using the SLTCAP calculator[92] (Table 3.1).

Table 3.1: Number of ions and water molecules added to each siRNA-hAgo2 complex model.

System	Water	Na^+	Cl^-
RNA	44,356	92	117
OMeNA	44,338	97	122
FNA	44,347	97	122
Givosiran	44,352	92	117

3.2.2 MD Simulation Protocol

Initially, the positions of all solvent molecules and ions were minimized using 4,000 steps of steepest descent, followed by 6,000 steps of conjugate gradient minimization, while the solute (siRNA–hAgo2 complex) was constrained with a force constant of 100 $kcal \cdot mol^{-1} \cdot Å^{-2}$. Subsequently, heavy atoms of the solvent and ions were restrained with the same force constant, and hydrogen atoms in the system were minimized using 2,500 steps each of steepest descent and conjugate gradient minimization. Next, the solute (complex) was minimized using 10,000 steps of steepest descent, followed by 10,000 steps of conjugate gradient minimization, while solvent and ion molecules remained restrained

(100 kcal·mol^{-1}·Å^{-2}). Finally, the entire system was subjected to unrestrained minimization involving 2,000 steps of steepest descent and 3,000 steps of conjugate gradient minimization.

Following minimization, the solute was restrained with a force constant of 25 kcal·mol^{-1}·Å^{-2}, and the system was heated from 10 K to 310 K in 50 K increments using a Langevin thermostat with a collision frequency of 3 ps^{-1} and a 1 fs time step, over 120,000 simulation steps. The system was then equilibrated in five consecutive segments of 10,000 steps each, during which restraints on the solvent were gradually reduced from 25 to 1.5 kcal·mol^{-1}·Å^{-2}, ensuring a smooth relaxation to 310 K and a pressure of 1 bar.

Five independent 1 μs unrestrained production MD simulations were conducted for each system using the NPT ensemble in AMBER20.[87] The temperature was maintained at 310 K using the Langevin thermostat[93,94] (collision frequency = 3 ps^{-1}), and the pressure was controlled at 1 bar with a Berendsen barostat[95] (relaxation time = 2 ps). The periodic boundary condition was applied, and long-range electrostatics were treated using the particle mesh Ewald method[96,97] with a 12 Å cutoff for non-bonded interactions. The SHAKE[98] algorithm was employed to constrain bonds involving hydrogen atoms, allowing a 2 fs time step during production runs.

3.2.3 Analyses

The cpptraj[99] module of AmberTools21[87] was used to analyze each MD trajectory, with reported results averaged and standard deviations evaluated over the entire datasets. RMSDs with respect to the first frame of the production simulations were calculated for the heavy backbone atoms of the protein (Cα, C, and N) and RNA (P, O5′, C5′, C4′, C3′, and O3′) using cpptraj. Heavy atom RMSF of the protein residues during MD simulations

were also calculated using cpptraj. Hydrogen-bond occupancies were evaluated based upon the heavy atom distance (acceptor-donor) cut-off of 3.0 Å and an angle cut-off of ≥135°. To calculate the binding free energy of the complex, residues within 5 Å of the siRNA–hAgo2 interface were selected, and 5,000 snapshots were extracted from the MD trajectories at 100 ps intervals for subsequent analysis. The binding free energy for the siRNA−hAgo2 complex was computed using the molecular mechanics/Poisson−Boltzmann surface area (MM/PBSA) method.[100] Clustering was carried out to obtain representative structures based on the RMSD of all heavy atoms. Helical parameters were evaluated using the NAstruct command and in-house scripts according to the same algorithms, definitions, and units for helical parameters and groove sizes as employed by X3DNA.[99,101-104]

3.3 Results

3.3.1 Simulated siRNA–hAgo2 Complexes Retain Key Structural Features of Experimental Crystal Structure

The average structures derived from MD simulations of each siRNA–hAgo2 complex (canonical–hAgo2, FNA–hAgo2, OMeNA–hAgo2, and Givosiran–hAgo2) appear structurally similar. Therefore, the image shown in Figure 3.2a illustrates the canonical–hAgo2 complex as a representative example to visually convey the overall structural features common to all models. Structural overlays of the simulated complex with the crystallographic structures of hAgo2 (PDB IDs: 4W5O and 6N4O) reveal a high degree of conservation of the secondary structure of the protein. The structural alignment confirms that the overall architecture of hAgo2 remains intact during the simulation, as supported by an all-atom RMSD of less than 6.8 Å relative to the experimental starting

structure (Figure 3.2b and Appendix B.1). The conformational states depicted in the RMSD plot (Appendix B, Fig B.1) (blue trace) for the protein primarily reflect localized fluctuations, particularly within residues 819–831 of the PIWI domain. These variations are minor and do not significantly influence the overall structure or function of the complex, as the affected residues are situated over 5 Å away from the active site (seed region). Consequently, the observed RMSD deviations are considered negligible. These localized fluctuations are visually highlighted by the red rectangle in (Appendix B, Fig B.2). The target RNA (green plot) exhibits greater structural deviation compared to the guide RNA (red plot), with more fluctuation across the simulation timeframe. However, the guide RNA maintains relatively consistent RMSD values. Despite these differences, both remain below 3 Å, indicating structural stability during the simulation.

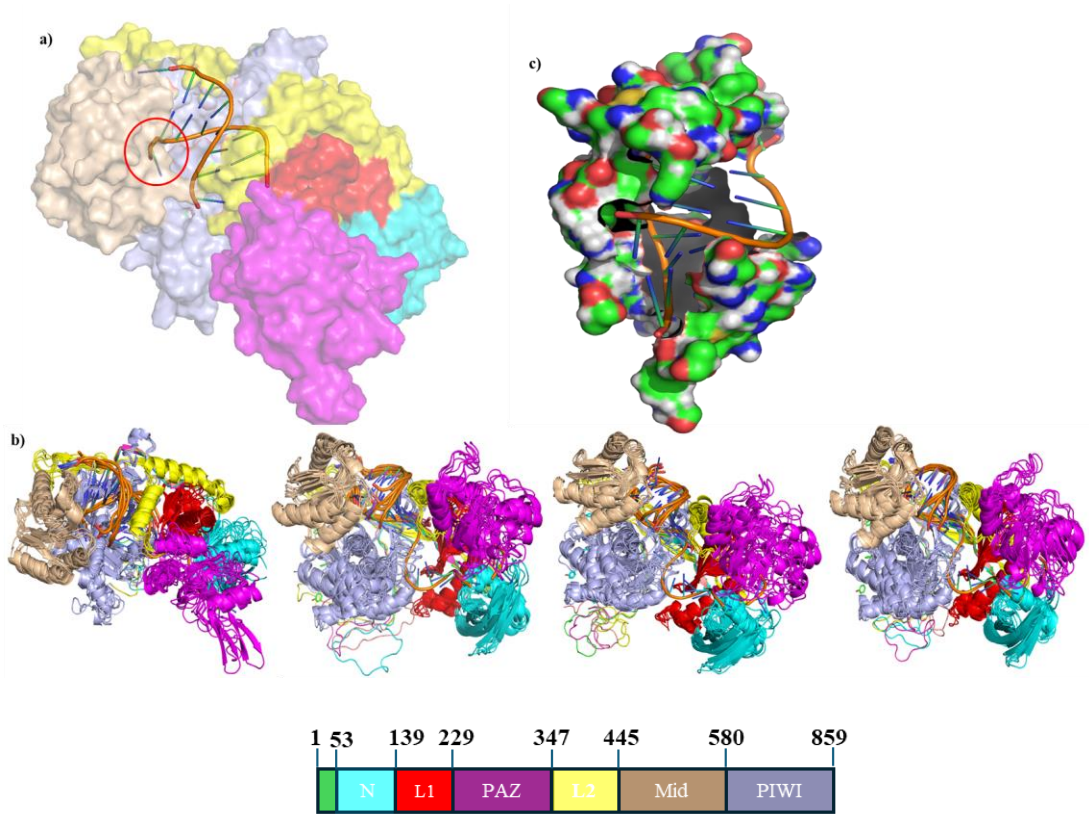

Figure 3.2: A) Average representative structure of canonical siRNA–hAgo2 complex from 5 replicas of 1 μs MD simulation. The area circled in red shows the 5'-end of the guide

*strand anchored in the MID domain of hAgo2. B) Best representative structures from 5 * 1 μs MD simulation superimposed on crystal structure (PDB ID: 4W5O). C) Model of the local interacting residues that are 5 Å away from the guide strand.*

The RoG of all heavy atoms was employed to assess the overall compactness of the interacting domain (5 Å away from the seed region) in siRNA–hAgo2 complexes during MD simulations (Appendix B, Figure B.3). As a measure of mass distribution relative to the center of mass, RoG provides insight into the global compactness of the complex,[105] where abrupt deviations may suggest system expansion or denaturation. All complexes (i.e., involving RNA, FNA, OMeNA, or Givosiran) maintained RoG values within a narrow range of 33–34 Å, with no significant fluctuations or sharp transitions observed throughout the trajectories. This indicates that the complexes remained structurally compact and conformationally stable across the simulations regardless of the type or pattern of modifications.

The RMSF plots (Appendix B, Fig B.4) of the protein backbone reveal that the N-terminal and PIWI domains are the most flexible regions in all complexes. The MID domain is less flexible and more rigid than all other domains in the complex. Furthermore, the modeled siRNA–hAgo2 complex preserves key structural features observed in crystal structures, including the stable anchoring of the 5′-end of the guide strand within the MID domain pocket (shown in red circle, Figure 3.2a), and the proper threading of the seed region through the nucleic acid binding channel.[31,33,36,37] These results demonstrate that the computational model developed in this chapter closely mirrors the experimental structure, and this agreement supports the reliability of the model for subsequent analyses.

3.3.2 Local Structural Stability, Flexibility, and Compactness of the Seed Region Are Maintained Across Chemically Modified siRNA–hAgo2 Complexes

To investigate the structural implications of chemical modifications on siRNA–hAgo2 interactions, we focused on the seed region of the guide strand, a critical domain known to mediate primary interactions within the RISC.[78,79] Indeed, crystallographic structures of siRNA–hAgo2 complexes[29, 33, 36] consistently identify the seed region as being crucial for hAgo2 recognition and binding. All analyses were restricted to residues within 5 Å of the guide strand (Figure 3.2c), effectively capturing the local environment and interaction network in this domain. The structural stability of the complexes was evaluated by computing the RMSD of protein and RNA backbone atoms with respect to the starting structure throughout the MD simulations (Figure 3.3a). All systems exhibited global conformational stability, with RMSD values consistently below 3.5 Å and typically ranging between 0.5 Å and 2.5 Å for both protein and RNA.

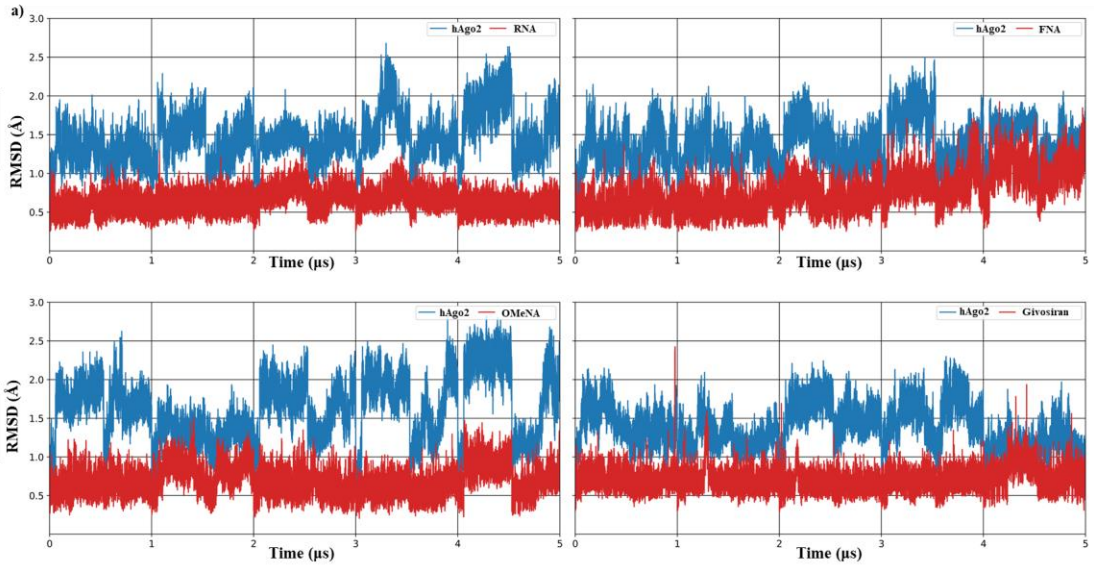

Figure 3.3a: Root-mean-square-deviation (RMSD) for the interacting region within the siRNA–hAgo2 complex (a) RNA (b) FNA (c) OMeNA (d) Givosiran over 1 µs MD simulations across 5 replicas.

RMSF analysis reveals the patterns of per residue movements across the protein and nucleic acid components (Figure 3.3b). In all complexes, the majority of hAgo2 residues within this interaction domain exhibit RMSF values ranging from 0.6 to 4.6 Å, indicating an overall stable complex. While the overall interaction domain is structurally stable, certain amino acid residues exhibit increased atomic fluctuations, indicating localized flexibility within specific regions of the protein structure. A603 within the PIWI domain consistently displays the highest degree of flexibility across all systems, with RMSF values of 4.44 Å (RNA), 4.61 Å (FNA), 6.24 Å (OMeNA), and 3.79 Å (Givosiran), identifying this residue as a conserved dynamic region independent of siRNA chemical modifications. Similarly, the second most dynamic residue within this interaction region is R814, located in the PIWI domain, which demonstrates higher flexibility, with RMSF values of 2.22 Å (RNA), 2.79 Å (FNA), 2.87 Å (OMeNA), and 2.02 Å (Givosiran). This further suggests localized structural flexibility within the PIWI domain. Interestingly, the lowest RMSF is observed in the Givosiran-modified system, potentially reflecting enhanced local rigidity due to the synergistic effects of 2′-F and 2′-*O*-Me modifications. In contrast to hAgo2, the guide strands of siRNA in all complexes exhibit lower RMSF values, fluctuating between 0.6 and 1.6 Å, indicative of a less flexible region within the siRNA–hAgo2 interacting domain and a tightly bound siRNA, resulting in reduced fluctuations.

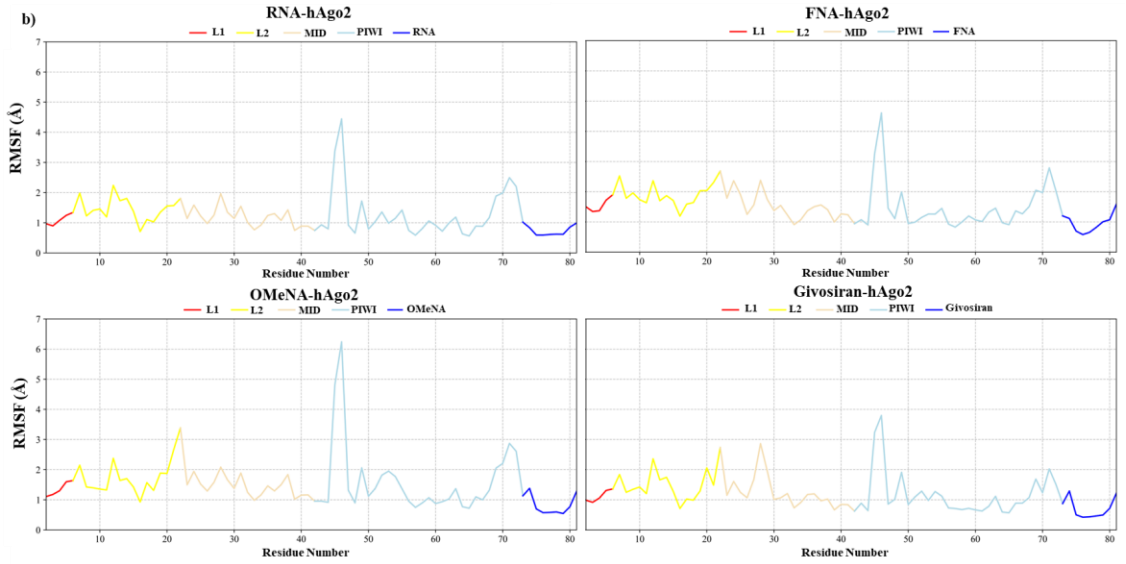

Figure 3.3b: Root-mean-square-fluctuations (RMSF) for the interacting region within the siRNA–hAgo2 complex (a) RNA (b) FNA (c) OMeNA (d) Givosiran over 1 µs MD simulations across 5 replicas.

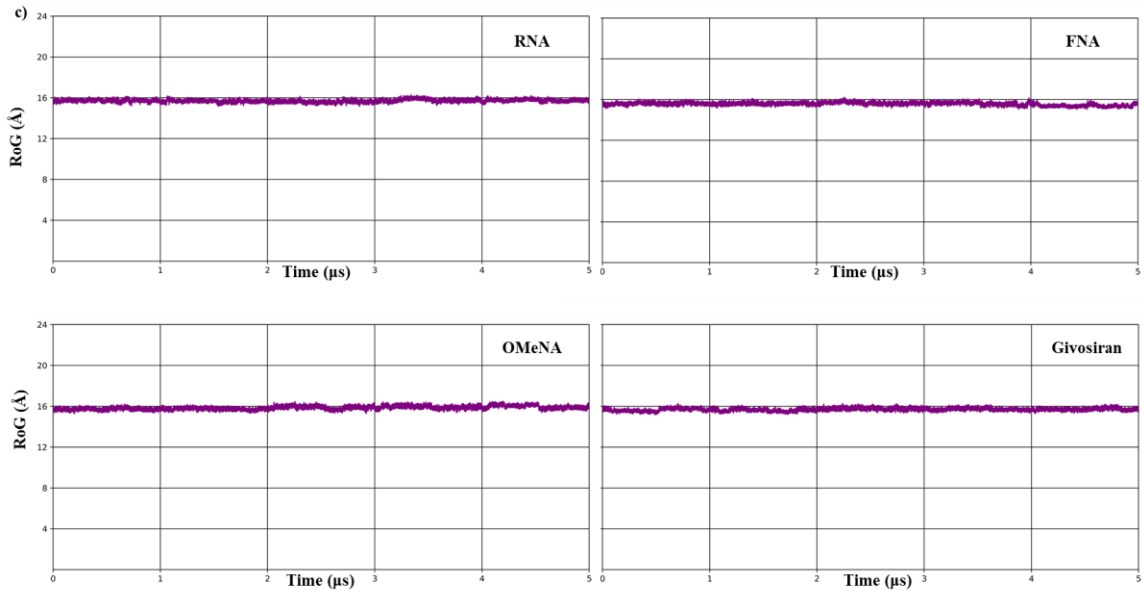

Figure 3.3c: Radius of gyration (RoG) for the interacting region within the siRNA-hAgo2 complex (a) RNA (b) FNA (c) OMeNA (d) Givosiran over 1 µs MD simulations across 5 replicas.

Consistently, all complexes involving RNA, FNA, OMeNA, or Givosiran maintain RoG values within a narrow range of 15–16 Å, with no significant fluctuations or sharp transitions observed throughout the trajectories (Figure 3.3c). This indicates that the

interacting domains remained structurally compact and conformationally stable across the simulations regardless of the type or pattern of modifications and are reliable for subsequent analysis.

3.3.3 Critical siRNA–hAgo2 Interactions in the MID Domain are Preserved but Modulated by 2′ Modifications

A previous crystallographic study has demonstrated that the seed sequence of the RNA occupies a narrow binding groove on hAgo2, where each backbone phosphate from the second nucleotide (A2) to the 8th nucleotide (C8) forms interactions with protein residues (Appendix B, Fig B.5).[29,74] The study confirmed that the Watson-Crick face of the first nucleotide interacts with the peptide backbone of G524 and T526, and the phosphate of A2 forms hydrogen bonds with the main and side chains of N551 and Q548. Furthermore, A3 and A4 interact with K566 and R792, respectively, G5 contacts Y804 and both the main chain and side chain of S798, U6 engages K709, G7 contacts R761, and C8 interacts with the main-chain amine of A221. Another complementary study identified contacts within the MID and PIWI domains of hAgo2.[9] The study revealed that residues K566, K709, H753, Y790, R792, S798, and Y804 interact with phosphates of nucleotide 3 through nucleotide 6 of the guide strand, while S220, R357, R714, and R761 engage phosphates of nucleotide 7 through 9.[9]

Building upon these experimental observations, our study employs MD simulations to systematically investigate how Givosiran-like chemical modifications influence these interactions between the seed region of the siRNA guide strand and hAgo2. Particular attention is given to whether the experimentally-observed contacts are preserved, disrupted, or modulated in the presence of ribose modifications. As an initial control, MD simulations

of the canonical siRNA–hAgo2 complex revealed that the nucleotide at the 5′-end of the guide strand is primarily recognized by the amino acid residues G524 (amide oxygen of the backbone) and T526 (backbone amide hydrogen) of hAgo2, forming stable hydrogen-bonds with the uracil base (Figure 3.4a). Specifically, U5···G524 and T526···U5 interactions were observed with percentage occupancies of 75 ± 6% and 32 ± 6%, respectively. FNA retains these hydrogen-bond interactions observed in the canonical siRNA–hAgo2 complex, with occupancies decreasing to 65 ± 6% for U5···G524 and relatively consistent 30 ± 7% for T526···U5, (Figure 3.4b), while in OMeNA, the percentage occupancies for the U5···G524 interaction decreased to 57 ± 28% from the observed value of canonical siRNA–hAgo2 complex and similar values of 32 ± 14% for T526···U5, respectively (Figure 3.4c). In Givosiran, these interactions with G524 and T526 of hAgo2 are still observed, but the average occupancies substantially reduce and have greater variability, being 42 ± 30% and 19 ± 12%, respectively (Figure 3.4d).

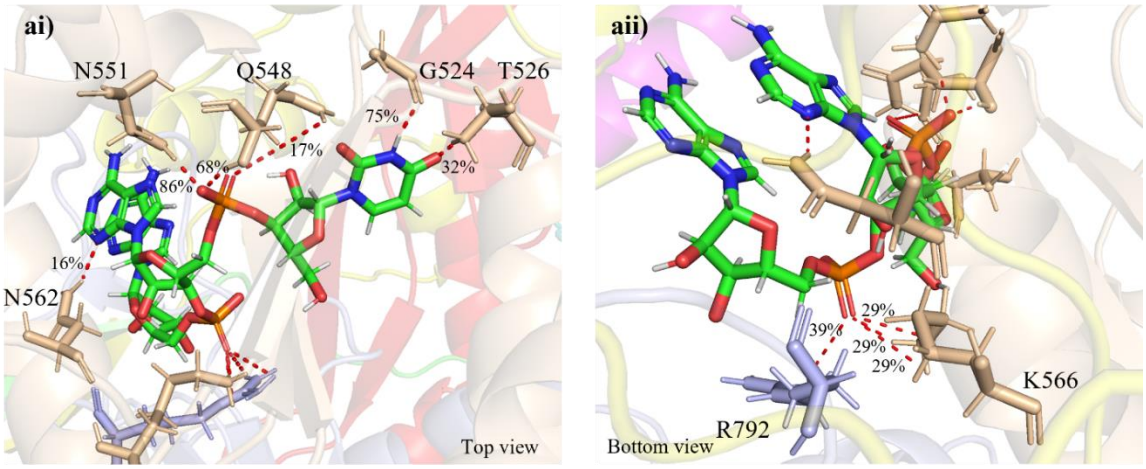

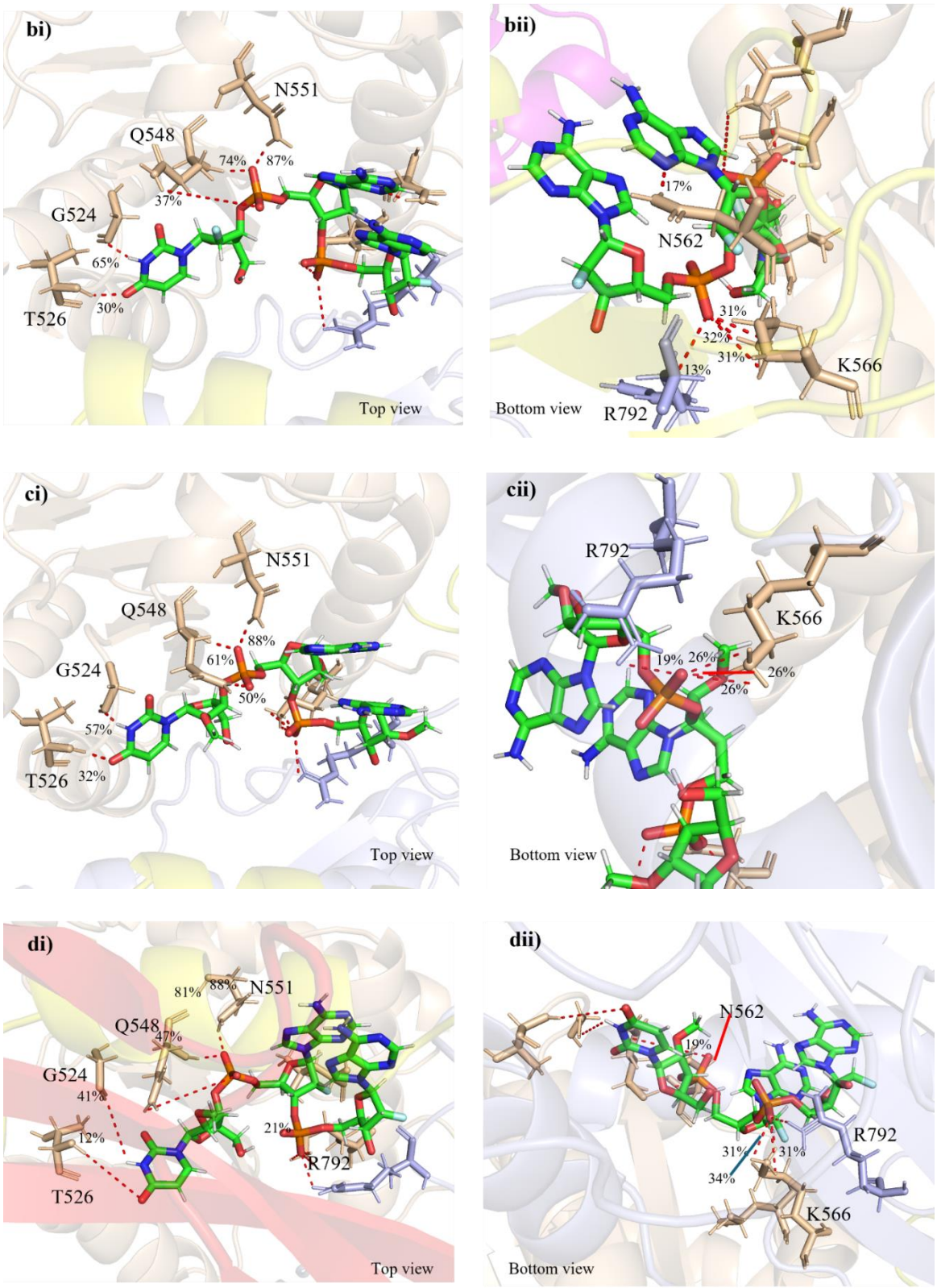

Figure 3.4: Representative structures of siRNA–hAgo2 complexes showing interactions at the MID domain for: (A) unmodified, (B) 2'-F, (C) 2'-O-Me, and (D) Givosiran (combined

2′-F/2′-O-Me) modified siRNA. Protein is colored in wheat and magenta, interacting siRNA residues are colored by atom. The red dashed lines indicate the noncovalent interactions between nucleotides of siRNA and MID domain residues of hAgo2.

The residue adjacent to the 5′-end of the guide strand, adenosine, is also recognized by the MID domain of hAgo2. [29, 37, 106] MD simulations of the canonical siRNA–hAgo2 complex shows that the interactions at this site are primarily mediated by the phosphate backbone, which forms noncovalent interactions with N551 and Q548 of hAgo2, along with a nucleobase-mediated contact involving N562 with N3 of adenosine (Figure 3.4a). The hydrogen-bond interactions occur between one amide hydrogen (HD22) of the side chain of N551 and the non-bridging phosphate oxygen (OP2, N551···A), the backbone and side chain amide hydrogen of Q548 and the non-bridging phosphate oxygens (two instances; OP2 and OP1) Q548···A, and amide hydrogen of the side chain of N562 with the N3 atom in the adenine base (N562···A), with percentage occupancies of 86 ± 3%, 68 ± 4%, 17 ± 5%, and 16 ± 1%, respectively (Figure 3.4a). Upon substitution of the 2′-OH group with 2′-F in the FNA–hAgo2 complex, these interactions are retained and while the occupancy of the (A)OP1···NE2(Q548) interaction increases to 37 ± 12%, the other interactions are similar with occupancies of 87 ± 3%, 74 ± 8%, and 17 ± 3%, respectively (Figure 3.4b) indicating somewhat similar interactions. In contrast, the 2′-*O*-Me modification in the OMeNA–hAgo2 complex preserves the noncovalent interactions with the backbone of adenosine, but disrupts the base-specific contact, thereby reducing the interactions to only N551···(A) and both Q548···(A), with the occupancy of (A)OP1···NE2(Q548) interaction increasing significantly to 50 ± 6%, and occupancies of the other interactions decreasing to 66 ± 28%, and 61 ± 9%, respectively (Figure 3.4c). The base interaction was lost because OMe at the 2′-position in the ribose extends towards N562, pushing the amino acid residue away from the siRNA. The Givosiran–hAgo2

complex that contains 2′-F modification in the ribose at this nucleotide maintains all key interactions of the canonical siRNA–hAgo2 complex, including the base-specific contact with increased persistence over the MD simulations. Specifically, the occupancies of both Q548···(A), and N562···(A) interactions rise to 81 ± 5%, 47 ± 10%, and 19 ± 3%, respectively and the N551···(A) interaction is consistent with canonical siRNA–hAgo2 complex with occupancy of 88 ± 1% (Figure 3.4d). This demonstrates that the 2′-F substitution found in FNA and Givosiran at position 2 preserves and amplifies key hydrogen-bond interactions, including those involving the nucleobase, but the bulkier 2′-*O*-Me modification disrupts nucleobase-level recognition by displacing residues such as N562.

Our MD simulations highlight that adenosine, the 3rd nucleotide of the guide strand, appears to mark the boundary of the 5′ terminal within the seed region and is recognized by residues from two distinct protein domains, albeit with relatively low occupancy (less than 50%). The primary non-covalent interactions at this site involve the non-bridging phosphate backbone (OP1) of the nucleotide and are mediated by all three hydrogen atoms on the terminal amino group of K566 (MID domain) and one of the terminal hydrogens on the NH1 guanidinium group of the R792 side chain (PIWI domain). In the unmodified complex, the most prominent interactions in the MD simulations are R792···A, with an occupancy of 39 ± 15%, and three hydrogen bonds involving K566···A (targeting the OP1 of the backbone), each having 29 ± 2% occupancy (Figure 3.4a). Upon full 2′-F modification (FNA), the R792···A occupancy drops substantially to 13 ± 2%, while K566···A interactions are maintained with occupancies of 32 ± 5%, 31 ± 0%, and 31 ± 4%, respectively (Figure 3.4b). In the OMeNA system, the occupancy of K566-mediated

interactions decreases slightly to 26 ± 4% for each interaction. Meanwhile, R792-H···A is rather inconsistent with occupancy of 19 ± 22% and thus likely represents a transient contact (Figure 3.4c). In Givosiran, where the nucleotide remains fluorinated, the K566···(A) interaction is more than observed for OMeNA (34 ± 4%, 31 ± 5%, and 31 ± 3%), while the occupancy of the R792···(A) interaction increases to 21 ± 4%, which is greater than the observed for OMeNA–hAgo2 and FNA–hAgo2 complexes, but less than the canonical siRNA–hAgo2 complex (Figure 3.4d). This interaction pattern in Givosiran resembles that of FNA and canonical RNA, as the 2′-F modification maintains more persistent protein contacts than the bulkier 2′-*O*-Me group in OMeNA.

Overall, the 2′-*O*-Me and 2′-F modifications in the guide strand preserve most of the interactions within the MID domain of hAgo2, maintaining recognition of the 5′ terminal nucleotides. However, the persistence of these interactions is modulated by the specific chemical modification, with 2′-F enhancing or finetuning the key contacts, especially those involving backbone and nucleobase recognition, while 2′-*O*-Me tends to decrease or displace such residues due to steric hindrance.

3.3.4 Key siRNA–PIWI Domain Contacts in hAgo2 Persist but are Influenced by 2′ Modifications

The PIWI domain of hAgo2 serves as the catalytic core of the RISC and is responsible for cleaving the target mRNA between positions 10 and 11 relative to the guide strand.[8,13,14] As a result, precise interactions between the guide strand and the PIWI domain are essential for efficient siRNA-mediated gene silencing. Given that all residues of the guide strand in the Givosiran-like siRNA are chemically modified, we investigated the effects of these modifications on siRNA–PIWI domain interactions in comparison to

OMeNA, FNA, and the unmodified siRNA.

Throughout the MD simulations of the canonical siRNA–hAgo2 complex, the fourth nucleotide from the 5′-end of the guide strand (a guanosine) is consistently recognized by the phenolic hydrogen (HH) of Y790, one of the terminal guanidinium hydrogens (HH21), and one of the hydrogen (HE) of the side chain nitrogen of the guanidinium group of R792 within the PIWI domain of hAgo2, forming hydrogen bonds with both non-bridging phosphate backbone (Figure 3.5a). Y790 establishes a highly conserved hydrogen bond with OP1 of the phosphate group, maintaining this interaction for 99 ± 0% of the simulation time. In addition, R792 engages in multiple hydrogen bonds with both OP1 and OP2 of the same phosphate group, utilizing distinct donor atoms. Specifically, hydrogen bonds are formed between OP1 and HE of R792 for 68 ± 12% of the simulation time, while a separate interaction between HH of R792 and OP2 persists for 78 ± 23% of the trajectory. Upon fluorine modification (i.e., in the FNA–hAgo2 complex), the interactions observed in the canonical complex are largely retained. Y790 continues to maintain the OP1 hydrogen bond for 99 ± 1% of the simulation time. R792 preserves two OP1 interactions, one involving HH atom (not observed in canonical complex) with an occupancy of 53 ± 9%, and another involving the HE atom, although the occupancy of this interaction decreases to 42 ± 15%. However, the hydrogen bond with OP2 is less frequent, occurring only 28 ± 11% of the time (Figure 3.5b). In OMeNA, the Y790···OP1 interaction remains persistent (98 ± 1%), and the R792···OP1 interaction involving HH is observed for 78 ± 9% of the simulation. A significant change is that the interaction with OP2 and the OP1 interaction involving HE are completely lost in this system (Figure 3.5c). Interestingly, in Givosiran, where the same nucleotide is modified with fluorine, the hydrogen-bonding interactions diverge from that of FNA. Specifically, only two prominent interactions are

maintained: the conserved Y790···OP1 hydrogen bond (99 ± 1%) and a consistent R792···OP1 interaction via the HH donor atom (90 ± 1%). All other hydrogen-bonding interactions, including those with OP2 and the HE interaction with OP1, are absent, as observed for OMeNA complex (Figure 3.5d).

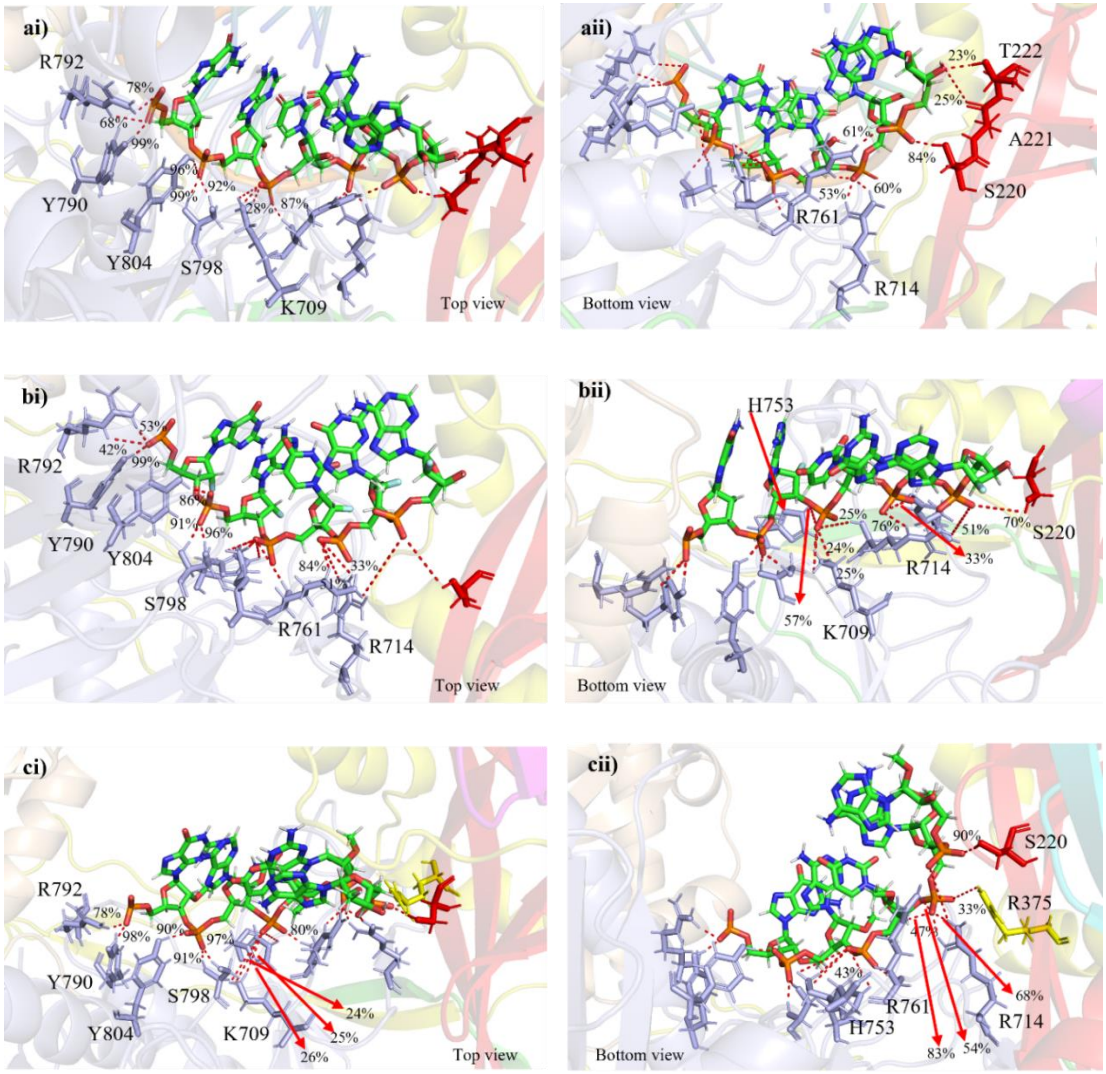

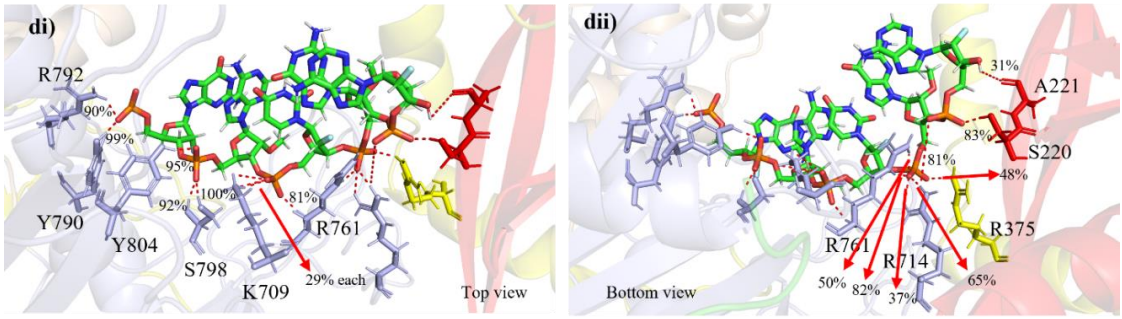

Figure 3.5: Representative structures of siRNA–hAgo2 complexes showing interactions at the PIWI domain for: (A) unmodified, (B) 2'-F, (C) 2'-O-Me, and (D) Givosiran (combined 2'-F/2'-O-Me) modified siRNA. Protein is colored in magenta, interacting siRNA residues are colored by atom. The red dashed lines indicate the noncovalent interactions between nucleotides of siRNA and PIWI domain residues of hAgo2.

For adenosine, the fifth nucleotide from the 5′-end of the guide strand, MD simulations highlight that S798 and Y804 form multiple hydrogen bonds with the phosphate backbone through both their side-chain hydroxyl groups and additional backbone NH (in the case of S798). The hydrogen bond formed between S798, and the phosphate group (via OP1) is highly conserved, with the occupancy exceeding 90% and standard deviation being < 3% across all complexes, including those involving unmodified RNA, FNA, OMeNA, and Givosiran. However, the interaction between Y804 and the OP2 atom of the adenine phosphate group displays varying degrees of occupancy depending on the chemical modification. In the unmodified RNA duplex, Y804···OP2 hydrogen bond is persistent for approximately 96 ± 2% of the simulation time. The occupancy decreases slightly in FNA (86 ± 13%) and OMeNA (90 ± 7%), while in Givosiran, which also contains a 2′-*O*-Me modification at this site, the interaction is largely preserved for 95 ± 1% of the simulation time (Figure 3.5a-d). This shows that while both 2′-*O*-Me and 2′-F modifications can slightly reduce the occupancy of the Y804···OP2 hydrogen bond relative to canonical RNA, the 2′-*O*-Me modification in the context of Givosiran closely preserves the native interaction pattern. This suggests that 2′-*O*-Me is better tolerated at this position

than 2′-F, enabling Givosiran to maintain interactions with hAgo2 comparable to canonical RNA.

The uridine nucleotide in the 6th position on the guide strand is consistently recognized by amino acids R761, K709, and H753 regardless of the chemical modification present on the ribose moiety. In the unmodified RNA duplex, the hydrogen attached to the backbone amide group of R761 forms a stable noncovalent interaction with one of the non-bridging phosphates atoms, (OP1), which is maintained for 87 ± 9% of the simulation time. K709 exhibits multiple hydrogen bonds from each hydrogen on the terminal amino group (HZ1, HZ2, and HZ3) and the other non-bridging phosphate atom (OP2), with individual occupancies of 28 ± 4% (Figure 3.5a). In the FNA–hAgo2 complex, the interaction with R761 is preserved (84 ± 15%), FNA interacts with H753 and exhibits an occupancy of 57 ± 9%. K709 maintains multiple OP2 interactions with each hydrogen on the terminal amino group, each occurring 25 ± 4% of the simulation time (Figure 3.5b). In the OMeNA–hAgo2 complex, the 2′-modification results in consistent occupancies in R761···U (80 ± 15%), H753···U (43 ± 28%), and K709···U interactions (24 ± 4% per interaction, Figure 3.5c). In Givosiran–hAgo2 complex, R761 continues to engage the OP1 atom, with 81 ± 3% occupancy, and K709 maintains the multiple OP2 interactions with the three hydrogen atoms on the terminal ammonio group, each occurring for 29 ± 2% of the simulation time (Figure 3.5d). While the core phosphate backbone interactions involving R761 and K709 are largely retained across all systems, modifications such as 2'-F and 2'-*O*-Me subtly alter the local hydrogen-bonding landscape, mostly impacting the H753 interaction.

Guanosine (nucleotide 7) of the guide strand in the siRNA–hAgo2 complex is recognized by an extensive hydrogen-bonding network involving primarily R761, R714, and R375 (L2; linker domain). In the unmodified duplex, R761 forms a dominant hydrogen

bond via the hydrogen attached to the backbone amide group with the OP2 atom of the phosphate backbone, with 61 ± 25% occupancy (Figure 3.5a). R714 also interacts robustly with the phosphate backbone, forming hydrogen bonds with OP2 through the hydrogen on the terminal guanidinium nitrogen groups (60 ± 40% and 40 ± 16%) donors. In the FNA–hAgo2 complex, guanosine remains coordinated through a similar network. R761 retains the primary interaction with OP2 via the guanidino hydrogen, with increased occupancy (76 ± 17%), and a secondary interaction through the other guanidino hydrogen on the terminal nitrogen (33 ± 11%). R714 preserves single interaction with OP2 via same donor atom as the unmodified nucleotide (51 ± 38%, Figure 3.5b). In the OMeNA–hAgo2 complex, R761 forms a highly persistent hydrogen bond with the non-bridging phosphate oxygen (OP2) through the backbone amide hydrogen, with an occupancy of 83 ± 7%. Additionally, one of the terminal guanidino hydrogens provides a stabilizing interaction (54 ± 5%). R714 shows the most prominent engagement across all complexes, donating hydrogen bonds to OP2 through both terminal guanidino hydrogens (68 ± 27% and 47 ± 18%). Meanwhile, the OMeNA modification introduces another interaction between R375 with OP1 observed for 33 ± 15% of the simulation time (Figure 3.5c). In the Givosiran–hAgo2 complex, R761 maintains robust interactions with OP2 through both its backbone amide hydrogen (82 ± 8%) and guanidino hydrogen (50 ± 8%) as observed in OMeNA. R714 retains dual engagement with OP2 via the guanidino hydrogens (65 ± 27% and 37 ± 27%), while R375 forms the most persistent interaction across all systems with a hydrogen bond to OP1 (48 ± 10%, Figure 3.5d). These results indicate that the FNA modification does not significantly disrupt the canonical phosphate recognition network, and the new contacts introduced in the OMeNA complex suggest that the 2′-*O*-Me substitution subtly reshapes the local hydrogen-bonding network, enabling broader residue

participation in guide strand recognition. This subtle fine-tuning of the local hydrogen-bonding landscape not only maintains native contacts but also recruits new residues, such as R375, to participate in guide strand recognition. Such fine-tuning may enhance the siRNA guide strand recognition.

The 8th nucleotide (adenosine) of the guide strand is primarily recognized through interactions with L1 domain residues S220, A221, and T222, along with R761. In the unmodified siRNA–hAgo2 complex, a persistent hydrogen bond is formed between OP1 and the side chain hydroxyl of S220, with high occupancy (84 ± 9%, Figure 3.5a). Additional local interactions include hydrogen bonds between the 3′-OH of the nucleotide and the backbone oxygen of A221 (25 ± 9%), as well as a transient interaction with the side chain hydroxyl of T222 (23 ± 13%). In the FNA–hAgo2 complex, this hydrogen-bonding pattern is largely conserved and the S220···OP1 interaction remains preserved (70 ± 26%), and R761 interacts with OP2 via the guanidino group (52 ± 26%). However, the T222···O3′ and A221···O3′ interactions are lost, suggesting a subtle conformational shift at the 3′ end due to the 2′-F modification (Figure 3.5b). In the OMeNA–hAgo2 complex, the S220···OP1 interaction is further enhanced (90 ± 7%), and the R761···OP2 interaction shows a slight increase (59 ± 26%). Also, as seen in the FNA complex, the hydrogen bonds with A221 and T222 are lost (Figure 3.5c). In the Givosiran–hAgo2 complex, the interaction with S220 remains highly conserved (83 ± 10%), and the R761–OP2 contact displays the highest occupancy among all systems (81 ± 12%), suggesting longer electrostatic interactions. The A221 interaction persists (31 ± 9%) as in the canonical context but the T222 interaction is lost (Figure 3.5d).

Overall, the PIWI domain of hAgo2 recognizes the guide strand of siRNA

regardless of 2'-F and 2′-*O*-Me modifications. However, the level of interaction varies with the modification pattern, with Givosiran exhibiting enhanced interactions throughout this domain likely due to the synergistic effect of the two types of 2′ substitutions. Chemical modifications at the ribose moiety such as those introduced in FNA and OMeNA do not disrupt this interaction network. Instead, they maintain or, in some instances, enhance the overall hydrogen-bonding framework, thereby supporting robust guide strand recognition by hAgo2 across chemically diverse siRNA analogs. However, differences in the occupancy and persistence of individual hydrogen bonds suggest nuanced effects of these modifications on local interaction dynamics. These findings align with prior experimental observations from the crystal structure indicating that hAgo2 does not critically depend on direct hydrogen bonding with the 2′-OH groups of the guide strand for RNA recognition.[9,33,36]

3.4 Synergistic Effects of 2′-F/*O*-Me Modifications Enhance siRNA–hAgo2 Binding

To evaluate the binding efficiency of each siRNA modification, MM/PBSA energy calculations[100] were performed for all siRNA–hAgo2 complexes. Specifically, the binding free energy (ΔG^0_{bind}) was calculated as below.

$$\Delta G_{bind} = \Delta G_{complex} - (\Delta G_{ligand} + \Delta G_{protein}) \qquad (eq.\ 3.1)$$

where each G (free energy) term is made up of:

$$G = E_{MM} + G_{solv} - TS \qquad (eq.3.2)$$

E_{MM} is the molecular mechanics energy from the force field calculations in the gas-phase made up of non-bonding interactions (sum of van der Waals and electrostatic).

G_{solv} represents how favorable it is to transfer molecules from vacuum into solvent and is composed of polar solvation, and nonpolar solvation energies.

The entropy term (TS) was not included, as its estimation through normal mode analysis is computationally expensive and often unreliable for RNA systems due to the need for extensive sampling and the poor convergence of entropy values, especially in biomolecules. Moreover, since the compared systems are structurally similar, entropic contributions are expected to cancel out, making their omission acceptable for capturing relative binding trends.

The resulting binding free energies, along with their respective energy components, (i.e., van der Waals (ΔE_{VDW}), electrostatic (ΔE_{ELEC}), polar solvation, and nonpolar solvation energies) are listed in Table 2. Across all complexes, electrostatic interactions are the primary contributors to siRNA–Ago2 binding affinity, with the Givosiran–hAgo2 complex exhibiting the most favorable electrostatics. While polar solvation energies are consistently unfavorable, these are offset by favorable gas-phase interactions. FNA–hAgo2 and canonical–hAgo2 complexes exhibit comparable binding free energies, both of which are more favorable than that of the OMeNA–hAgo2 complex. Despite similarities in ΔE_{VDW} and ΔE_{ELEC} across the modified and unmodified systems, the Givosiran modification pattern, which carries both 2'-F and 2'-*O*-Me modifications, demonstrates the strongest overall binding. This suggests a synergistic effect of these chemical modifications and corroborates the enhanced hydrogen-bond interactions for Givosiran discussed in the previous subsections. Overall, the MM/PBSA results indicate that siRNA–hAgo2 binding is primarily driven by electrostatics and further modulated by solvation and dispersion forces, with mixed 2'-F/*O*-Me modifications enhancing complex binding interactions.

Table 3.2: Binding free energy components (using MMPBSA) of the siRNA– hAgo2 complexes (RNA, FNA, OMeNA, and Givosiran) calculated from 5 replicas of 1 μs MD

simulations. Values are presented as mean ± standard error of the mean (SEM), with standard deviation (SD) across datasets are shown in parentheses.

Systems	ΔE_{VDW}	ΔE_{elec}	ΔE_{PB}	ΔE_{npolar}	ΔE_{disper}	ΔG_{gas}	ΔG_{solv}	ΔG
RNA	–122.4 (6.9)	–2458.6 (50.1)	2424.8 (44.8)	–89.3 (2.2)	167.3 (2.9)	–2580.9 (49.3)	2502.7 (44.8)	–78.3 ± 2.0 (14.6)
OMeNA	–121.0 (8.3)	–2434.3 (72.9)	2403.7 (70.1)	–92.3 (3.7)	170.9 (4.6)	–2555.3 (72.1)	2482.3 (71.2)	–73.0 ± 2.4 (20.1)
FNA	–120.2 (7.6)	–2451.1 (58.3)	2417.7 (49.3)	–89.8 (3.2)	165.9 (5.3)	–2571.3 (59.0)	2493.7 (50.4)	–77.5 ± 2.8 (16.8)
Givosiran	–121.6 (10.4)	–2479.2 (36.6)	2441.7 (34.9)	–91.2 (3.5)	167.1 (4.7)	–2600.8 (38.1)	2517.6 (34.8)	–83.2 ± 2.2 (15.6)

3.5 Conclusion

This study provides the first detailed computational account of how chemical modifications at each residue in the seed region influence siRNA interactions with hAgo2, the core protein effector of the RISC. To our knowledge, no previous modeling or simulation-based studies have systematically examined the residue-level impact of such modifications on hAgo2 recognition. Through MD simulations, we demonstrate that 2′-*O*-Me and 2′-F modifications preserve the key binding interaction at the siRNA–hAgo2 interface, particularly in the MID and PIWI domains, where the seed region of siRNA is anchored. Importantly, our findings show that these chemical modifications do not totally disrupt the canonical siRNA–hAgo2 contacts, but rather subtly fine-tune the persistence of key interactions depending on their chemical nature. When both modifications are present within the same duplex (i.e., the Givosiran-like design), the modifications act synergistically to further enhance guide strand recognition by hAgo2. This suggests that such synergistic effects improve the siRNA–hAgo2 interaction, could potentially contribute to the increased silencing potency of fully-modified siRNA, which is a key factor

in the therapeutic efficacy of siRNA drugs.[40,47,49,50,52,58,107-110] Overall, the siRNA–hAgo2 models and simulation strategies developed herein offer a valuable benchmark for structure-based optimization of chemically-modified siRNAs. Furthermore, the results for the modified duplexes deepen our understanding of the consequences of guide strand modifications and lay the groundwork for the rational design of next-generation RNAi therapeutics.

3.6 References

(1) Wu, J.; Yang, J.; Cho, W. C.; Zheng, Y. Argonaute proteins: Structural features, functions and emerging roles. *J. Adv. Res.* **2020**, *24*, 317-324.
(2) Faehnle, C. R.; Joshua-Tor, L. Argonautes confront new small RNAs. *Curr. Opin. Chem. Biol.* **2007**, *11* (5), 569-577.
(3) Pfaff, J.; Hennig, J.; Herzog, F.; Aebersold, R.; Sattler, M.; Niessing, D.; Meister, G. Structural features of Argonaute-GW182 protein interactions. *PNAS USA* **2013**, *110* (40), E3770-3779.
(4) Hauptmann, J.; Dueck, A.; Harlander, S.; Pfaff, J.; Merkl, R.; Meister, G. Turning catalytically inactive human Argonaute proteins into active slicer enzymes. *Nat. Struct. Mol. Biol* **2013**, *20* (7), 814-817.
(5) Kobayashi, H.; Tomari, Y. RISC assembly: Coordination between small RNAs and Argonaute proteins. *Biochim. Biophys. Acta.* **2016**, *1859* (1), 71-81.
(6) Tsuboyama, K.; Tadakuma, H.; Tomari, Y. Conformational Activation of Argonaute by Distinct yet Coordinated Actions of the Hsp70 and Hsp90 Chaperone Systems. *Mol. Cell* **2018**, *70* (4), 722-729 e724.
(7) Elbashir, S., Harborth, J., Lendeckel, W., Yalcin, A., Weber, K., Tuschl, T. Duplexes of 21-nucleotide RNAs mediate RNA interference in cultured mammalian cells. *Nature* **2001**, *411* (6836), 494-498.
(8) Elbashir, S. M.; Lendeckel, W.; Tuschl, T. RNA interference is mediated by 21- and 22-nucleotide RNAs. *Genes Dev.* **2001**, *15* (2), 188-200.
(9) Schirle, N. T.; MacRae, I. J. The Crystal Structure of Human Argonaute2. *Science* **2012**, *336* (6084), 1037-1040.
(10) Hutvagner, G.; Simard, M. J. Argonaute proteins: key players in RNA silencing. *Nat. Rev. Mol. Cell Biol.* **2008**, *9* (1), 22-32.
(11) Olina, A. V.; Kulbachinskiy, A. V.; Aravin, A. A.; Esyunina, D. M. Argonaute Proteins and Mechanisms of RNA Interference in Eukaryotes and Prokaryotes. *Biochemistry (Mosc)* **2018**, *83* (5), 483-497.
(12) Hock, J.; Meister, G. The Argonaute protein family. *Genome Biol* **2008**, *9* (2), 210.
(13) Rivas, F. V.; Tolia, N. H.; Song, J.-J.; Aragon, J. P.; Liu, J.; Hannon, G. J.; Joshua-Tor, L. Purified Argonaute2 and an siRNA form recombinant human RISC. *Nat. Struct. Mol. Biol* **2005**, *12* (4), 340-349.

(14) Song, J.-J.; Smith, S. K.; Hannon, G. J.; Joshua-Tor, L. Crystal Structure of Argonaute and Its Implications for RISC Slicer Activity. *Science* **2004**, *305* (5689), 1434-1437.
(15) Tolia, N. H.; Joshua-Tor, L. Slicer and the Argonautes. *Nat. Chem. Biol.* **2007**, *3* (1), 36-43.
(16) Xu, Y.; Zhang, Y.; Li, Z.; Soloria, A. K.; Potter, S.; Chen, X. The N-terminal extension of Arabidopsis ARGONAUTE 1 is essential for microRNA activities. *PLoS Genet.* **2023**, *19* (3), e1010450.
(17) Miyoshi, T.; Ito, K.; Murakami, R.; Uchiumi, T. Structural basis for the recognition of guide RNA and target DNA heteroduplex by Argonaute. *Nat. Commun.* **2016**, *7*, 11846.
(18) Frank, F.; Sonenberg, N.; Nagar, B. Structural basis for 5'-nucleotide base-specific recognition of guide RNA by human AGO2. *Nature* **2010**, *465* (7299), 818-822.
(19) Lau, N. C.; Lim, L. P.; Weinstein, E. G.; Bartel, D. P. An Abundant Class of Tiny RNAs with Probable Regulatory Roles in Caenorhabditis elegans. *Science* **2001**, *294* (5543), 858-862.
(20) Boland, A.; Huntzinger, E.; Schmidt, S.; Izaurralde, E.; Weichenrieder, O. Crystal structure of the MID-PIWI lobe of a eukaryotic Argonaute protein. *PNAS USA* **2011**, *108* (26), 10466-10471.
(21) Wang, Y.; Sheng, G.; Juranek, S.; Tuschl, T.; Patel, D. J. Structure of the guide-strand-containing argonaute silencing complex. *Nature* **2008**, *456* (7219), 209-213.
(22) Wang, Y.; Juranek, S.; Li, H.; Sheng, G.; Wardle, G. S.; Tuschl, T.; Patel, D. J. Nucleation, propagation and cleavage of target RNAs in Ago silencing complexes. *Nature* **2009**, *461* (7265), 754-761.
(23) Sheng, G.; Zhao, H.; Wang, J.; Rao, Y.; Tian, W.; Swarts, D. C.; van der Oost, J.; Patel, D. J.; Wang, Y. Structure-based cleavage mechanism of Thermus thermophilus Argonaute DNA guide strand-mediated DNA target cleavage. *PNAS* **2014**, *111* (2), 652-657.
(24) Parker, J. S.; Roe, S. M.; Barford, D. Structural insights into mRNA recognition from a PIWI domain–siRNA guide complex. *Nature* **2005**, *434* (7033), 663-666.
(25) Ghildiyal, M.; Seitz, H.; Horwich, M. D.; Li, C.; Du, T.; Lee, S.; Xu, J.; Kittler, E. L. W.; Zapp, M. L.; Weng, Z.; Zamore, P. D. Endogenous siRNAs Derived from Transposons and mRNAs in Drosophila Somatic Cells. *Science* **2008**, *320* (5879), 1077-1081.
(26) Lingel, A.; Simon, B.; Izaurralde, E.; Sattler, M. Structure and nucleic-acid binding of the Drosophila Argonaute 2 PAZ domain. *Nature* **2003**, *426* (6965), 465-469.
(27) Yan, K. S.; Yan, S.; Farooq, A.; Han, A.; Zeng, L.; Zhou, M.-M. Structure and conserved RNA binding of the PAZ domain. *Nature* **2003**, *426* (6965), 469-474.
(28) Kwak, P. B.; Tomari, Y. The N domain of Argonaute drives duplex unwinding during RISC assembly. *Nat. Struct. Mol. Biol* **2012**, *19* (2), 145-151.
(29) Elkayam, E.; Kuhn, C. D.; Tocilj, A.; Haase, A. D.; Greene, E. M.; Hannon, G. J.; Joshua-Tor, L. The structure of human argonaute-2 in complex with miR-20a. *Cell* **2012**, *150* (1), 100-110.
(30) Lim, L. P.; Lau, N. C.; Garrett-Engele, P.; Grimson, A.; Schelter, J. M.; Castle, J.; Bartel, D. P.; Linsley, P. S.; Johnson, J. M. Microarray analysis shows that some microRNAs downregulate large numbers of target mRNAs. *Nature* **2005**, *433* (7027), 769-773.
(31) Chandradoss, Stanley D.; Schirle, Nicole T.; Szczepaniak, M.; MacRae, Ian J.; Joo, C. A Dynamic Search Process Underlies MicroRNA Targeting. *Cell* **2015**, *162* (1), 96-107.

(32) Czauderna, F.; Fechtner, M.; Dames, S.; Aygun, H.; Klippel, A.; Pronk, G. J.; Giese, K.; Kaufmann, J. Structural variations and stabilising modifications of synthetic siRNAs in mammalian cells. *Nucleic Acids Res.* **2003**, *31* (11), 2705-2716.
(33) Schirle, N. T.; Sheu-Gruttadauria, J.; MacRae, I. J. Structural basis for microRNA targeting. *Science* **2014**, *346* (6209), 608-613.
(34) Nakanishi, K.; Weinberg, D. E.; Bartel, D. P.; Patel, D. J. Structure of yeast Argonaute with guide RNA. *Nature* **2012**, *486* (7403), 368-374.
(35) Wang, Y.; Juranek, S.; Li, H.; Sheng, G.; Tuschl, T.; Patel, D. J. Structure of an argonaute silencing complex with a seed-containing guide DNA and target RNA duplex. *Nature* **2008**, *456* (7224), 921-926.
(36) Schirle, N. T.; Kinberger, G. A.; Murray, H. F.; Lima, W. F.; Prakash, T. P.; MacRae, I. J. Structural Analysis of Human Argonaute-2 Bound to a Modified siRNA Guide. *J. Am. Chem. Soc.* **2016**, *138* (28), 8694-8697.
(37) Schirle, N. T.; Sheu-Gruttadauria, J.; Chandradoss, S. D.; Joo, C.; MacRae, I. J. Water-mediated recognition of t1-adenosine anchors Argonaute2 to microRNA targets. *Elife* **2015**, *4*.
(38) Ya-Lin Chiu, T. M. R. RNAi in Human Cells: Basic Structural and Functional Features of Small Interfering RNA. *Mol. Cell* **2002**, *Volume 10* (Issue 3), Pages 549-561.
(39) Chiu, Y. L.; Rana, T. M. siRNA function in RNAi: a chemical modification analysis. *RNA.* **2003**, *9* (9), 1034-1048.
(40) Egli, M.; Manoharan, M. Chemistry, structure and function of approved oligonucleotide therapeutics. *Nucleic Acids Res.* **2023**, *51* (6), 2529-2573.
(41) Egli, M.; Pallan, P. S. Crystallographic studies of chemically modified nucleic acids: a backward glance. *Chem. Biodivers.* **2010**, *7* (1), 60-89.
(42) Egli, M.; Manoharan, M. Re-Engineering RNA Molecules into Therapeutic Agents. *Acc. Chem. Res.* **2019**, *52* (4), 1036-1047.
(43) Matsuda, S.; Bala, S.; Liao, J. Y.; Datta, D.; Mikami, A.; Woods, L.; Harp, J. M.; Gilbert, J. A.; Bisbe, A.; Manoharan, R. M.; et al. Shorter Is Better: The alpha-(l)-Threofuranosyl Nucleic Acid Modification Improves Stability, Potency, Safety, and Ago2 Binding and Mitigates Off-Target Effects of Small Interfering RNAs. *J. Am. Chem. Soc.* **2023**, *145* (36), 19691-19706.
(44) Crooke, S. T.; Witztum, J. L.; Bennett, C. F.; Baker, B. F. RNA-Targeted Therapeutics. *Cell Metab.* **2018**, *27* (4), 714-739.
(45) Seth, P. P.; Tanowitz, M.; Bennett, C. F. Selective tissue targeting of synthetic nucleic acid drugs. *J Clin Invest* **2019**, *129* (3), 915-925.
(46) Bennett, C. F. Therapeutic Antisense Oligonucleotides Are Coming of Age. *Annu. Rev. Med.* **2019**, *70*, 307-321.
(47) Gangopadhyay, S.; Gore, K. R. Advances in siRNA therapeutics and synergistic effect on siRNA activity using emerging dual ribose modifications. *RNA Biol.* **2022**, *19* (1), 452-467.
(48) Ku, S. H.; Jo, S. D.; Lee, Y. K.; Kim, K.; Kim, S. H. Chemical and structural modifications of RNAi therapeutics. *Adv. Drug Deliv. Rev.* **2016**, *104*, 16-28.
(49) Behlke, M. A. Chemical modification of siRNAs for in vivo use. *Oligonucleotides* **2008**, *18* (4), 305-319.
(50) Deleavey, G. F.; Damha, M. J. Designing chemically modified oligonucleotides for targeted gene silencing. *Chem. Biol.* **2012**, *19* (8), 937-954.

(51) Ali Zaidi, S. S.; Fatima, F.; Ali Zaidi, S. A.; Zhou, D.; Deng, W.; Liu, S. Engineering siRNA therapeutics: challenges and strategies. *J. Nanobiotechnology* **2023**, *21* (1), 381.
(52) Allerson, C. R.; Sioufi, N.; Jarres, R.; Prakash, T. P.; Naik, N.; Berdeja, A.; Wanders, L.; Griffey, R. H.; Swayze, E. E.; Bhat, B. Fully 2'-modified oligonucleotide duplexes with improved in vitro potency and stability compared to unmodified small interfering RNA. *J. Med. Chem.* **2005**, *48* (4), 901-904.
(53) Zhang, M. M.; Bahal, R.; Rasmussen, T. P.; Manautou, J. E.; Zhong, X. B. The growth of siRNA-based therapeutics: Updated clinical studies. *Biochem. Pharmacol.* **2021**, *189*, 114432.
(54) Das, G.; Harikrishna, S.; Gore, K. R. Influence of Sugar Modifications on the Nucleoside Conformation and Oligonucleotide Stability: A Critical Review. *Chem. Rec.* **2022**, *22* (12), e202200174.
(55) Lundin, K. E.; Gissberg, O.; Smith, C. I. Oligonucleotide Therapies: The Past and the Present. *Hum. Gene. Ther.* **2015**, *26* (8), 475-485.
(56) Sajid, M. I.; Moazzam, M.; Kato, S.; Yeseom Cho, K.; Tiwari, R. K. Overcoming Barriers for siRNA Therapeutics: From Bench to Bedside. *Pharmaceuticals* **2020**, *13* (10), 294.
(57) Guo, F.; Li, Y.; Yu, W.; Fu, Y.; Zhang, J.; Cao, H. Recent Progress of Small Interfering RNA Delivery on the Market and Clinical Stage. *Mol Pharm* **2024**, *21* (5), 2081-2096.
(58) Hu, B.; Zhong, L.; Weng, Y.; Peng, L.; Huang, Y.; Zhao, Y.; Liang, X. J. Therapeutic siRNA: state of the art. *Signal Transduct. Target. Ther.* **2020**, *5* (1), 101.
(59) Peacock, H.; Kannan, A.; Beal, P. A.; Burrows, C. J. Chemical modification of siRNA bases to probe and enhance RNA interference. *J. Org. Chem.* **2011**, *76* (18), 7295-7300.
(60) Setten, R. L.; Rossi, J. J.; Han, S.-p. The current state and future directions of RNAi-based therapeutics. *Nat. Rev. Drug Discov.* **2019**, *18* (6), 421-446.
(61) Gao, S.; Dagnaes-Hansen, F.; Nielsen, E. J.; Wengel, J.; Besenbacher, F.; Howard, K. A.; Kjems, J. The effect of chemical modification and nanoparticle formulation on stability and biodistribution of siRNA in mice. *Mol. Ther.* **2009**, *17* (7), 1225-1233.
(62) Varley, A. J.; Hammill, M. L.; Salim, L.; Desaulniers, J. P. Effects of Chemical Modifications on siRNA Strand Selection in Mammalian Cells. *Nucleic Acid Ther.* **2020**, *30* (4), 229-236.
(63) Mook, O. R.; Baas, F.; de Wissel, M. B.; Fluiter, K. Evaluation of locked nucleic acid–modified small interfering RNA in vitro and in vivo. *Mol. Cancer Ther.* **2007**, *6* (3), 833-843.
(64) Das, G.; Harikrishna, S.; Gore, K. R. Investigating the Effect of Chemical Modifications on the Ribose Sugar Conformation, Watson-Crick Base Pairing, and Intrastrand Stacking Interactions: A Theoretical Approach. *J. Phys. Chem. B* **2024**, *128* (35), 8313-8331.
(65) Sponer, J.; Bussi, G.; Krepl, M.; Banas, P.; Bottaro, S.; Cunha, R. A.; Gil-Ley, A.; Pinamonti, G.; Poblete, S.; Jurecka, P.; et al. RNA Structural Dynamics As Captured by Molecular Simulations: A Comprehensive Overview. *Chem. Rev.* **2018**, *118* (8), 4177-4338.
(66) Mallick, B.; Sharma, A. R.; Lee, S. S.; Chakraborty, C. Understanding the molecular interaction of human argonaute-2 and miR-20a complex: A molecular dynamics approach. *J. Cell. Biochem.* **2019**, *120* (12), 19915-19924.
(67) Karplus, M.; McCammon, J. Molecular dynamics simulations of biomolecules. *Nat. Struct. Mol. Biol.* **2002**, *9*, 646-652.

(68) Wang, Y.; Li, Y.; Ma, Z.; Yang, W.; Ai, C. Mechanism of microRNA-target interaction: molecular dynamics simulations and thermodynamics analysis. *PLoS Comput. Biol.* **2010**, *6* (7), e1000866.
(69) Xia, Z.; Clark, P.; Huynh, T.; Loher, P.; Zhao, Y.; Chen, H. W.; Ren, P.; Rigoutsos, I.; Zhou, R. Molecular dynamics simulations of Ago silencing complexes reveal a large repertoire of admissible 'seed-less' targets. *Sci Rep* **2012**, *2*, 569.
(70) Nam, S.; Ryu, H.; Son, W. J.; Kim, Y. H.; Kim, K. T.; Balch, C.; Nephew, K. P.; Lee, J. Mg2+ effect on argonaute and RNA duplex by molecular dynamics and bioinformatics implications. *PLoS One.* **2014**, *9* (10), e109745.
(71) Zhu, L.; Jiang, H.; Sheong, F. K.; Cui, X.; Gao, X.; Wang, Y.; Huang, X. A Flexible Domain-Domain Hinge Promotes an Induced-fit Dominant Mechanism for the Loading of Guide-DNA into Argonaute Protein in Thermus thermophilus. *J. Phys. Chem. B.* **2016**, *120* (10), 2709-2720.
(72) Uppuladinne, M. V. N.; Koulgi, S.; Jani, V.; Sonavane, U.; Joshi, R. Unlocking the potential of RNAi as a therapeutic strategy against infectious viruses: an in-silico study. *Chem. Pap.* **2023**, *78* (3), 1537-1552.
(73) Harikrishna, S.; Pradeepkumar, P. I. Probing the Binding Interactions between Chemically Modified siRNAs and Human Argonaute 2 Using Microsecond Molecular Dynamics Simulations. *J. Chem. Inf. Model.* **2017**, *57* (4), 883-896.
(74) Bhandare, V.; Ramaswamy, A. Structural Dynamics of Human Argonaute2 and Its Interaction with siRNAs Designed to Target Mutant tdp43. *Adv. Bioinformatics* **2016**, *2016*, 8792814.
(75) Wan, S.; Bhati, A. P.; Wade, A. D.; Coveney, P. V. Ensemble-Based Approaches Ensure Reliability and Reproducibility. *J. Chem. Inf. Model.* **2023**, *63* (22), 6959-6963.
(76) Knapp, B.; Ospina, L.; Deane, C. M. Avoiding False Positive Conclusions in Molecular Simulation: The Importance of Replicas. *J. Chem. Theory Comput.* **2018**, *14* (12), 6127-6138.
(77) Webb, B.; Sali, A. Comparative Protein Structure Modeling Using MODELLER. *Curr Protoc Bioinformatics.* **2016**, *54* (1), 5.6.1-5.6.37.
(78) Nakanishi, K. Anatomy of four human Argonaute proteins. *Nucleic Acids Res.* **2022**, *50* (12), 6618-6638.
(79) Jackson, A. L.; Burchard, J.; Leake, D.; Reynolds, A.; Schelter, J.; Guo, J.; Johnson, J. M.; Lim, L.; Karpilow, J.; Nichols, K.; et al. Position-specific chemical modification of siRNAs reduces "off-target" transcript silencing. *RNA.* **2006**, *12* (7), 1197-1205.
(80) Sheu-Gruttadauria, J.; Xiao, Y.; Gebert, L. F.; MacRae, I. J. Beyond the seed: structural basis for supplementary microRNA targeting by human Argonaute2. *EMBO J.* **2019**, *38* (13), e101153.
(81) Pettersen, E. F.; Goddard, T. D.; Huang, C. C.; Couch, G. S.; Greenblatt, D. M.; Meng, E. C.; Ferrin, T. E. UCSF Chimera--a visualization system for exploratory research and analysis. *J. Comput. Chem.* **2004**, *25* (13), 1605-1612.
(82) Kuhrova, P.; Mlynsky, V.; Zgarbova, M.; Krepl, M.; Bussi, G.; Best, R. B.; Otyepka, M.; Sponer, J.; Banas, P. Improving the Performance of the Amber RNA Force Field by Tuning the Hydrogen-Bonding Interactions. *J. Chem. Theory. Comput.* **2019**, *15* (5), 3288-3305.
(83) Tian, C.; Kasavajhala, K.; Belfon, K. A. A.; Raguette, L.; Huang, H.; Migues, A. N.; Bickel, J.; Wang, Y.; Pincay, J.; Wu, Q.; Simmerling, C. ff19SB: Amino-Acid-Specific

Protein Backbone Parameters Trained against Quantum Mechanics Energy Surfaces in Solution. *J. Chem. Theory. Comput.* **2020**, *16* (1), 528-552.
(84) Vanquelef, E.; Simon, S.; Marquant, G.; Garcia, E.; Klimerak, G.; Delepine, J. C.; Cieplak, P.; Dupradeau, F. Y. R.E.D. Server: a web service for deriving RESP and ESP charges and building force field libraries for new molecules and molecular fragments. *Nucleic Acids Res.* **2011**, *39* (Web Server issue), W511-517.
(85) Dupradeau, F. Y.; Pigache, A.; Zaffran, T.; Savineau, C.; Lelong, R.; Grivel, N.; Lelong, D.; Rosanski, W.; Cieplak, P. The R.E.D. tools: advances in RESP and ESP charge derivation and force field library building. *Phys. Chem. Chem. Phys.* **2010**, *12* (28), 7821-7839.
(86) Wang, J.; Wolf, R. M.; Caldwell, J. W.; Kollman, P. A.; Case, D. A. Development and testing of a general amber force field. *J. Comput. Chem.* **2004**, *25* (9), 1157-1174.
(87) Case, D. A. B., K.; Ben-Shalom, I. Y.; Brozell, S. R.; Cerutti, D. S.; Cheatham III, T. E.; Cruzeiro, V. W. D.; Darden, T. A.; Duke, R. E.; Giambasu, G.; Gilson, M. K.; Gohlke, H.; Goetz, A. W.; Harris, R.; Izadi, S.; Izmailov, S. A.; Kasavajhala, K.; Kovalenko, A.; Krasny, R.; Kurtzman, T.; Lee, T. S.; LeGrand, S.; Li, P.; Lin, C.; Liu, J.; Luchko, T.; Machado, M.; Man, V.; Merz, K. M.; Miao, Y.; Mikhailovskii, O.; Monard, G.; Nguyen, H.; Onufriev, A.; Pan, F.; Pantano, S.; Qi, R.; Rahaman, O.; Roitberg, A.; Sagui, C.; Schott-Verdugo, S.; Shajan, A.; Shen, J.; Simmerling, C. L.; Skrynnikov, N. R.; Smith, J.; Swails, J.; Walker, R. C.; Wang, J.; Wilson, L.; Wolf, R. M.; Wu, X.; Xue, Y.; York, D. M.; Zhu, Y. Amber 2021. *University of California, San Francisco.* **2021**.
(88) Gordon, J. C.; Myers, J. B.; Folta, T.; Shoja, V.; Heath, L. S.; Onufriev, A. H++: a server for estimating p Ka s and adding missing hydrogens to macromolecules. *Nucleic Acids Res.* **2005**, *33* (suppl_2), W368-W371.
(89) Jorgensen, M. A five-site model for liquid water and the reproduction of the density anomaly by rigid, nonpolarizable potential functions. *J. Chem. Phys.* **2000**, *112*, 8910-8922.
(90) Jorgensen, W. L.; Chandrasekhar, J.; Madura, J. D.; Impey, R. W.; Klein, M. L. Comparison of simple potential functions for simulating liquid water. *J. Chem. Phys.* **1983**, *79* (2), 926-935.
(91) Mark, P.; Nilsson, L. Structure and Dynamics of the TIP3P, SPC, and SPC/E Water Models at 298 K. *J. Phys. Chem. A.* **2001**, *105* (43), 9954-9960.
(92) Schmit, J. D.; Kariyawasam, N. L.; Needham, V.; Smith, P. E. SLTCAP: A Simple Method for Calculating the Number of Ions Needed for MD Simulation. *J. Chem. Theory Comput.* **2018**, *14* (4), 1823-1827.
(93) Pastor, R. W.; Brooks, B. R.; Szabo, A. An analysis of the accuracy of Langevin and molecular dynamics algorithms. *Mol. Phys.* **1988**, *65* (6), 1409-1419.
(94) Schneider, T.; Stoll, E. Molecular-dynamics study of a three-dimensional one-component model for distortive phase transitions. *Phys. Rev. B* **1978**, *17* (3), 1302-1322.
(95) Berendsen, H. J. C.; Postma, J. P. M.; van Gunsteren, W. F.; DiNola, A.; Haak, J. R. Molecular dynamics with coupling to an external bath. *J. Chem. Phys.* **1984**, *81* (8), 3684-3690.
(96) Essmann, U.; Perera, L.; Berkowitz, M. L.; Darden, T.; Lee, H.; Pedersen, L. G. A smooth particle mesh Ewald method. *J. Chem. Phys.* **1995**, *103* (19), 8577-8593.
(97) Darden, T.; York, D.; Pedersen, L. Particle mesh Ewald: An N·log(N) method for Ewald sums in large systems. *J. Chem. Phys.* **1993**, *98* (12), 10089-10092.

(98) Macuglia, D. SHAKE and the exact constraint satisfaction of the dynamics of semi-rigid molecules in Cartesian coordinates, 1973–1977. *Archive for History of Exact Sciences* **2023**, *77* (4), 345-371.
(99) Roe, D. R.; Cheatham, T. E., 3rd. PTRAJ and CPPTRAJ: Software for Processing and Analysis of Molecular Dynamics Trajectory Data. *J. Chem. Theory Comput.* **2013**, *9* (7), 3084-3095.
(100) Hou, T.; Wang, J.; Li, Y.; Wang, W. Assessing the Performance of the MM/PBSA and MM/GBSA Methods. 1. The Accuracy of Binding Free Energy Calculations Based on Molecular Dynamics Simulations. *J. Chem. Inf. Model.* **2011**, *51* (1), 69-82.
(101) Knappeova, B.; Mlynsky, V.; Pykal, M.; Sponer, J.; Banas, P.; Otyepka, M.; Krepl, M. Comprehensive Assessment of Force-Field Performance in Molecular Dynamics Simulations of DNA/RNA Hybrid Duplexes. *J. Chem. Theory. Comput.* **2024**, *20* (15), 6917-6929.
(102) Lu, X. J.; Olson, W. K. 3DNA: a software package for the analysis, rebuilding and visualization of three-dimensional nucleic acid structures. *Nucleic Acids Res.* **2003**, *31* (17), 5108-5121.
(103) Babcock, M. S.; Pednault, E. P. D.; Olson, W. K. Nucleic Acid Structure Analysis: Mathematics for Local Cartesian and Helical Structure Parameters That Are Truly Comparable Between Structures. *J. Mol. Biol.* **1994**, *237* (1), 125-156.
(104) Olson, W. K.; Bansal, M.; Burley, S. K.; Dickerson, R. E.; Gerstein, M.; Harvey, S. C.; Heinemann, U.; Lu, X. J.; Neidle, S.; Shakked, Z.; et al. A standard reference frame for the description of nucleic acid base-pair geometry. *J. Mol. Biol.* **2001**, *313* (1), 229-237.
(105) Case, D. A.; Aktulga, H. M.; Belfon, K.; Cerutti, D. S.; Cisneros, G. A.; Cruzeiro, V. W. D.; Forouzesh, N.; Giese, T. J.; Gotz, A. W.; Gohlke, H.; et al. AmberTools. *J. Chem. Inf. Model.* **2023**, *63* (20), 6183-6191.
(106) Kobayashi, Y.; Fukuhara, D.; Akase, D.; Aida, M.; Ui-Tei, K. siRNA Seed Region Is Divided into Two Functionally Different Domains in RNA Interference in Response to 2'-OMe Modifications. *ACS Omega* **2022**, *7* (2), 2398-2410.
(107) Choung, S.; Kim, Y. J.; Kim, S.; Park, H.-O.; Choi, Y.-C. Chemical modification of siRNAs to improve serum stability without loss of efficacy. *Biochem. Biophys. Res. Commun.* **2006**, *342* (3), 919-927.
(108) Sun, Y.; Zhao, Y.; Zhao, X.; Lee, R. J.; Teng, L.; Zhou, C. Enhancing the Therapeutic Delivery of Oligonucleotides by Chemical Modification and Nanoparticle Encapsulation. *Molecules* **2017**, *22* (10).
(109) Shukla, S.; Sumaria, C. S.; Pradeepkumar, P. I. Exploring chemical modifications for siRNA therapeutics: a structural and functional outlook. *ChemMedChem* **2010**, *5* (3), 328-349.
(110) Qiu, L.; Jing, Q.; Li, Y.; Han, J. RNA modification: mechanisms and therapeutic targets. *Mol. Biomed.* **2023**, *4* (1), 25.

CHAPTER 4: THESIS SUMMARY AND FUTURE DIRECTIONS

4.1 Summary

The development of siRNA-based therapeutics has been advanced by the strategic incorporation of chemical modifications, especially at the 2′-position of ribose. Among these modifications, 2′-O-methyl (2′-*O*-Me) and 2′-fluoro (2′-F) have gained prominence for their ability to modulate siRNA function because of their use in FDA-approved siRNA therapeutics.[1] The introduction of chemical modifications into siRNA may affect several structural and functional properties, including the susceptibility to ribonuclease degradation, recognition, and processing by the RNAi machinery, toxicity, thermal stability (melting temperature), and maintenance of the A-form RNA helical structure.[2-5] While several studies have explored the impact of modifications on properties such as the thermal stability of siRNA,[6,7] resistance to ribonucleases,[8-10] and circulation time in the bloodstream,[11] the knowledge about the impact of chemical modifications on the structure of siRNA is missing. This gap is particularly important because experimental evidence underscores that maintaining the A-form helical structure is essential for siRNA function and any significant deviation from this structure has been shown to abolish RNAi activity.[12-14] This thesis has employed computational methodologies to investigate the structural impacts of chemical modifications on siRNA, particularly focusing on their effects on the siRNA duplex and duplex interactions with hAgo2, a key protein in the RISC. Using all-atom molecular dynamics (MD) simulations, this work provides detailed insights into how these chemical modifications affect the geometry, flexibility, and biological recognition of siRNA molecules.

In Chapter 2, I systematically analyzed fully-modified RNA duplexes derived from

the first five FDA-approved siRNA drugs to assess how 2′-*O*-Me and 2′-F substitutions influence the structural features of A-form helices. The results revealed that 2′-*O*-Me modifications introduce conformational rigidity and effectively compress the RNA duplex. This structural rigidity may hinder the ability of the duplex to adapt to the conformational requirements of RISC loading and activity. On the other hand, the 2′-F modification better preserves RNA-like structural characteristics, but makes the pucker adopted by the sugar throughout the helix more diverse and disrupts the helical structure of the duplex when fully modified without the restraint, suggesting a potential trade-off between thermal stability and preservation of the helix. Most importantly, duplexes containing a combination of 2′-*O*-Me and 2′-F substitutions, such as those observed in Givosiran, Lumasiran, Inclisiran and Vutrisiran, exhibit a synergistic effect, whereby the 2′-F modification appears to counterbalance the rigidity induced by 2′-*O*-Me, and the diverse sugar pucker adopted by the sugar throughout the helix introduced by 2′-F is tempered by the presence of 2′-*O*-Me, collectively fine-tuning the duplex conformation to more closely resemble that of canonical RNA. Structural fingerprinting using heatmaps of helical parameters (e.g., roll, inclination, x-displacement) further illustrates how individual and combined modifications distinctly influence RNA geometry. A particularly interesting observation is the nucleobase sequence-independence of the structural changes induced by the modifications. Across different siRNA nucleobase sequences, the presence of 2′-*O*-Me and 2′-F modifications consistently altered structural parameters in a reproducible manner. This finding underscores the dominant role of chemical modifications over nucleobase sequence in dictating RNA conformation. Importantly, these structural trends were consistent across all five FDA-approved siRNA drugs studied, underscoring the generalizability of the observed effects, and offering a robust framework for generalizing

design principles in siRNA drug development.

In Chapter 3, I examined how the structural effects seen for isolated duplexes manifest in the context of the siRNA–hAgo2 complex using the nucleobase sequence of Givosiran for the siRNA. The consistency across diverse sequence contexts is the reason for focusing on a single representative drug, in the siRNA–hAgo2 interaction modeling presented in Chapter 3. To my knowledge, no previous modeling or simulation-based studies have systematically investigated the residue-level impact of chemical modifications within the seed region on hAgo2 recognition, nor has a structural model of a fully-modified seed region siRNA–hAgo2 complex been reported. In this work, we present and characterize the first such model, featuring a fully chemically-modified seed region of siRNA guide strand bound to hAgo2. All-atom MD simulations of modified guide strands bound to hAgo2 revealed that both 2′-*O*-Me and 2′-F modifications are well tolerated within the MID and PIWI domains, which are critical for anchoring the seed region. The modifications do not completely disrupt canonical siRNA–hAgo2 interactions. Instead, they subtly modulate the persistence of hydrogen bonds, most often enhancing interaction lifetimes throughout the simulations. This likely contributes to the increased binding affinity, which is essential for sustained silencing activity *in vivo*.[3, 15-17] These findings offer molecular-level insights into how guide strand design influences RISC loading, thereby providing a valuable platform for future structure-based optimization of siRNA therapeutics.

The insights from this thesis help bridge the knowledge gap between clinically-relevant chemical modification strategies and their structural consequences at both the RNA duplex and protein-binding levels. By elucidating how specific 2′-*O*-Me and 2′-F modifications influence siRNA conformation and hAgo2 recognition, this work reinforces

the rationale behind current therapeutic designs and provides a predictive framework for developing novel siRNA sequences that preserve RNA-like helical integrity. The detailed atomistic understanding developed here is broadly applicable and can be extended to guide the rational design of other RNA-based therapeutic platforms that rely on the introduction of chemical modifications, including miRNA mimics, antisense oligonucleotides, and mRNA vaccines.

4.2 Future Directions

While this thesis provides key insights into the structural effects of 2′-modifications on siRNA duplexes and their interactions with hAgo2, several important questions remain for future investigation. One such question revolves around the positional effects of chemical modifications. The current work focused on fully-modified duplexes to explain the global structural consequences of 2′-*O*-Me, 2′-F, and their combination according to existing FDA-approved drugs. However, therapeutic siRNAs often feature asymmetric or position-specific modification patterns, such as selective placement of 2′-*O*-Me at seed positions and 2′-F at other locations.[18-24] Future simulations should systematically explore how the position of the modifications along the siRNA strands influence key RNAi-related outcomes, including cleavage efficiency, strand selection, and off-target binding. Another important direction involves mechanistic studies of RNAi catalysis. While this work focuses on structural interactions between the seed region of siRNA guide strand and hAgo2, an essential determinant of RNAi efficacy is the ability of hAgo2 to catalyze target mRNA cleavage.[25-33]

Another important direction for future work is expanding the chemical modification landscape. While this thesis focused on 2′-*O*-Me and 2′-F modifications, several other

chemical modifications, including phosphorothioates, unlocked nucleic acids (UNAs),[34] glycol nucleic acids (GNAs),[35] locked nucleic acid (LNAs),[34,36, 37] ethyl-bridged nucleic acids (ENAs),[38] and 2′-O-methoxyethyl (2′-*O*-MOE)[19] (Figures 1.7–1.9) are increasingly being explored for use in siRNA therapeutics. Incorporating these modifications into similar MD simulation models will deepen our understanding of how different chemistries modulate siRNA structure, flexibility, and protein binding, and will expand the design toolkit for next-generation siRNA drugs. Lastly, as structural datasets on RNA modifications continue to grow,[39,40] there is a valuable opportunity to integrate atomistic simulation data with machine learning approaches. By training models on structural features such as helical parameters, and sugar pucker distributions, it may become possible to predict the functional efficacy of novel siRNA designs prior to experimental validation. This data-driven strategy could enable high-throughput screening of chemically-modified siRNAs, accelerating the discovery and optimization pipeline for RNA therapeutics.

4.3 Final Remarks

Taken together, this thesis provides a novel understanding of the structural consequences of ribose modifications in siRNA therapeutics. By linking detailed RNA duplex-level conformational analyses with molecular modeling of siRNA–hAgo2 interactions, this work established a computational framework for the rational design of next-generation siRNA drugs. The observed synergistic effects of 2′-*O*-Me and 2′-F modifications, along with the discovery that these structural alterations are largely nucleobase sequence independent, present a compelling strategy for enhancing siRNA stability and efficacy. As a result, the models, structural insights, and computational approaches developed herein lay a foundation for the precision engineering of siRNA

therapeutics with improved potency.

4.4 References

(1) Gangopadhyay, S.; Gore, K. R. Advances in siRNA therapeutics and synergistic effect on siRNA activity using emerging dual ribose modifications. *RNA Biol.* **2022**, *19* (1), 452-467.
(2) Manoharan, M. RNA interference and chemically modified small interfering RNAs. *Curr. Opin. Chem. Biol.* **2004**, *8* (6), 570-579.
(3) Behlke, M. A. Chemical modification of siRNAs for in vivo use. *Oligonucleotides* **2008**, *18* (4), 305-319.
(4) Chernikov, I. V.; Vlassov, V. V.; Chernolovskaya, E. L. Current Development of siRNA Bioconjugates: From Research to the Clinic. *Front. Pharmacol.* **2019**, *10*, 444.
(5) Chernikov, I. V.; Gladkikh, D. V.; Meschaninova, M. I.; Ven'yaminova, A. G.; Zenkova, M. A.; Vlassov, V. V.; Chernolovskaya, E. L. Cholesterol-Containing Nuclease-Resistant siRNA Accumulates in Tumors in a Carrier-free Mode and Silences MDR1 Gene. *Mol. Ther. Nucleic Acids* **2017**, *6*, 209-220.
(6) Bobst, A. M.; Rottman, F.; Cerutti, P. A. Effect of the methylation of the 2′-hydroxyl groups in polyadenylic acid on its structure in weakly acidic and neutral solutions and on its capability to form ordered complexes with polyuridylic acid. *J. Mol. Biol.* **1969**, *46* (2), 221-234.
(7) Pallan, P. S.; Greene, E. M.; Jicman, P. A.; Pandey, R. K.; Manoharan, M.; Rozners, E.; Egli, M. Unexpected origins of the enhanced pairing affinity of 2'-fluoro-modified RNA. *Nucleic Acids Res.* **2011**, *39* (8), 3482-3495.
(8) Takahashi, M.; Nagai, C.; Hatakeyama, H.; Minakawa, N.; Harashima, H.; Matsuda, A. Intracellular stability of 2'-OMe-4'-thioribonucleoside modified siRNA leads to long-term RNAi effect. *Nucleic Acids Res.* **2012**, *40* (12), 5787-5793.
(9) Volkov, A. A.; Kruglova, N. y. S.; Meschaninova, M. I.; Venyaminova, A. G.; Zenkova, M. A.; Vlassov, V. V.; Chernolovskaya, E. L. Selective Protection of Nuclease-Sensitive Sites in siRNA Prolongs Silencing Effect. *Oligonucleotides* **2009**, *19* (2), 191-202.
(10) Morrissey, D. V.; Lockridge, J. A.; Shaw, L.; Blanchard, K.; Jensen, K.; Breen, W.; Hartsough, K.; Machemer, L.; Radka, S.; Jadhav, V.; et al. Potent and persistent in vivo anti-HBV activity of chemically modified siRNAs. *Nat. Biotechnol.* **2005**, *23* (8), 1002-1007.
(11) Liu, X.; Wang, W.; Samarsky, D.; Liu, L.; Xu, Q.; Zhang, W.; Zhu, G.; Wu, P.; Zuo, X.; Deng, H.; et al. Tumor-targeted in vivo gene silencing via systemic delivery of cRGD-conjugated siRNA. *Nucleic Acids Res.* **2014**, *42* (18), 11805-11817.
(12) Ku, S. H.; Jo, S. D.; Lee, Y. K.; Kim, K.; Kim, S. H. Chemical and structural modifications of RNAi therapeutics. *Adv. Drug Deliv. Rev.* **2016**, *104*, 16-28.
(13) Crooke, S. T.; Witztum, J. L.; Bennett, C. F.; Baker, B. F. RNA-Targeted Therapeutics. *Cell Metab.* **2018**, *27* (4), 714-739.
(14) Ya-Lin Chiu, T. M. R. RNAi in Human Cells: Basic Structural and Functional Features of Small Interfering RNA. *Mol. Cell* **2002**, *Volume 10* (Issue 3), Pages 549-561.
(15) Deleavey, G. F.; Damha, M. J. Designing chemically modified oligonucleotides for targeted gene silencing. *Chem. Biol.* **2012**, *19* (8), 937-954.

(16) Allerson, C. R.; Sioufi, N.; Jarres, R.; Prakash, T. P.; Naik, N.; Berdeja, A.; Wanders, L.; Griffey, R. H.; Swayze, E. E.; Bhat, B. Fully 2'-modified oligonucleotide duplexes with improved in vitro potency and stability compared to unmodified small interfering RNA. *J. Med. Chem.* **2005**, *48* (4), 901-904.
(17) Choung, S.; Kim, Y. J.; Kim, S.; Park, H.-O.; Choi, Y.-C. Chemical modification of siRNAs to improve serum stability without loss of efficacy. *Biochem. Biophys. Res. Commun.* **2006**, *342* (3), 919-927.
(18) Hu, B.; Zhong, L.; Weng, Y.; Peng, L.; Huang, Y.; Zhao, Y.; Liang, X. J. Therapeutic siRNA: state of the art. *Signal Transduct. Target. Ther.* **2020**, *5* (1), 101.
(19) Prakash, T. P.; Allerson, C. R.; Dande, P.; Vickers, T. A.; Sioufi, N.; Jarres, R.; Baker, B. F.; Swayze, E. E.; Griffey, R. H.; Bhat, B. Positional Effect of Chemical Modifications on Short Interference RNA Activity in Mammalian Cells. *J. Med. Chem.* **2005**, *48* (13), 4247-4253.
(20) Kenski, D. M.; Butora, G.; Willingham, A. T.; Cooper, A. J.; Fu, W.; Qi, N.; Soriano, F.; Davies, I. W.; Flanagan, W. M. siRNA-optimized Modifications for Enhanced In Vivo Activity. *Mol. Ther. Nucleic Acids* **2012**, *1* (1), e5.
(21) Shinohara, F.; Oashi, T.; Harumoto, T.; Nishikawa, T.; Takayama, Y.; Miyagi, H.; Takahashi, Y.; Nakajima, T.; Sawada, T.; Koda, Y.; et al. siRNA potency enhancement via chemical modifications of nucleotide bases at the 5'-end of the siRNA guide strand. *RNA.* **2021**, *27* (2), 163-173.
(22) Yu, A.-M.; Choi, Y. H.; Tu, M.-J. RNA Drugs and RNA Targets for Small Molecules: Principles, Progress, and Challenges. *Pharmacol. Rev.* **2020**, *72* (4), 862-898.
(23) Guo, F.; Li, Y.; Yu, W.; Fu, Y.; Zhang, J.; Cao, H. Recent Progress of Small Interfering RNA Delivery on the Market and Clinical Stage. *Mol Pharm* **2024**, *21* (5), 2081-2096.
(24) Egli, M.; Manoharan, M. Re-Engineering RNA Molecules into Therapeutic Agents. *Acc. Chem. Res.* **2019**, *52* (4), 1036-1047.
(25) Mallick, B.; Sharma, A. R.; Lee, S. S.; Chakraborty, C. Understanding the molecular interaction of human argonaute-2 and miR-20a complex: A molecular dynamics approach. *J. Cell. Biochem.* **2019**, *120* (12), 19915-19924.
(26) Sheng, G.; Zhao, H.; Wang, J.; Rao, Y.; Tian, W.; Swarts, D. C.; van der Oost, J.; Patel, D. J.; Wang, Y. Structure-based cleavage mechanism of Thermus thermophilus Argonaute DNA guide strand-mediated DNA target cleavage. *PNAS* **2014**, *111* (2), 652-657.
(27) Bhandare, V.; Ramaswamy, A. Structural Dynamics of Human Argonaute2 and Its Interaction with siRNAs Designed to Target Mutant tdp43. *Adv. Bioinformatics* **2016**, *2016*, 8792814.
(28) Miyoshi, T.; Ito, K.; Murakami, R.; Uchiumi, T. Structural basis for the recognition of guide RNA and target DNA heteroduplex by Argonaute. *Nat. Commun.* **2016**, *7*, 11846.
(29) Frank, F.; Sonenberg, N.; Nagar, B. Structural basis for 5'-nucleotide base-specific recognition of guide RNA by human AGO2. *Nature* **2010**, *465* (7299), 818-822.
(30) Jiang, H.; Sheong, F. K.; Zhu, L.; Gao, X.; Bernauer, J.; Huang, X. Markov State Models Reveal a Two-Step Mechanism of miRNA Loading into the Human Argonaute Protein: Selective Binding followed by Structural Re-arrangement. *PLoS Comput. Biol.* **2015**, *11* (7), e1004404.
(31) Zhu, L.; Jiang, H.; Sheong, F. K.; Cui, X.; Gao, X.; Wang, Y.; Huang, X. A Flexible Domain-Domain Hinge Promotes an Induced-fit Dominant Mechanism for the Loading of Guide-DNA into Argonaute Protein in Thermus thermophilus. *J. Phys. Chem. B.* **2016**, *120* (10), 2709-2720.

(32) Hutvagner, G.; Simard, M. J. Argonaute proteins: key players in RNA silencing. *Nat. Rev. Mol. Cell Biol.* **2008**, *9* (1), 22-32.
(33) Olina, A. V.; Kulbachinskiy, A. V.; Aravin, A. A.; Esyunina, D. M. Argonaute Proteins and Mechanisms of RNA Interference in Eukaryotes and Prokaryotes. *Biochemistry (Mosc)* **2018**, *83* (5), 483-497.
(34) Doessing, H.; Vester, B. Locked and Unlocked Nucleosides in Functional Nucleic Acids. *Molecules* **2011**, *16* (6), 4511-4526.
(35) Janas, M. M.; Schlegel, M. K.; Harbison, C. E.; Yilmaz, V. O.; Jiang, Y.; Parmar, R.; Zlatev, I.; Castoreno, A.; Xu, H.; Shulga-Morskaya, S.; et al. Selection of GalNAc-conjugated siRNAs with limited off-target-driven rat hepatotoxicity. *Nat. Commun.* **2018**, *9* (1), 723.
(36) Elmen, J.; Lindow, M.; Schutz, S.; Lawrence, M.; Petri, A.; Obad, S.; Lindholm, M.; Hedtjarn, M.; Hansen, H. F.; Berger, U.; et al. LNA-mediated microRNA silencing in non-human primates. *Nature* **2008**, *452* (7189), 896-899.
(37) Mook, O. R.; Baas, F.; de Wissel, M. B.; Fluiter, K. Evaluation of locked nucleic acid–modified small interfering RNA in vitro and in vivo. *Mol. Cancer Ther.* **2007**, *6* (3), 833-843.
(38) Morita, K.; Hasegawa, C.; Kaneko, M.; Tsutsumi, S.; Sone, J.; Ishikawa, T.; Imanishi, T.; Koizumi, M. 2′-O, 4′-C-Ethylene-bridged nucleic acids (ENA) with nuclease-resistance and high affnity for RNA. *Nucleic Acids Symposium Series* **2001**, *1* (1), 241-242.
(39) Liu, W. W.; Zheng, S. Q.; Li, T.; Fei, Y. F.; Wang, C.; Zhang, S.; Wang, F.; Jiang, G. M.; Wang, H. RNA modifications in cellular metabolism: implications for metabolism-targeted therapy and immunotherapy. *Signal Transduct. Target. Ther.* **2024**, *9* (1), 70.
(40) Cappannini, A.; Ray, A.; Purta, E.; Mukherjee, S.; Boccaletto, P.; Moafinejad, S. N.; Lechner, A.; Barchet, C.; Klaholz, B. P.; Stefaniak, F.; Bujnicki, J. M. MODOMICS: a database of RNA modifications and related information. 2023 update. *Nucleic Acids Res.* **2024**, *52* (D1), D239-D244.

APPENDIX A: SUPPLEMENTARY INFORMATION FOR CHAPTER 2

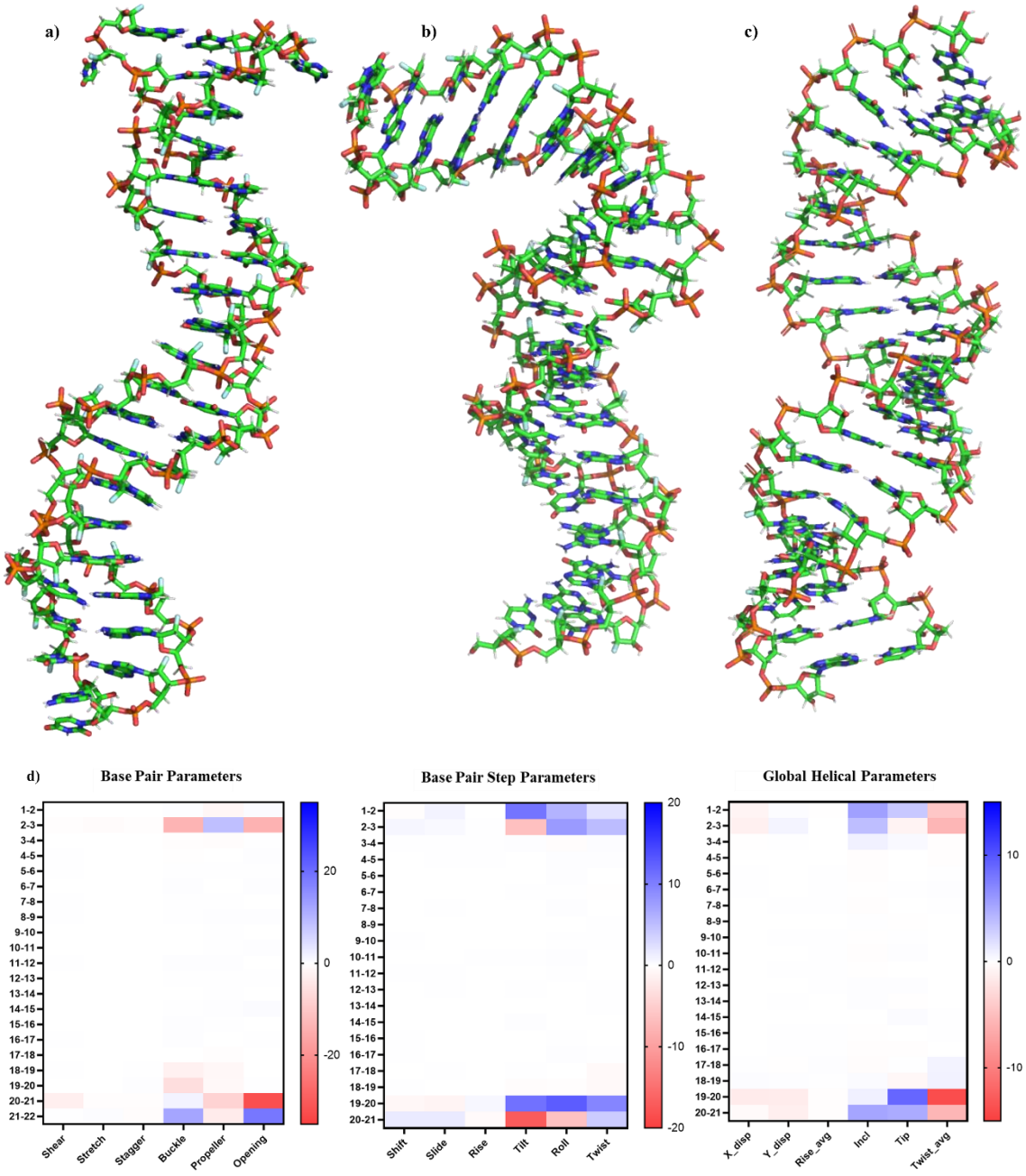

Figure A.1: (a) U-FNA showing base pair fraying at the subterminal (b) U-FNA with the helix disrupted (c) A-FNA showing no fraying at the terminal as a result of reduction in the number of F-modifications (d) Base pair parameters showing the deviation between unrestrained (U-) and fully restrained (R-) FNA for Givosiran.

To assess the structural stability of FNA duplexes in the context of Givosiran, we compared the base pair parameters of unrestrained (U-FNA) and fully distant restrained (R-FNA) MD simulations. The unrestrained FNA duplex exhibited extensive base pair fraying **(Figure A.1a)**, particularly at the termini, resulting in a disruption in the helical structure **(Figure**

A.1b). Interestingly, this fraying was absent in other modification patterns that included F substitutions, suggesting that the destabilization is specific to the fully fluorinated system. To test this hypothesis, we designed an alternating FNA duplex (A-FNA) where the fluorine modifications were introduced in an alternating pattern across the duplex. This strategy successfully eliminated the terminal fraying **(Figure A.1c)**, reinforcing the conclusion that excessive fluorination is responsible for the observed structural instability. Given our interest in characterizing a fully fluorinated duplex, we applied distance restraints between all heavy atoms involved in Watson–Crick base pairing. To validate this restraint strategy, we compared helical parameters between U-FNA and R-FNA **(Figure A.1d)**. The analysis revealed no significant deviations across the duplex, apart from minor differences at the termini, confirming that the applied restraints preserved native-like structural features.

Table A.1: Average (and standard deviation) of structural parameters of canonical and chemically modified nucleic acids from 5 replicas of 1 μs MD simulations.

Features	**RNA**	**DNA**	**OMeNA**	**FNA**	**Lumasiran**
Sugar Pucker	C3'-endo	C2'-endo	C3'-endo	C3'-endo	C3'-endo
Rise/ Base Pair	2.63 (0.17) Å	3.25 (0.12) Å	2.17 (0.26) Å	2.73 (0.13) Å	2.48 (0.18) Å
Base Pairs/Turn	11	10	11	11	11
	RNA	**DNA**	**OMeNA**	**FNA**	**Inclisiran**
Sugar Pucker	C3'-endo	C2'-endo	C3'-endo	C3'-endo	C3'-endo
Rise/Base Pair	2.67 (0.15) Å	3.22 (0.14) Å	2.40 (0.15) Å	2.72 (0.17) Å	2.55 (0.18) Å
Base Pairs/Turn	11	10	11	11	11
	RNA	**DNA**	**OMeNA**	**FNA**	**Vutrisiran**
Sugar Pucker	C3'-endo	C2'-endo	C3'-endo	C3'-endo	C3'-endo
Rise/Base Pair	2.63 (0.12) Å	3.24 (0.12) Å	2.34 (0.16) Å	2.68 (0.12) Å	2.42 (0.12) Å
Base Pairs/Turn	11	10	11	11	11

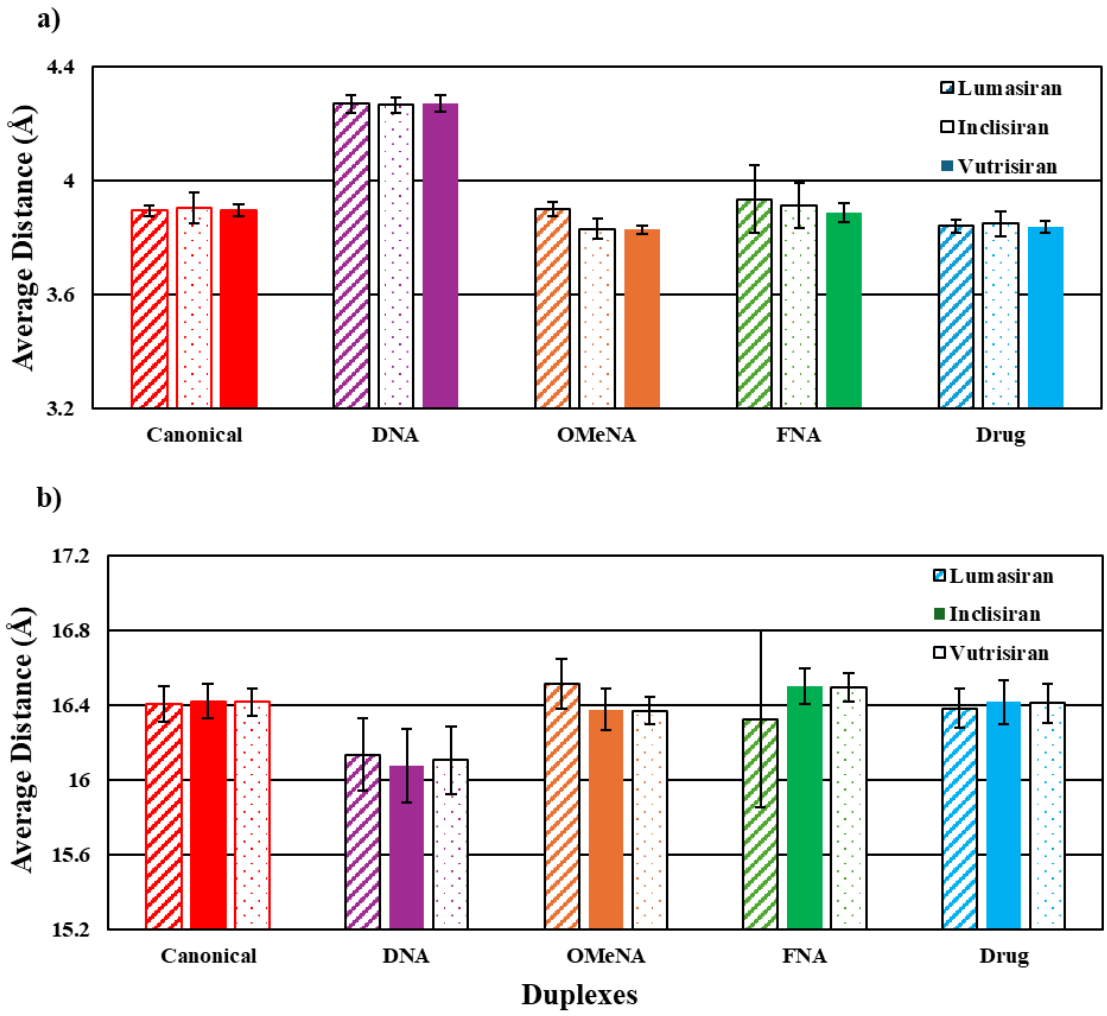

Figure A.2: Interstrand and intrastrand backbone distances for Lumasiran, Inclisiran and Vutrisiran.

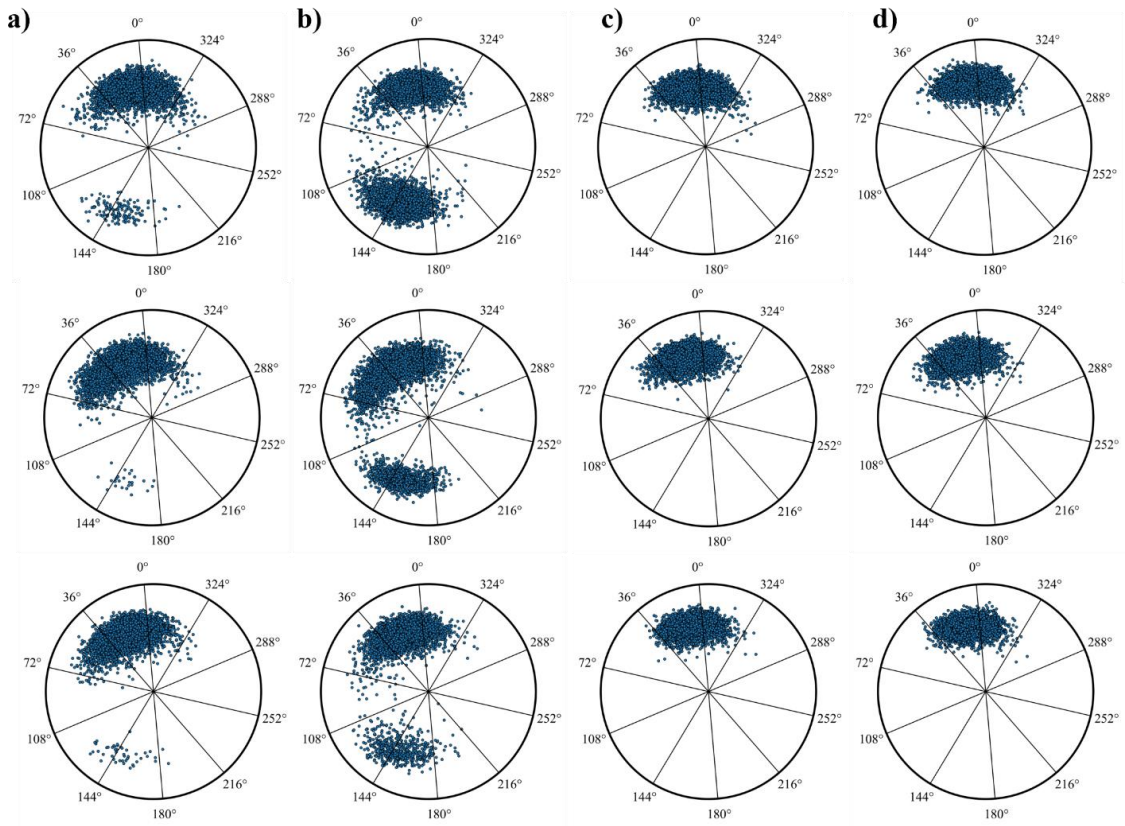

Figure A.2:(a-d) Schematic of the distribution of the pseudorotation phase angle (P) sampled by the ribose of canonical RNA, FNA, OMeNA and drugs (Lumasiran, Inclisiran and Vutrisiran) from (top-bottom) throughout 1 μs MD simulations across 5 replicas.

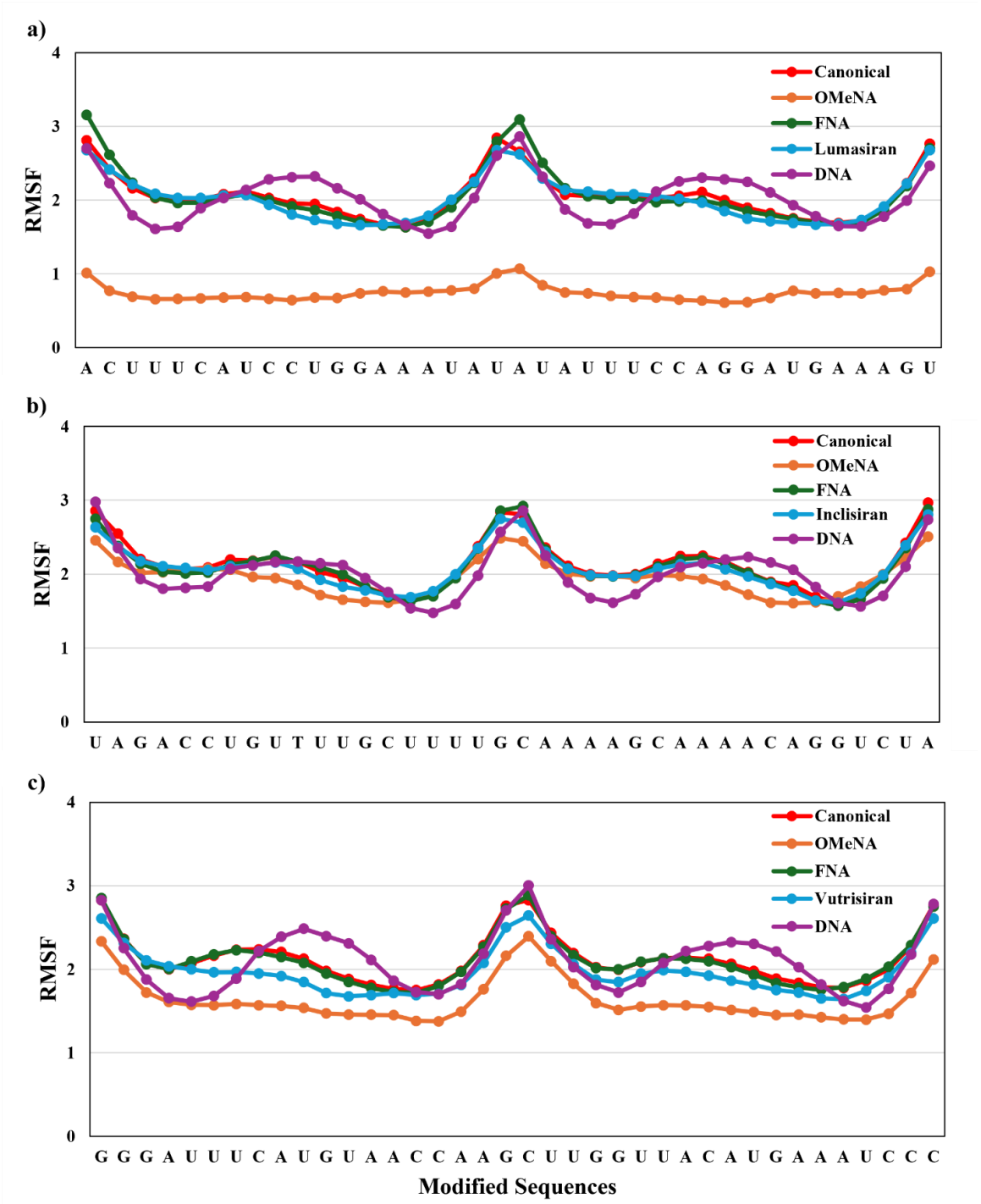

Figure A.3: Root-mean-square fluctuations (RMSF) for canonical and chemically modified nucleic acids (in Å) over 1 μs MD simulations across 5 replicas.

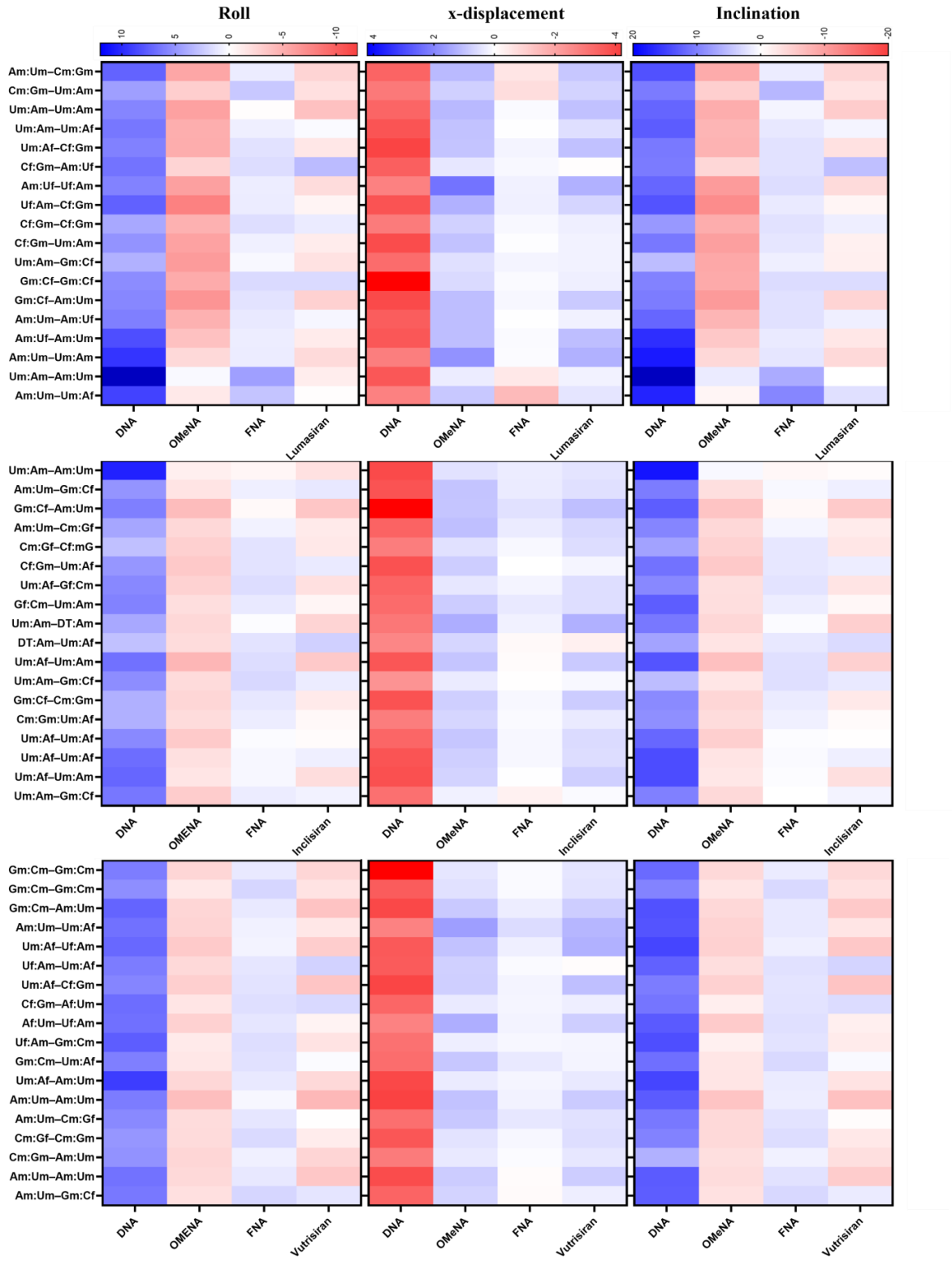

Figure A.4: Heatmaps illustrating the deviations in structural parameters of modified nucleic acids relative to canonical RNA.

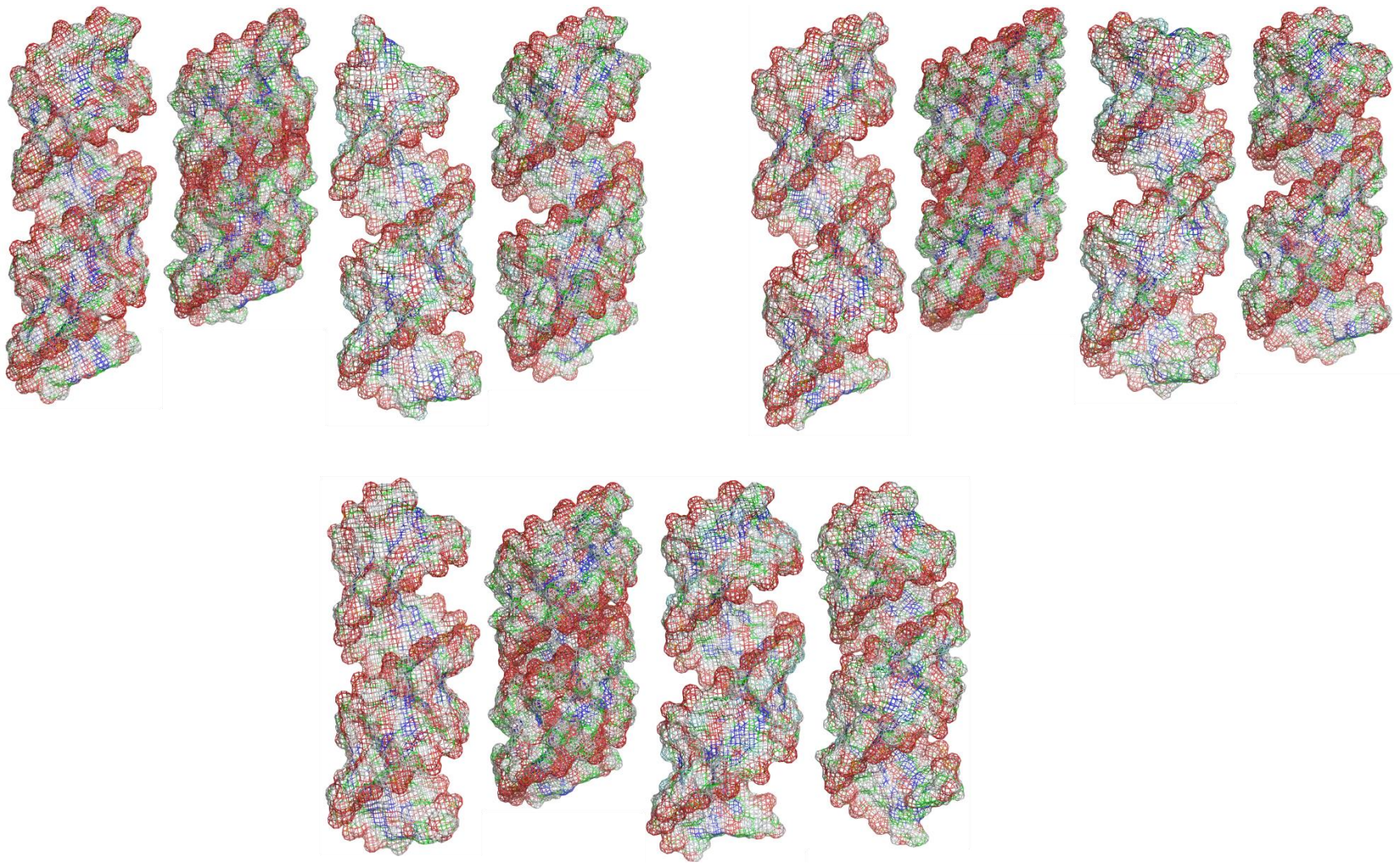

Figure A.5: L-R: RNA, OMeNA, FNA, and drugs global structures.

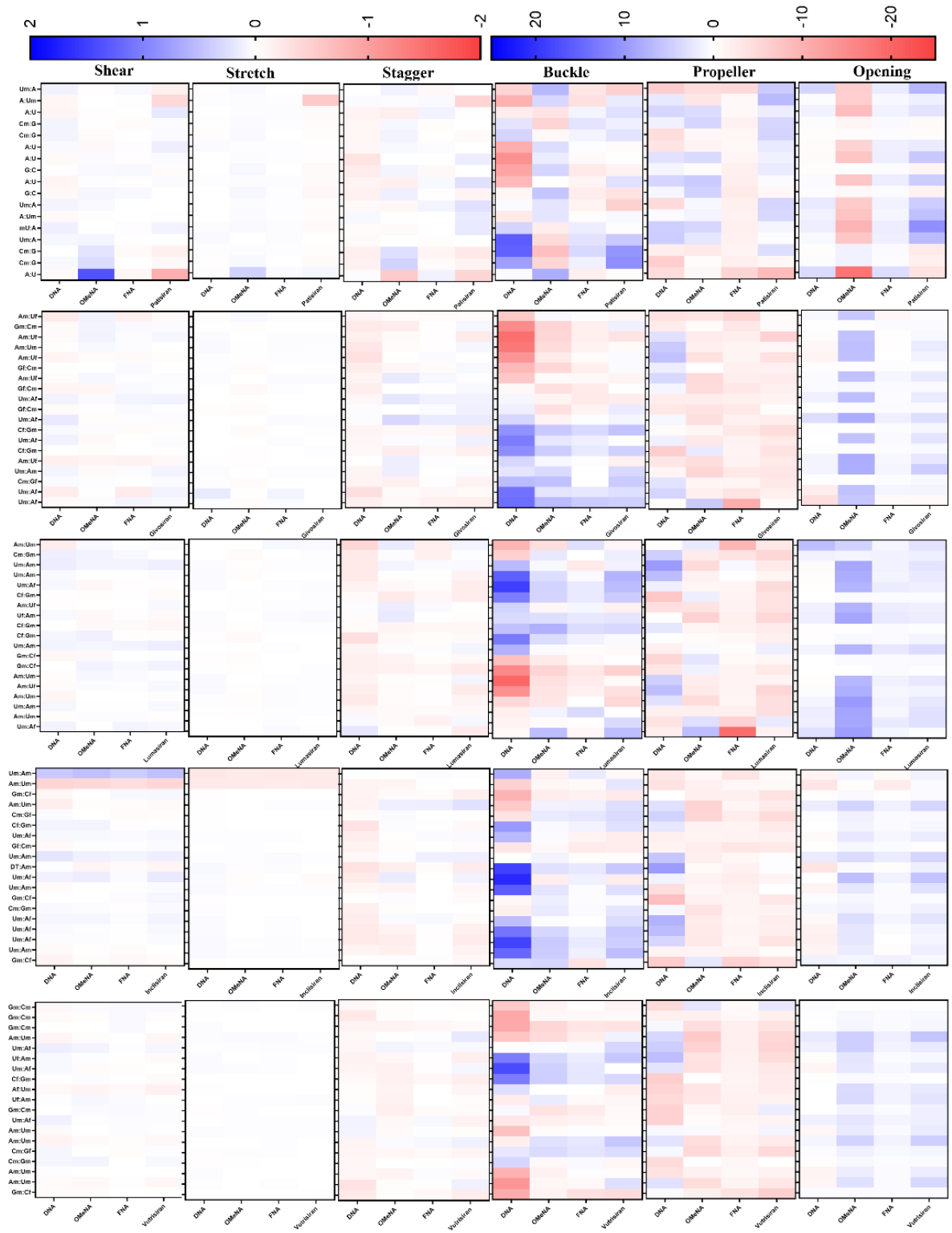

Figure A.6: Heatmaps illustrating the deviations in structural parameters (base pair) of modified nucleic acids relative to canonical RNA.

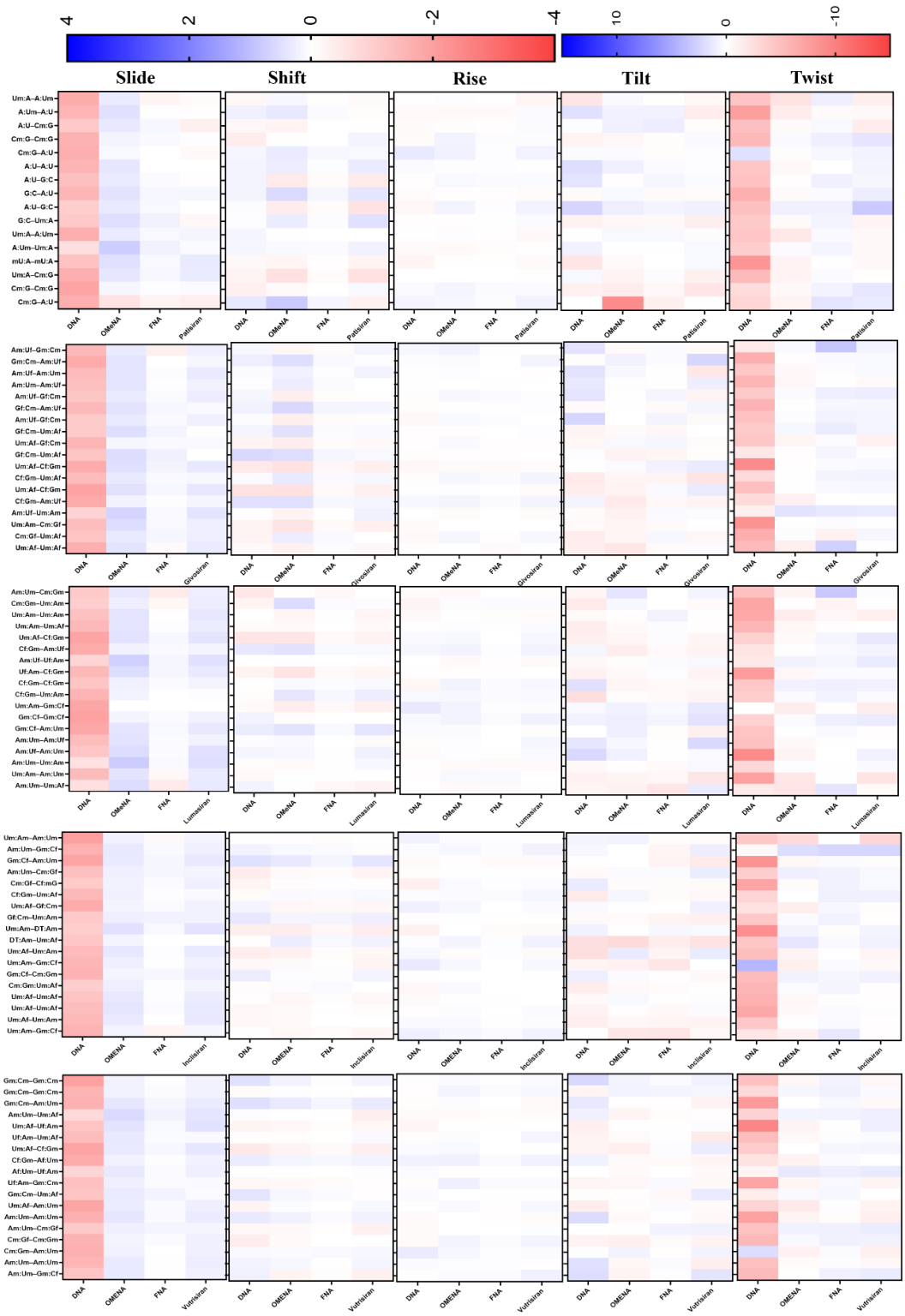

Figure A.7: Heatmaps illustrating the deviations in structural parameters (base pair step) of modified nucleic acids relative to canonical RNA.

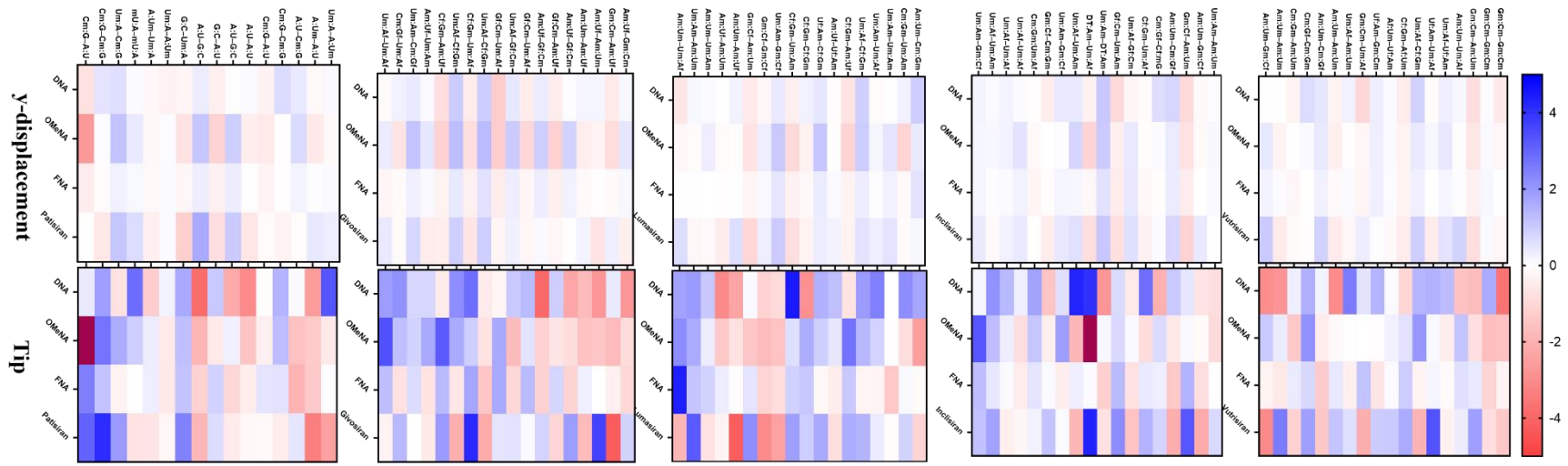

Figure A.8: Heatmaps illustrating the deviations in structural parameters (helix) of modified nucleic acids relative to canonical RNA.

Reproducibility Tests for Averages for Helical Parameters Among Replicas Used to Make Heatmaps and Confidence Interval At 95%

An excel document with all the data is attached to this supplementary information.

Atomic Coordinates For RNA, Drug, Omena, FNA And DNA For Patisiran, Givosiran, Lumasiran, Inclisiran and Vutrisiran Respectively

All atomic coordinates files have been attached to the document.

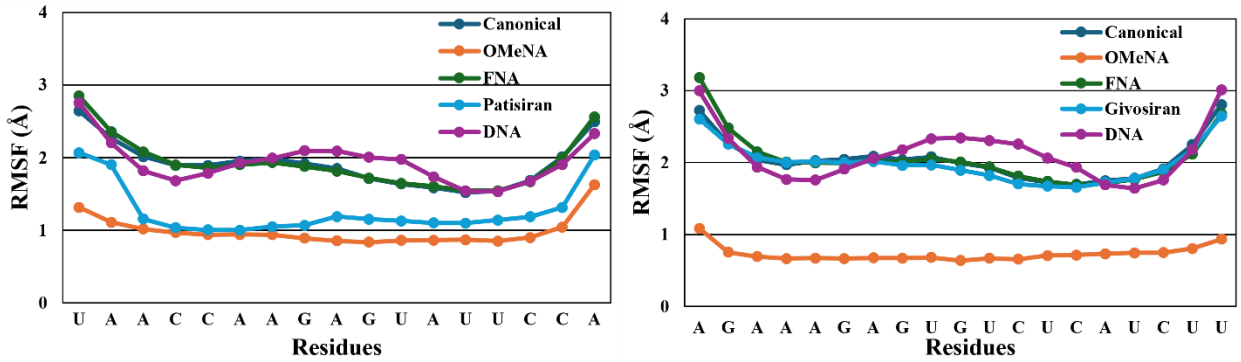

Figure A.9: Root-mean-square fluctuations (RMSF) for the sense strand of canonical and chemically modified nucleic acids of Patisiran and Givosiran (in Å) over 1 μs MD simulations across 5 replicas.

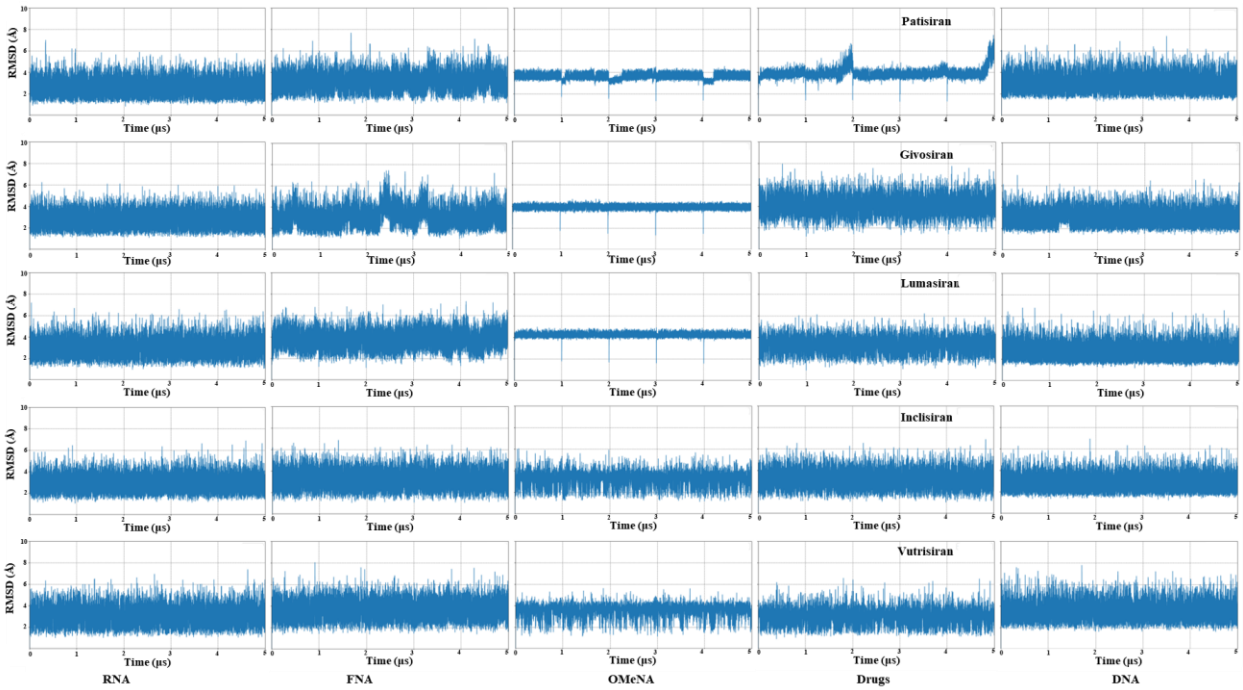

Figure A.11: Root-mean-square deviation (RMSD) for all duplexes (in Å) over 1 μs MD simulations across 5 replicas.

APPENDIX B: SUPPLEMENTARY INFORMATION FOR CHAPTER 3

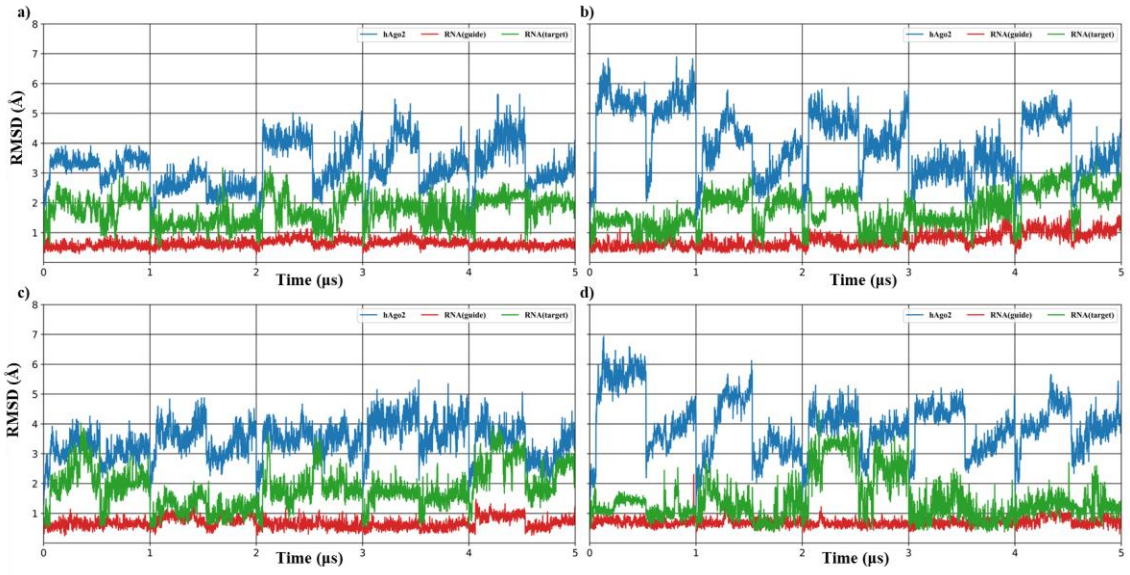

Figure B.1: Root-Mean-Square-Deviation (RMSD) for the whole siRNA-hAgo2 complex (a) RNA (b) FNA (c) OMeNA (d) Givosiran over 1 μs MD simulations across 5 replicas.

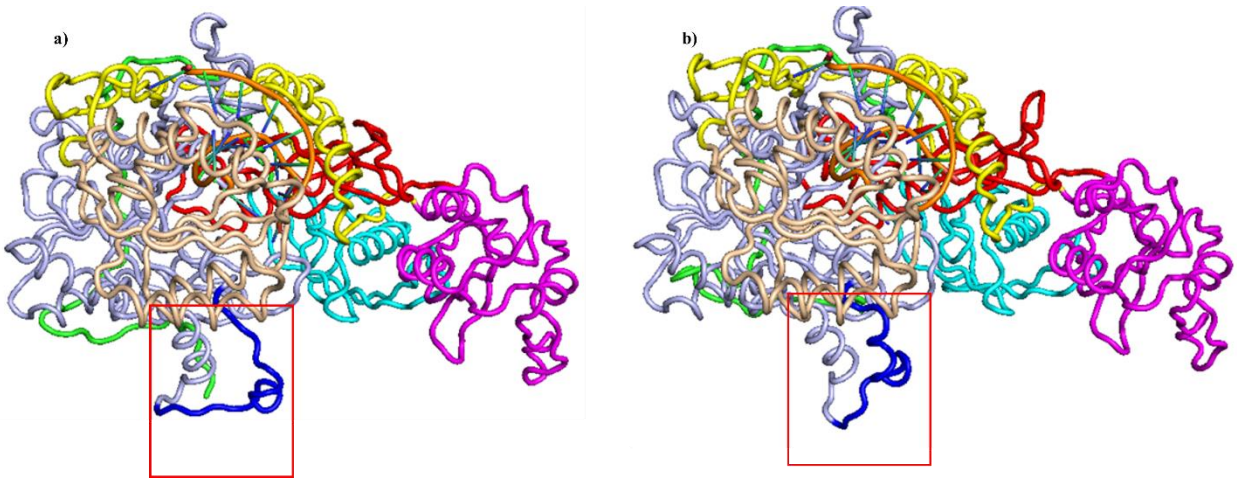

Figure B.10: Localized conformational fluctuations within the hAgo2 domain (residue 819-831) are highlighted by the red rectangle.

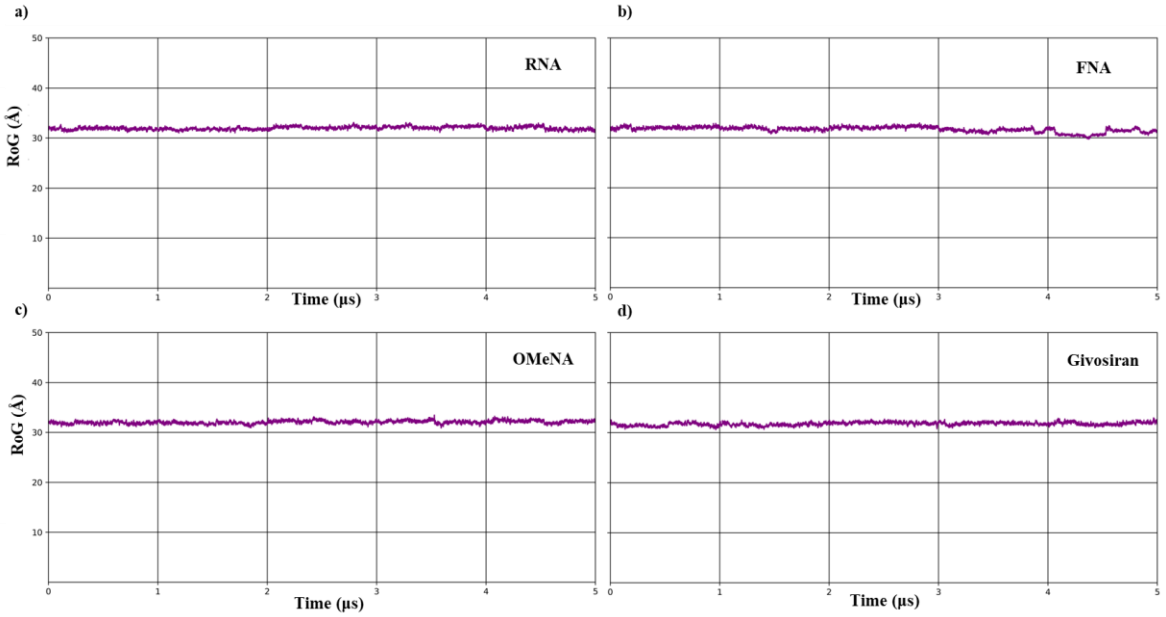

Figure B.3: Radius of Gyration (RoG) for the whole siRNA-hAgo2 complex (a) RNA (b) FNA (c) OMeNA (d) Givosiran over 1 µs MD simulations across 5 replicas.

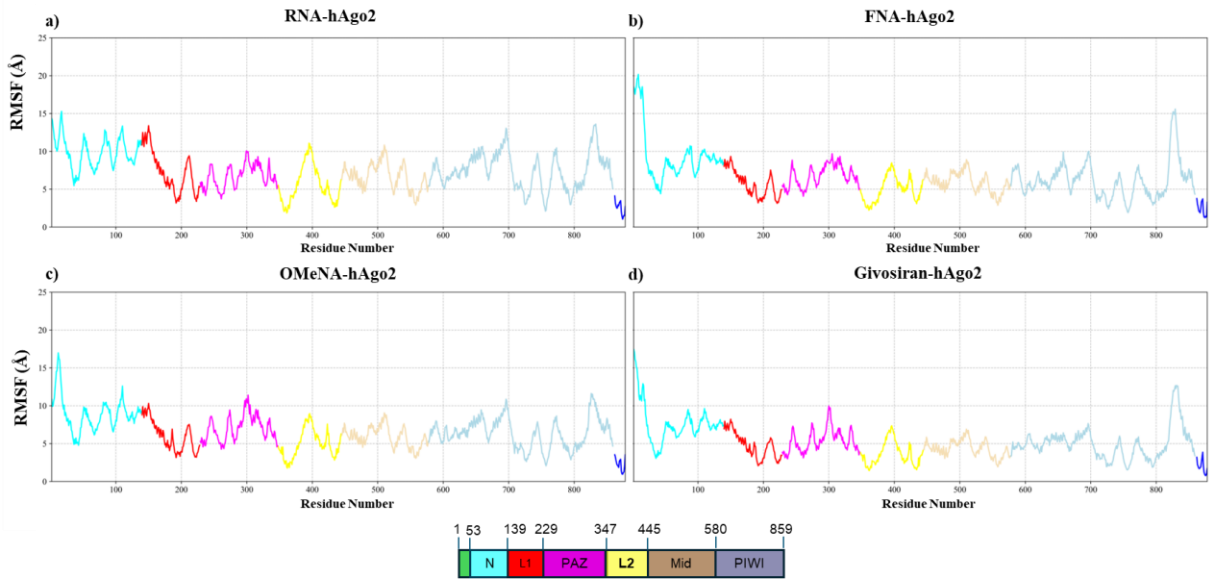

Figure B.4: Root-Mean-Square-Fluctuations (RMSF) for the whole siRNA-hAgo2 complex (a) RNA (b) FNA (c) OMeNA (d) Givosiran over 1 µs MD simulations across 5 replicas.

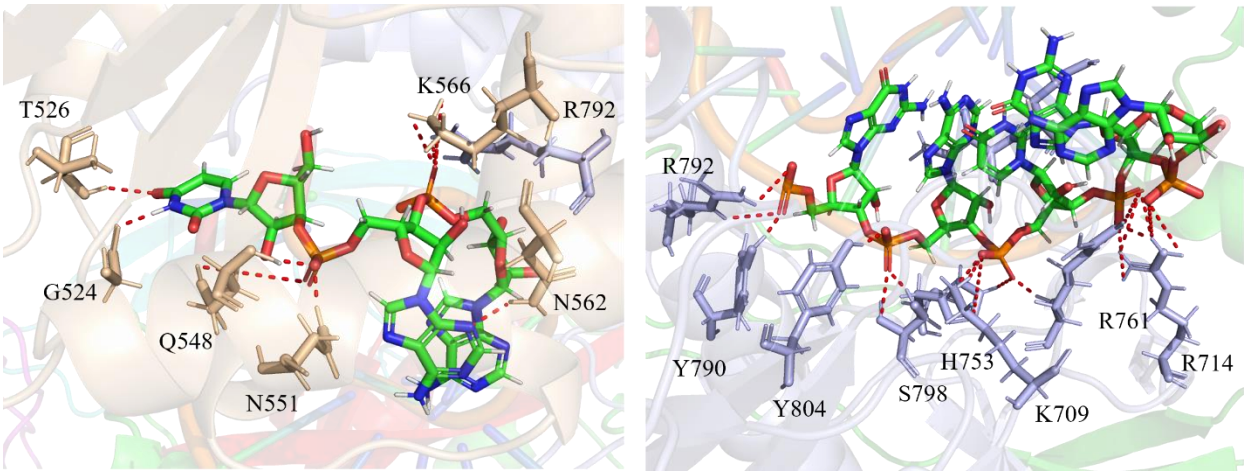

Figure B.5: Guide siRNA recognition by domains of hAgo2 reported in experimental crystal structure (PDB ID:4W5O)